



Université Pierre et Marie Curie

Sorbonne Universités

École doctorale d'Astronomie et
Astrophysique d'Île-de-France (ED 127)

Institut d'Astrophysique de Paris (IAP)

Cosmology with Cosmic Voids

Par Alice Pisani

Thèse de doctorat de Cosmologie

Dirigée par Benjamin Wandelt (Chaire Internationale à l'UPMC)

Présentée et soutenue publiquement le 22/09/2014

Devant un jury composé de (par ordre alphabétique):

Pr. James Bartlett	APC	Examinateur
Pr. Valérie de Lapparent	IAP, CNRS	Invitée
Dr. Stéphanie Escoffier	CPPM, CNRS	Rapporteure
Pr. Luigi Guzzo	INAF	Examinateur
Pr. Michael Joyce	LPNHE	Examinateur
Pr. Rien van de Weygaert	Kapteyn Institute	Rapporteur
Pr. Benjamin Wandelt	IAP, UMPC, CNRS, ILP	Examinateur

Contents

Introduction **4**

1 The large-scale structure of the Universe, cosmic voids, and the pillars of Cosmology **7**

1.1 Historical overview of the large-scale structure discovery . . . 8

1.1.1 Looking outside our galaxy 8

1.1.2 1976: first surveys 10

1.1.3 The discovery of cosmic voids and the large-scale structure 12

1.1.4 The large-scale surveys 16

1.2 An abridged history of Cosmology 19

1.2.1 The pillars of Cosmology 20

1.2.2 Friedmann equations 27

1.2.3 Distances 31

1.3 Recent developments in Cosmology 40

1.3.1 Our Universe 43

1.3.2 The most boring Universe? 50

2 Understanding the Universe with Voids **54**

2.1 Standard objects 55

2.2 Cosmic voids 60

2.2.1 Voids as a tool for dark energy 63

2.2.2 Alcock-Paczyński test with voids 65

2.2.3 Questions and challenges 67

3 Redshift space distortions: To real space and beyond 71
3.1 Redshift-space distortions . . . 71
3.2 To real space . . . 73
3.2.1 Using sphericity . . . 73
3.2.2 Notation . . . 75
3.2.3 The inverse Abel transform . . . 75
3.3 Ill-conditioning . . . 77
3.3.1 Polynomial regularisation . . . 77
3.3.2 Singular value decomposition . . . 79
3.3.3 Differences between the methods . . . 80
3.3.4 Technical details . . . 81

4 Testing void reconstruction 83
4.1 The ideal case: no-noise . . . 83
4.2 The toy model: constructing and using a simple benchmark . 86
4.3 Dark matter particles . . . 90
4.3.1 Reconstructed density profile of a stacked void with the polynomial regularisation method . . . 91
4.3.2 The reprojection, a quality test for the reconstruction . 95
4.3.3 The singular value decomposition method for the simulated void . . . 96
4.4 Galaxy mocks . . . 97

5 Results: real space density profiles for stacked voids from SDSS DR7 101
5.1 Results . . . 101
5.2 Discussion . . . 109
5.3 Possible direct applications . . . 111
5.3.1 Mass compensation and theoretical prediction of velocity profile . . . 112
5.3.2 Velocity reconstruction . . . 121

6 The effect of peculiar velocities and `VIDE` 126
6.1 `VIDE` . . . 128

6.2 Peculiar velocities affect voids and `VIDE` 131
6.2.1 Simulation and HOD details 131
6.2.2 The matching algorithm 132
6.2.3 One-to-one comparison 133
6.3 Results 134
6.3.1 Matched fraction 136
6.3.2 Average ellipticity variation due to peculiar velocities . 140
6.3.3 Guidelines 144
6.4 Effect of velocities on HOD stacks 145
6.5 Discussion on peculiar velocities 147

7 Constraints from cosmic voids: Alcock-Paczyński test and abundances 149
7.1 Recent Alcock-Paczyński test application 150
7.2 Constraints from void abundances 152

Conclusion 159

Acknowledgements 162

Appendix A 166

Appendix B 170

Bibliography 173

***La Cosmologie avec les Vides Cosmiques** (Résumé de la thèse)* **190**

Introduction

Cosmology is the science that studies the Universe as a whole, with the objective of explaining its structure and evolution. To reach information about the Universe, one way is to observe the largest scales possible, considering galaxies — groups of stars bound by gravity — as points, and tracing their positions and movements. The large-scale movement of these tracers tracks for us the evolution of the Universe. At large scales, clusters of galaxies, sheets, voids and filaments shape the Universe — it is the Cosmic Web.

While most of the work to understand the large-scale structure of the Universe has focussed on the over-dense regions, emptier regions are gaining interest: *cosmic voids*, discovered in 1978, are the under-dense regions in the Universe, with sizes from ten to hundreds of Mpcs.

Until very recently, due to the difficulty of extracting data from low density zones, the potential of voids has been under-explored. Modern surveys allow us now to access to high quality large-scale-structure measurements, by sampling the galaxy distribution in great detail also in sparse regions: the appeal of cosmic voids becomes thus considerable.

Being devoid of matter, cosmic voids might be mainly composed of dark energy — which strongly justifies their importance for Cosmology, as dark energy is believed to be 70% of the Universe and we still do not understand it. The efforts of cosmologists seem to converge to a cosmological model (called ΛCDM) that leaves many unknowns. The nature — and we could say even more, the existence — of dark energy remains a mystery; and so does the nature of dark matter. In this framework cosmic voids appear as a new potential probe for our quest of a correct model for Cosmology.

Cosmic voids fill most of the Universe, and have simpler dynamics than high density regions of the Universe. As such, they constitute a promising laboratory to test dark energy, constrain cosmic expansion and discriminate between cosmological models such as modified gravity models. Despite of being simpler, Cosmology with cosmic voids is only at its commencement. In the era of precision Cosmology, each cosmological probe needs a careful understanding of the systematic effects affecting measurements and, to become competitive with other probes, requires detailed study. Aiming to constrain cosmological parameters with voids, we need to ensure that we are able to correctly understand and model them.

The use of voids to constrain Cosmology is based on studying their shapes, their number density and their evolution. These properties are indeed dependent on the cosmological model and can thus be used to constrain it. In this framework the major source of systematics is the presence of peculiar velocities.

When we observe cosmic voids, we observe them in *redshift-space*: their real shape remains inaccessible to us, thus greatly limiting our knowledge about such structures. To employ voids as a precision tool for Cosmology, it is fundamental to obtain their real shape and eventually to understand how peculiar velocities affect them.

The purpose of this thesis is to find a model-independent way to access the real shape of the voids, i. e. the *real-space information*, adopting as few assumptions as possible about the cosmological model. This work aims to answer to the following questions: how can we extract real-space information from cosmic voids in a model-independent way? Can we understand the systematics in the use of cosmic voids? Can we obtain real-space information from real data? The application of any method we consider to real data it another fundamental point of this work: as voids are to be used as cosmological probes, we cannot disentangle us from real data, which have the ultimate word in assessing the quality of models. Furthermore, using realistic HOD models mimicking real data, it is possible to study the major systematics affecting the use of voids as cosmological probes: peculiar velocities. Obtaining

the real-space shape of voids and understanding how velocities affect our measurements are crucial steps towards the goal of precision-level Cosmology with cosmic voids.

Chapter 1 presents the large-scale structure of the Universe and the discovery of cosmic voids, as well as the standard cosmological model. The second chapter illustrates the use of voids as cosmological probes and the systematics that affect their use. The third Chapter lays out the fundamental idea of this work: the method to obtain the real-space information for cosmic voids in a model independent way. Chapter 4 tests the model in multiple ways, first with a toy model; then with a dark matter particle simulation and finally using galaxy mocks mimicking real data.

The application to real data from the Sloan Digital Sky Survey (Data Release 7) is presented in Chapter 5, providing the first model-independent average density profiles of cosmic voids *in real space*. In Chapter 6, I analyse the effect of peculiar velocities with mock galaxy catalogues, and provide guidelines to minimise the systematics when using cosmic voids for cosmological purposes. Finally the last chapter presents the latest constraints from cosmic voids, as well as a forecast of the abundances of voids from the upcoming Euclid survey, providing us with realistic estimates of what can be achieved with voids in the next decade[1].

[1]Portions of this work have been used in the following publications:

- A. Pisani, G. Lavaux, P. M. Sutter, B. D. Wandelt. "*Real-space density profile reconstruction of stacked voids*", arχiv:1306.3052, accepted for publication in **Monthly Notices of the Royal Astronomical Society Main Journal** (Pisani et al., 2014a);
- A. Pisani, B. D. Wandelt. "*The challenge of cosmic voids*", to appear in the **Proceedings of the International School of Physics** "Enrico Fermi" of the Italian Physical Society – SIF-Course CLXXXVI: "New Horizons for Observational Cosmology"(Pisani and Wandelt, 2013);

Other portions will be used as results and discussions in forthcoming papers: Pisani, Sutter and Wandelt 2014 *"Mastering the effects of peculiar velocities on voids"*(Pisani et al. (2014c), in prep.); Pisani, Sutter, Alizadeh, Biswas and Wandelt 2014 *"Constraining dark energy with cosmic void abundances"* (Pisani et al. (2014b), in prep.).

Chapter 1

The large-scale structure of the Universe, cosmic voids, and the pillars of Cosmology

Cosmologists aim to understand the Universe, its components and its evolution. The study of the large-scale structure of the Universe is a powerful tool to reach such an understanding, since structures map both the evolution and the content of the Universe through their growth. Although physical Cosmology is a relatively recent science (compared for instance to Biology, Chemistry or Mathematics), it has now reached a high level of completeness, at the point that we can observe the Universe at large scale and try to understand its evolution.

We are able to define a standard cosmological model, in the framework of which many concepts can be understood. The global picture for the large-scale structure of the Universe and Cosmology — although leaving many challenging unknowns — is thus established.

The first section of this Chapter introduces the large-scale structure of the Universe, starting with an overview of its discovery and describing the first galaxy maps, as well as the most recent surveys. It particularly focuses on the discovery of cosmic voids, the topic of this thesis. The second section sums up the current status of cosmological knowledge by defining the standard

cosmological model and the content of our Universe. Finally the third section discusses more in details the recent developments of Cosmology.

1.1 Historical overview of the large-scale structure discovery

In this introduction I will review the observational milestones that lead us to an understanding of the Universe at large scale. Without any claim of completeness, I single out the steps that I consider crucial in our path towards the actual knowledge of the large-scale structure of the Universe.

1.1.1 Looking outside our galaxy

Our story with the Universe at large scales began the first time we looked outside our galaxy. As in many first attempts to look further in science, humankind misunderstood what was seen (obvious examples of such misunderstandings are the concepts of flat Earth and the belief of Earth as being the center of the Solar system, both particularly difficult to eradicate).

The first extragalactic objects (nearby galaxies such as the Andromeda galaxy) were erroneously though to be part of our galaxy and were called nebulae (a detailed review is Biviano (2000)). Interestingly, among the first to support the idea that these nebulae were in fact other systems than our Via Lactea, was the philosopher Immanuel Kant (Kant, 1755). His interest in the subject had been kindled by a paper of the English astronomer Thomas Wright (Wright and Hoskin, 1972), stating:

> "*That this in all probability may be the real Case, is in some Degree made evident by the many cloudy Spots, just perceivable by us, as far without our starry Regions, in which tho' visibly luminous Spaces no one Star or particular constituent Body can possibly be distinguished; those in all likelyhood may be external Creation, bordering upon the known one, too remote for even our Telescopes to reach.*".

A "great debate" between the ideas of "island Universes" and the "nebulae hypothesis" took place in 1920, involving Heber Curtis and Harlow Shapley (for a detailed and quite interesting review see Smith and Berendzen (1982)[1]).

To obtain a proof that the "island Universes" were indeed other galaxies, outside ours, the scientific community had to wait for the work of Henrietta Leavitt, one of the so-called Harward computers, the group of women hired by Edward Charles Pickering to analyse astronomical data. In 1908 she had produced a catalogue of 1777 variable stars and noticed that some of them had longer periods (Leavitt, 1908). Pursuing her research in the following years she confirmed the relation between the apparent magnitudes and the periods of the stars (Leavitt and Pickering, 1912) (a discussion about Leawitt work is given by Fernie (1969)). Her discovery that the period of Cepheid luminosity was related to luminosity allowed astronomer Edwin Hubble to estimate the real distance of the Andromeda Nebula, finally placing it outside our galaxy.

However Edwin Hubble was not the first to argue, supported by data, that the nebulae were in fact other galaxies. Eight years before, in 1917, the American astronomer Vesto Melvin Slipher had measured the redshift of the "nebulae" and stated the following:

> *"We may in like manner determine our motion relative to the spiral nebulae, when sufficient material becomes available. A preliminary solution of the material at present available indicates that we are moving in the direction of right ascension 22 hours and declination* $-22°$ *with a velocity of about 700 km. While the number of nebulae is small and their distribution poor this result may still be considered as indicating that we have some such drift through space. For us to have such motion and the stars not show it means that our whole stellar system moves and carries us with it. It has for a long time been suggested that the spiral nebulae are stellar systems seen at great distances [...] This theory, it seems to me, gains favor in the present observations."*

[1]Among the astronomers, a strong supporter of the idea of "island Universes" was Sir William Herschel.

As Peacock (2013) points out in a recent review of Slipher's work (Slipher, 1917), this reasoning is a masterpiece of logic and an astounding example of scientific analysis. Although others suggested this interpretation of redshift measurements (such as Sullivan (1916)), they all used Slipher's data — which should thus be considered as the first proof that we are in an "island Universe" moving with respect to others "islands".

For the first time, scientists were looking outside our galaxy and could prove it. Thus, understanding the existence of other galaxies is — historically — the beginning of the study of the Universe at large scales, where galaxies are considered as points of which we can follow the distribution.

1.1.2 1976: first surveys

The following important conceptual step in the study of the large-scale structure of the Universe had to wait for the advent of large-scale surveys and, more precisely, for the possibility to better access the 3D information. In the early 1960's the existence of superclusters (called "second order cluster" in Abell (1958, 1961)) was driving the attention of the scientific community: as a result many groups started to study the distribution of galaxies.

Some groups argued that the distribution of galaxies had to be random; interestingly among those, Fritz Zwicky strongly claimed that superclusters could not exist: *"These results are: First, there exists no pronounced clustering tendency of clusters of galaxies[...]"* (Zwicky, 1957)[2], while other groups claimed the existence of a distinct structure for the Universe at large scales.

According to Laird Thompson (Thompson, 2005), Gerard de Vaucouleurs was one of the first to use the redshift information accessible at those times for a limited amount of galaxies. While in a paper from 1970 de Vaucouleurs clearly states the existence of *"obvious non-random clustering which dominated the galaxy distribution on all scales out to the limit of the deepest survey"* and declares *"I believe, nevertheless, that there is some indication of nonrandom density fluctuations[...]"* (de Vaucouleurs, 1970), the uncertainty

[2]Even great scientists, of the calibre of Zwicky (the first to suggest the existence of dark matter (Zwicky, 1933), see 1.3.1), can make mistakes.

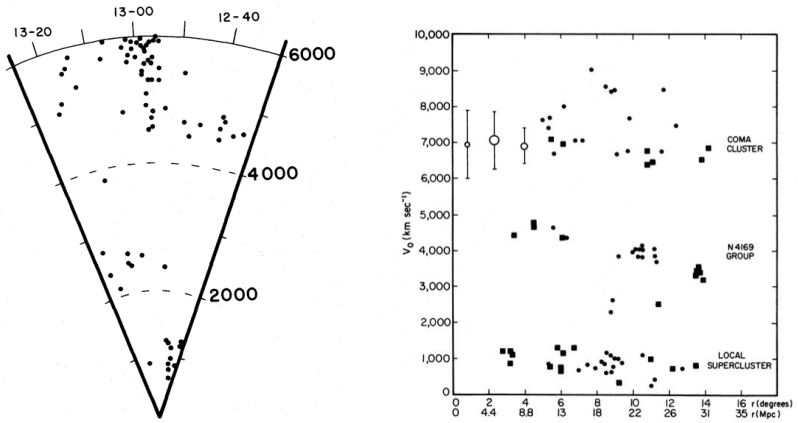

Figure 1.1: The first 3D surveys: left and right plots show the results of, respectively, Tifft & Gregory (Tifft and Gregory, 1976) and Chincarini & Rood (Chincarini and Rood, 1976).

about the large-scale structure was considerable, to the point that he was casting doubt on the big bang model for Cosmology.

A few years later, in 1976, William G. Tifft and Stephen A. Gregory presented the results of the Coma cluster redshift survey: a slice showing data in polar coordinates, where the ascension is used as the angular polar coordinate and redshift as the radial coordinate (while galaxy declination is projected on the plane) (see Figure 1.1, right plot). With the benefit of hindsight, one can observe that this way of presenting data allowed to have a glimpse of the large-scale structure of the Universe even though the area of the survey was small (Thompson, 2005). Unfortunately, the observed area was too small for the authors to make any deduction about the distributions at larger scales.

The same year, another group had the possibility to see the large-scale structure of the Universe, possibility that did not become reality. Guido Chincarini and Herb Rood presented data from a larger redshift survey. The group could have seen the voids and hints of the great CfA wall, if they had not chosen an unlucky representation, where the same quantities represented by Tifft and Gregory where plotted in x and y axis — which in some way hides the 3D visualisation (see Figure 1.1, left plot).

All these "close to the target" results prove that a milestone was about to

be reached. Who was going to give the first glance to the cosmic web?

1.1.3 The discovery of cosmic voids and the large-scale structure

As Thompson (2005) and Thompson and Gregory (2011) describe, two groups independently achieved this exploit. Laird A. Thompson and Stephen A. Gregory (Gregory and Thompson, 1978) sampled 238 galaxies up to a limiting magnitude of 15.0 while Mikhel Jôeveer, Jaan Einasto and Erik Tago (Jõeveer et al., 1978) used data from previous catalogues such as the Second Reference Catalog of Bright Galaxies from de Vaucouleurs (de Vaucouleurs et al., 1976) and Karachentsev's catalogue (Karachentsev, 1972) up to a magnitude of 14.5.

Gregory and Thompson had just obtained their respective Doctor of Philosophy degrees, as Thomson himself states, and had set a clear goal for their future research: measure the 3D distribution of a larger patch of the sky to finally see the large-scale structure of the Universe. Meanwhile Mikhel Jôeveer and Jaan Einasto, from the Tartu Astrophysical Observatory in Estonia, had started putting together galaxy reshifts from the available catalogues to obtain 3D maps of the large-scale galaxy distribution.

Quite rapidly, Gregory and Thompson found striking results: by 1977 they had unveiled the void-like structure of the Universe for the first time and started to write a publication. While Thompson and Gregory were submitting to the Astrophysical Journal (7 September 1977), Jôeveer and Einasto were independently preparing a presentation of similar results for a very timely meeting to be held: *The large scale structure of the Universe, symposium no. 79 in Tallinn, Estonia, U.S.S.R., September 12-16, 1977* (see Figure 1.2). Thompson and Gregory had not been invited to the conference, but their former thesis supervisor, William G. Tifft was, and he was planning to discuss the recent results (Thompson, 2005).

With the advantage of hindsight, many elements could have indicated that the meeting would have been a crucial milestone for the knowledge about the large-scale structure of the Universe. Many of the scientists present at the meeting are today known to have set the basis for the study of the large-scale



Figure 1.2: The 79. symposium of IAU "The large-scale structure of the Universe" in Tallinn, September 1977. In the photo J. Peebles, G. Abell, M. Longair and J. Einasto (photo from academician Jaan Einasto's private collection).

structure and Cosmology: among them I cannot avoid mentioning G. Abell, J. Audouze, J. Binney, G. I. Chincarini, A. G. Doroshkevich, J. Einasto, J. P. Huchra, M. Jôeveer, M. S. Longair, P. J. E. Peebles, H. J. Rood, S. F. Shandarin, J. Silk, R.A. Sunyaev, E. Tago, M. Tarenghi, W. C. Tifft, S. D. Tremaine, R. B. Tully, G. H. De Vaucouleurs and Ya. B. Zeldovich.

With the set ready, the meeting began. Tifft discussed the results from the 3D map of the large-scale structure in a paper written by Tifft and Gregory — with reference to the submitted paper of his former students. He states *"There are regions more than 20 Mpc in radius which are totally devoid of galaxies"*. It is historically interesting to read the discussion that followed, of which I particularly mention J. Silk's comment, showing how the idea of voids was innovative and unexpected, at the point that it gave rise to legitimate doubts and investigation about all the points of the analysis: *"The apparently sharp boundaries and holes over large scales that are being inferred may partly be a function of the nature of the magnitude-limited sample. At the distance of the Coma Cluster, one is barely at the knee in the galaxy luminosity function. Many fainter galaxies could be present, and it is possible that the more luminous galaxies are only found in dense regions."*(Tifft and Gregory, 1978).

The observational data were quite robust: in order to avoid critics stating that empty regions were due to incomplete sampling and not to real emptiness, the surveys used by Gregory and Thompson were magnitude-limited, but this could also raise doubts in the scientific community.

The work from Jôeveer and Einasto was subject to similar criticism, all the more since they had used redshifts collected from previous catalogues. Particularly they encountered some scepticism when they stated *"Disk of superclusters intersect at right angles, forming walls of cells in the Universe. In cells interiors the density of galaxies is very small and there we see big holes in the Universe. The mean diameter of big holes as well as superclusters is ∼100 Mpc."*(Joeveer and Einasto, 1978).

A comment from Davis illustrates the doubts that the Estonian group had to face: *"Most of your redshifts are derived from the second reference catalogue of the Vaucouleurs and since the sky coverage of the catalogue is quite patchy, one must exercise caution in judging the reality of the holes between superclusters"*(Joeveer and Einasto, 1978).

Davis's and Silk's comments give an idea of the initial scepticism that those observational data received, which is also mentioned by Thompson in (Thompson and Gregory, 2011), due to the fact that there was no accepted explanation for the existence of voids and filaments in the homogeneous Universe prescribed by theory.

The need for a solid theory explaining voids is clearly stated in the Gregory and Thompson paper: *"It is an important challenge for any cosmological model to explain the origin of these vast, apparently empty regions of space."*

Voids — the under-dense regions in the galaxy distribution — were the most interesting subject of the conference, as pointed out by Longair in the conclusion of the Symposium:

> *"But perhaps even more surprising are the great holes in the Universe. Peeble's picture, Einasto's analysis of the velocity distribution of galaxies which suggests a "cell-structure" and Tifft's similar analysis argue that galaxies are found in interlocking chains over scales ∼ 50-100 Mpc forming a pattern similar to a lace-tablecloth.*

> *The holes are particularly interesting since they might appear to be at variance with the idea of continuous clustering on all scales [...]"* (Longair, 1978)[3].

The observational data had thus a great importance in this meeting, despite some initial incredulity. But a similarly important part is played by theory. The meeting is also a crucial place for the first presentation of theoretical results that would shape the study of the large-scale structure of the Universe in the forthcoming years.

Zeldovich words in the proceedings of the Symposium point out the role of theory in the game:

> *"The present symposium has really opened up a new direction in the search for geometrical patterns governing the distribution of luminous matter in space. We heard about ribbons or filaments along which clusters of galaxies are aligned; the model of a honeycomb was presented with walls containing most of matter; the presence of large empty spaces was emphasized [...]. Cosmological theory must be aware of this information and try to use it [...]."*

After this introduction he presents the latest developments of his group's work — that included, among others, Doroshkevich, Sunyaev, Novikov and Shandarin and is based on the work from theoretical cosmologists such as Lifshitz, Bonnor, Silk, Peebles, Yu — to study the evolution of perturbations using approximate linear theory and numerical simulations (Zeldovich, 1978).

As stated in the paper of the Estonian group (Jõeveer et al., 1978), the collaboration between Zeldovich and his colleagues was advancing a theoretical model able to explain the non-random distribution of galaxies at large scales: *"We note that a theory of galaxy formation which leads to the formation of similar structure [cell structure] has been suggested and developed by*

[3]A complete discussion about who saw voids first can be found in Thompson and Gregory (2011), however I point out that, in the proceedings of the talk of Joeveer and Einasto, there is an added note referring to the presentation of Tifft, that was presenting results from Gregory and Thomson: *"The presence of holes of various diameters was demonstrated during the symposium by B. Tully and W.G. Tifft."*(Joeveer and Einasto, 1978).

Zeldovich (1970–1978) and his collaborators (Doroshkevich, Saar & Shandarin 1977).”

Simulations also play a role in this discovery, by validating a possible theoretical scenario. Longair himself comments the film presented by Zeldovich and developed by his group with the following words: *“All of us have been impressed by the film of the development of “pancakes” by Doroshkevich and his colleagues and by the remarkable resemblance to the cell-structure of the Universe described by Einasto, Tifft and others.”* (Longair, 1978)

To conclude, the symposium is an important crossing point between observations, theory and simulations, setting another crucial milestone in the timeline of the discovery of the large-scale structures. Figure 1.3 shows the first clear images of the large-scale structure of the Universe, where voids finally emerge.

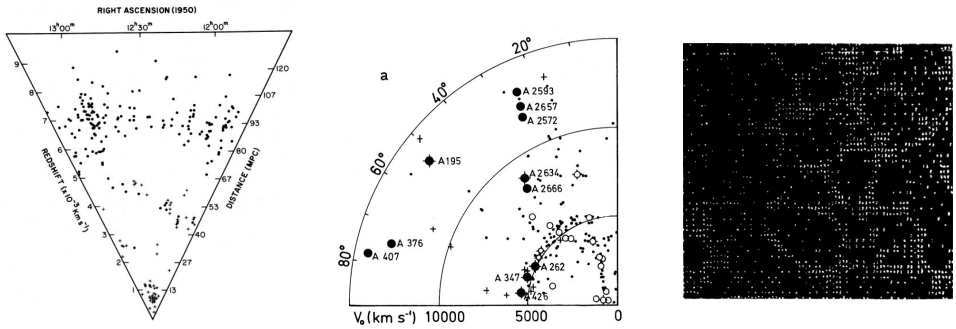

Figure 1.3: Finally, the large-scale structure: voids and superclusters. Left and central plots show the results of, respectively, Gregory & Thompson (Gregory and Thompson, 1978) and Jôeveer, Einasto & Tago (Jõeveer et al., 1978). Right panel shows a numerical simulation from Zeldovich et al. (Zeldovich, 1978) presented at the 79. symposium of IAU.

1.1.4 The large-scale surveys

The previous Section described how the idea of a foam-like *cosmic web*[4] arose from observations and stood — despite some initial theoretical doubts — to

[4]The *cosmic web* is the term nowadays used to design the distribution of clusters, voids, filaments and sheets in the Universe.

become a pillar of modern Cosmology. In the beginning of the 1980s, the picture started to be widely accepted. Many papers were published in both scientific and popular journals. In those years, the group lead by Kirshner (Kirshner et al., 1981) investigated an empty region in the previous redshift surveys and found the so-called "Boötes void"(or Great void), a 34 h^{-1}Mpc void. For a more complete review of the papers in these years, see Thompson and Gregory (2011).

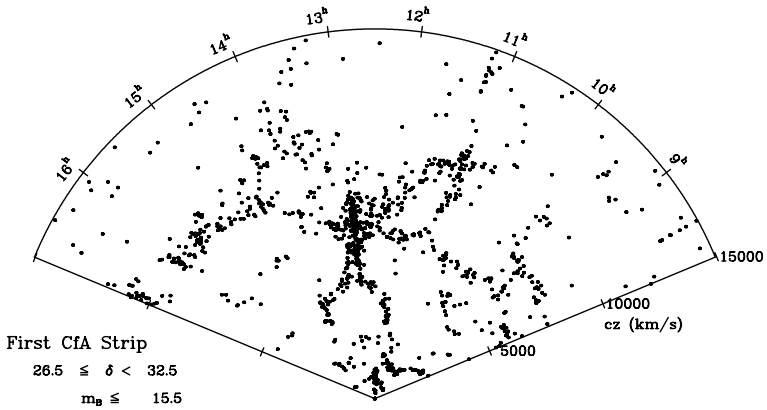

Figure 1.4: The second CfA survey. Image credit: The Smithsonian Astrophysical Observatory (de Lapparent et al., 1986).

The year 1986 marks an important step in the discovery and study of the large-scale structure of the Universe: Valérie de Lapparent — a French Ph.D student doing her thesis in Cambridge (Massachusetts) under the supervision of Margaret Geller and John Huchra — published a redshift galaxy catalogue reaching $m = 15.5$. The work was part of the CfA (Centre for Astrophysics) Redshift Survey, of which the first part had started in 1977. The map resulting from the second CfA spectroscopic survey is shown in Figure 1.4. The angle is much wider compared to previous surveys and confirms the idea that the distribution of galaxies is not random.

To illustrate the improvement that a few years had allowed in terms of survey's area, we show in Figure 1.5 (Thompson and Gregory, 2011) a comparison of the de Lapparent 1986 results with the earlier redshift survey from Gregory and Thompson (1978).

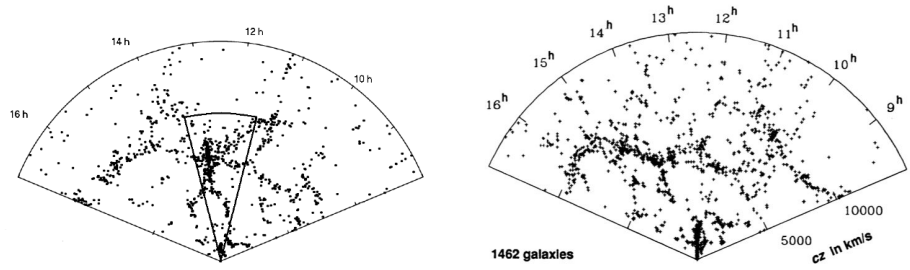

Figure 1.5: Left panel: comparison between the second CfA survey (de Lapparent et al., 1986) and the Gregory and Thompson original plots (Thompson and Gregory, 2011); right panel: pushing a to different declination to see the extent of the CfA Great Wall (Geller and Huchra, 1989) ($8.5° < \delta < 14.5°$, while the de Lapparent was $26.5° < \delta < 32.5°$).

The slice from de Lapparent et al. (1986) can be seen as the passage to a new era, the era of large scale surveys. More than hints of structures could be clearly seen, enhancing certainty to the void-filament-sheet-cluster panorama of the large-scale structures. In the following years the map was further improved by completing the sampling in the area, which led to the detection of the CfA Great Wall, the largest sheet of galaxies ever detected until that time (see right plot of Figure 1.5, from Geller and Huchra (1989)).

To complete this review of the history of the large-scale structure, I will cite and represent some of the most significative surveys of the following years, with no claim of completeness.

The joined CfA2 and SSRS2 (a magnitude-limited survey covering the region around the south Galactic Pole) covered more that 30 % of the sky (da Costa et al., 1994). The LCRS (Las Campanas Redshift Survey) is also an important example, since it made use of an improvement in the technology to measure redshifts: fiber-fed multi-object spectrographs and wide-filed telescopes allowed to sample a five times larger volume (Shectman et al., 1996).

Jumping to most recent times, I cannot avoid mentioning the two largest redshift surveys completed until now: the 2dF Galaxy Redshift Survey and the Sloan Digital Sky Survey. All these most recent surveys are shown in Figure 1.6, allowing to observe the improvements from the first to the last.

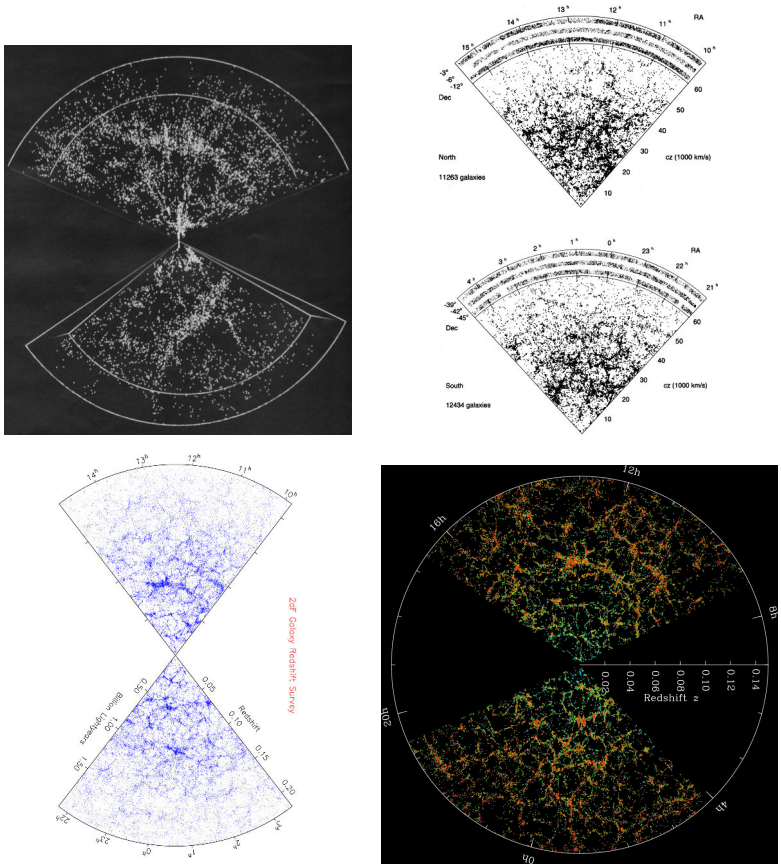

Figure 1.6: From left to right, upper row: CfA-SSRS2 (da Costa et al., 1994) joint map, the LCRS (Shectman et al., 1996); lower row: the 2dF survey (last release, image credit 2dF Galaxy Redshift Survey) and the SDSS results (image credit: Sloan Digital Sky Survey).

After having presented the discovery of voids and of the Universe at large scales, the next Section briefly sums up the history of Cosmology.

1.2 An abridged history of Cosmology

Cosmology became a modern science when scientists started measuring the expansion of the Universe. Historically, this happened exactly after the awareness that there were other galaxies outside ours. While studying the story of

the large-scale structure, I jumped from Slipher's work (in 1917) and the claim that the "nebulae" are in fact other galaxies to the first surveys of 1976.

Among the two, I skipped an important event that constitutes the first pillar of nowadays Cosmology: the discovery of the expansion of the Universe through the redshift-distance relation. The astronomer Edwin Hubble is the most known for the discovery of the expansion of the Universe. Nevertheless, as pointed out by Peacock (2013), Vesto Melvin Slipher had already measured the expansion of the Universe before him and advanced the perceptive hypothesis that galaxies recede in all directions — his redshift measures were used by Hubble to reach the conclusion that the Universe is expanding. To the interested reader, I add details about his research in Appendix A.

Furthermore, the idea of expanding Universe had also been introduced *before* Hubble by another scientist, the Belgian abbey Georges Lemaître. In 1927, Lemaître had published *"Un univers homogène de masse constance et de rayon croissant, rendant compte de la vitesse radiale des nébuleuses extra-galactiques"* (Lemaître, 1927), in which — based on Slipher's velocity measurements and on Hubble 1926's distances (obtained using Leavitt's relation) — Lemaître had in fact obtained the expansion rate of the Universe.

Livio (2011) discovered the reason for which Lemaître's results were unnoticed by the scientific community and the Belgian astrophysicist did not have the deserved recognition; details about this interesting anecdote can be found in Appendix A.

After this brief reminder about the discovery of the expansion of the Universe I introduce the pillars of modern Cosmology.

1.2.1 The pillars of Cosmology

In this Section I introduce the three pillars of Cosmology: the redshift-distance relation, the cosmological principle and the Friedmann-Lemaitre-Robertson-Walker metric.

Pillar I: The redshift-distance relation:

The redshift-distance relation (known as the Hubble[5] law) is one of the basis of Cosmology. To illustrate the relation we remind the definition of redshift. The observed shift of a galaxy's spectrum through the identification of spectral absorption lines allows the calculation of the relative motion between source and observer on the basis of the Doppler effect:

$$z = \frac{\lambda_o - \lambda_e}{\lambda_e} \tag{1.1}$$

where λ_e is the emission wavelength and λ_o the observed wavelength. There are three possible cases:

- If $z < 0$, the source is approaching the observer, this will result in a so-called *blueshift* (all spectral lines are displaced towards shorter wavelengths).
- If $z = 0$, the source would not be moving either towards or away from the observer.
- If $z > 0$, the source is moving away from the observer. This will result in a *redshift* (all spectral lines are displaced towards longer wavelengths).

A linear relationship can be established between a galaxy's speed of recession v and the distance of the galaxy from the observer. This relationship has been confirmed by the Hubble Space Telescope. As previously discussed, most of the redshifts used in the 1929 paper from Edwin Hubble to obtain the relation were measured by Vesto Melvin Slipher, and a robust measurement was not reached until unexpectedly recent times (Peacock, 2013). The law states:

$$v \simeq H_0 d = cz \tag{1.2}$$

where c is the speed of light and H_0 is the Hubble constant[6]. I anticipate that H_0 corresponds (as will be shown) to the value of H (the so-called Hubble

[5]We discussed in Appendix A the role of Edwin Hubble in the discovery, the perceptive hypothesis by Slipher, the use of his data and the earlier discovery by Lemaître.

[6]For completeness, I show that equation 1.2 is a linear approximation that can be obtained from the results in Section 1.2.3. Expanding $a(t_o)$ in a power series we have:

$$a(t_o) = a(t_e) + \dot{a}(t_e)(t_o - t_e) + ... \tag{1.3}$$

parameter) in Friedmann's equations at the time of observation. The measurement of the H_0 is thus a measurement of the expansion of the Universe.

Pillar II: The cosmological principle:

The second pillar of Cosmology is the *cosmological principle* which states **isotropy** (invariance in rotation) and **homogeneity** (invariance in translation) of the Universe on large scales (larger than 100-200 Mpc). This leads to the absence of a privileged position or direction in the cosmos. To better understand the difference between homogeneity and isotropy, we illustrate in Figure 1.7 two cases: a case of isotropy without homogeneity and a case of homogeneity without isotropy.

The application of the cosmological principle significantly limits the great variety of possible cosmological models. The cosmological principle is an assumption, since it has not been proved. On large scales however isotropy has been confirmed by many factors, such as:

- the distribution of clusters and superclusters of galaxies
- the distribution of radiosources
- the uniformity of the background radiation — particularly the Cosmic Microwave Background radiation (CMB) which describes a strongly isotropic Universe at the time of the emission of the radiation, or the background X-radiation between 2 and 20 keV produced by unresolved sources up to distances of thousands of Mpc.

Although isotropy is not proved, by increasing the number of samples of cosmological objects, isotropy rises. According to the Copernican principle, there is no reason to consider our position privileged, hence there must be isotropy in each point of the Universe. This strongly implies homogeneity.

considering equation 1.25 and multiplying on both sides by c, we obtain:

$$cz = \frac{\dot{a}(t_e)}{a(t_e)} c(t_o - t_e) + ... \tag{1.4}$$

where it is possible to identify the Hubble law, with $c(t_o - t_e)$ being the distance and $\frac{\dot{a}(t_e)}{a(t_e)}$ the Hubble parameter.

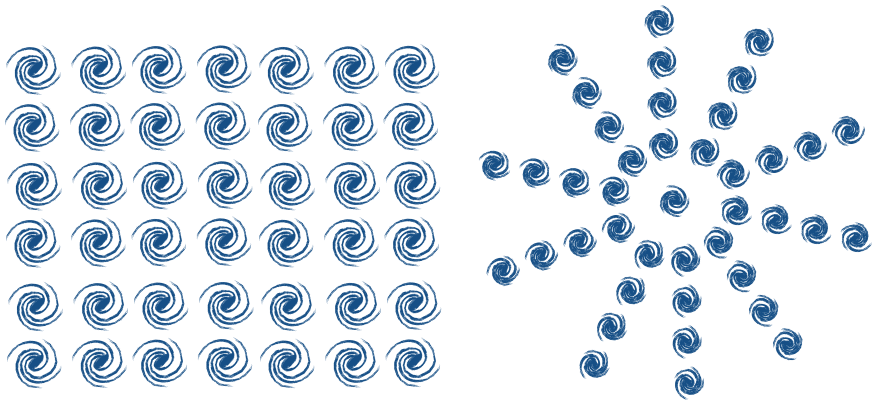

Figure 1.7: *Left:* illustration of **homogeneity without isotropy**, the image is invariant under translation, but would variate under rotation (the vertical and horizontal directions are preferred; if rotated of a certain angle, the two preferred directions would change, thus the image would change under rotation). *Right:* **isotropy without homogeneity** (translating the image would change it, but the image is invariant under rotation).

Since the Universe is expanding, it has reached the present low-density state from an initial hot and dense state, in a homogeneous and isotropic way. The model that predicts an initial hot and dense state is the Big Bang model.

The homogeneity and isotropy of the Universe at large scales is a fundamental assumption to work with cosmic voids, as explained in the next Chapter.

Pillar III: The Friedmann-Lemaitre-Robertson-Walker Metric

In the years between 1920 and 1930, four scientists worked independently on the model of an expanding Universe. Alexandre Friedmann was the first to look for exact solutions of the theory of General Relativity and published in 1922 a theory of expansion. Independently, in 1927, Georges Lemaître (as discussed in the previous section) wrote a paper establishing the expansion of the Universe. Furthermore, Howard Percy Robertson and Arthur Geoffrey Walker autonomously developed a metric able to describe a homogeneous and isotropic Universe. Assuming the cosmological principle, it is thus possible to define the Friedmann-Lemaître-Robertson-Walker model for the expansion of the Universe. This model studies the Universe as a whole to understand its

evolution thanks to the assumption of homogeneity and isotropy that greatly simplifies the study.

To describe the Universe, we set a system of coordinates in space-time: three space coordinates (x^α where $\alpha = 1, 2, 3$) and a temporal coordinate (t) which indicates the time, measured by an observer that is moving with the point. Generally, the geometrical properties of the coordinate system are determined by the *metric tensor* $g_{\mu\nu}$. This approach allows to include the effects of gravity in the metric, which means that the motion of particles will be simply described as a motion in a distorted space-time. The interval ds between two events in space-time is defined by the most general expression:

$$ds^2 = \sum_{\mu,\nu} g_{\mu\nu} dx^\mu dx^\nu \tag{1.5}$$

μ and ν have values from 0 to 3, where indices 1, 2 and 3 represent spatial coordinates and 0 is referred to the time-coordinate. When assuming the cosmological principle, the metric $g_{\mu\nu}$ will take a simple form. To reach this form, the coordinate system is chosen so that the space-time slices are homogeneous and isotropic at fixed t. This is equivalent to impose $g_{0i} = 0$, such that the slicing in time is orthogonal to the spatial part. The spatial grid is comoving[7], so that an observer moving with it measures zero velocity for the cosmic fluid (Lyth and Liddle, 2009): this guarantees isotropy also in an expanding Universe. Furthermore, we define

- The parameter t, called *proper cosmological time* (or *cosmic time*), is the time measured by an observer who sees the Universe evolving in a uniform expansion around him. To impose homogeneity, we set the proper[8] time interval between slices as position independent, thus we impose $g_{00} = -1$.

[7]The comoving distance is the distance between two points measured with a grid that expands. If the Universe is expanding the physical distance between points will increase, but the comoving distance is defined as remaining constant. More details can be found in Section 1.2.3.

[8]Here the adjective proper defines the time measured by an observer that is at rest compared to the clock.

- The *scale factor a(t)*, which takes into account distances stretching over time, is normalized to $a(H_0^{-1}) = 1$ at the present time. The scale factor is extremely important in Cosmology, since it represents the relation between the physical distance and the comoving distance between objects. It is thus proportional to the distance between points and, if inserted into the metric for the spatial coordinates, it allows to preserve homogeneity and isotropy during expansion. With the addition of this factor in the metric, the cosmological principle is preserved on a surface of constant t, but it is no longer a static Universe. We note that the scale factor can be related to redshift in an intuitive way: from 1.1, we can obtain:

  $$z + 1 = \frac{\lambda_o}{\lambda_e}$$

  The expansion of the Universe can be thought as a proportional relation between the observed and the emitted wavelengths, where the scale factor is the proportionality coefficient :

  $$\lambda_e = a(t_e)\lambda_o$$

  This is just a first intuitive description, a more complete derivation will be given in Section 1.2.3.

Taking into account all the above considerations, if the Universe is flat, the metric would be:

$$g_{\mu\nu} = \begin{pmatrix} -1 & 0 & 0 & 0 \\ 0 & a^2(t) & 0 & 0 \\ 0 & 0 & a^2(t) & 0 \\ 0 & 0 & 0 & a^2(t) \end{pmatrix}$$

This is the *Friedmann-Lemaître-Robertson-Walker metric*. We made the assumption of a flat Universe. If you want to consider curvature, the interval *ds* can be written as:

$$ds^2 = -c^2dt^2 + a^2(t)\left[dr^2 + S_k^2(r)d\Omega^2\right] \tag{1.6}$$

where the value of function S_k depends on the curvature of the Universe. The spatial part of the metric is the spatial metric for a Universe with uniform and constant curvature k of radius R_0. The *curvature constant* k is dimensionless and can take the values: -1 (a Universe with constant negative curvature), 0 (a Universe that is spatially flat) and $+1$ (a Universe with constant positive curvature).

Depending on the values of the constant k, the function $S_k(r)$ can take different values: $R\sinh(r/R)$ if $k = -1$, r if $k = 0$ and $R\sin(r/R)$ if $k = +1$. In this way three different metrics can be obtained for a Universe in isotropic expansion or contraction:

- $k = -1 \longrightarrow$ The Universe is negatively curved and the metric is $ds^2 = -c^2dt^2 + a^2(t)\left[dr^2 + R^2\sinh^2(r/R)d\Omega^2\right]$
- $k = 0 \longrightarrow$ The Universe is spatially flat and the metric is $ds^2 = -c^2dt^2 + a^2(t)\left[dr^2 + r^2d\Omega^2\right]$
- $k = +1 \longrightarrow$ The spatial curvature is positive and the metric is $ds^2 = -c^2dt^2 + a^2(t)\left[dr^2 + R^2\sin^2(r/R)d\Omega^2\right]$

  Another form[9] of the Friedmann-Lemaître-Robertson-Walker metric is:

$$ds^2 = -c^2dt^2 + a^2(t)\left[\frac{dx^2}{1 - \frac{kx^2}{R_0^2}} + x^2d\Omega^2\right] \tag{1.7}$$

  where we have switched from radial coordinate r to $x = S_k(r)$ (Ryden, 2003).

The Friedmann-Lemaître-Robertson-Walker model describes the expansion of the Universe under the hypothesis of the cosmological principle (namely isotropy and homogeneity). To correctly describe the Universe under the approximation of the cosmological principle, the metric must be a solution of Einstein's equation of General Relativity. The metric can indeed be related

[9]The difference between the two formulas is that when r is the radial coordinate, the radial distances would be Euclidean, while angular distance are not. When x is the radial coordinate we have the contrary, so here we are only making a coordinate's change.

to the energy and matter content of the Universe. This is the subject of the next section.

1.2.2 Friedmann equations

In order to explain the dynamic of the Universe, it is necessary to determine the evolution of the scale factor. This can be done by establishing the relationship between the description of the metric of an homogeneous and isotropic space and the mass-energy contained in the Universe. This relationship is given by Einstein's field equations which describe the dynamics of the Universe by determining the evolution of the scale factor $a(t)$. If $G_{\mu\nu}$ is the Einstein tensor, T^{μ}_{ν} the stress-energy tensor (also called energy-momentum tensor), $R_{\mu\nu}$ the Ricci curvature tensor and R, the scalar curvature, defined by $R = g^{\mu\nu}R_{\mu\nu}$, then **Einstein's equations** can be written:

$$G_{\mu\nu} \equiv R_{\mu\nu} - \frac{1}{2}Rg_{\mu\nu} = 8\pi G T_{\mu\nu} \tag{1.8}$$

This set of ten equations describes the fundamental interaction of gravity as a result of space-time being curved by matter and energy. It gives the relationship between space-time geometry (represented by the metric and the Ricci tensor and scalar) and the energy and pressure at a point in space-time (related to the stress-energy tensor). Einstein's equations will eventually require the calculation of the tensor components of the equation. First we consider the left side of 1.8. The Ricci tensor $R_{\mu\nu}$ can be expressed through the *Christoffel symbols* Γ^{i}_{jk} (Dodelson, 2003) in the following way:

$$R_{\mu\nu} = \Gamma^{\alpha}_{\mu\nu,\alpha} - \Gamma^{\alpha}_{\mu\alpha,\nu} + \Gamma^{\alpha}_{\beta\alpha}\Gamma^{\beta}_{\mu\nu} - \Gamma^{\alpha}_{\beta\nu}\Gamma^{\beta}_{\mu\alpha} \tag{1.9}$$

where the commas indicate the derivatives with respect to the coordinate. The Christoffel symbols are linked to the metric $g_{\mu\nu}$ by the relationship:

$$\Gamma^{\mu}_{\alpha\beta} = \frac{g_{\mu\nu}}{2}\left[\frac{\partial g_{\alpha\nu}}{\partial x^{\beta}} + \frac{\partial_{\beta\nu}}{\partial x_{\alpha}} - \frac{\partial g_{\alpha\beta}}{\partial x^{\nu}}\right]$$

Using the expression of the metric given by equation 1.6 in the above

expression of $\Gamma^{\mu}_{\alpha\beta}$, we obtain the Christoffel symbols and, consequently, the Ricci tensor and Ricci scalar. This allows the calculation of the Einstein tensor, which can then be written:

$$G_{00} = 3\left(\frac{\dot{a}}{a}\right)^2 + \frac{3k}{a^2} \tag{1.10}$$

$$G_{11} = G_{22} = G_{33} = -2\frac{\ddot{a}}{a} - \left(\frac{\dot{a}}{a}\right)^2 - \frac{k}{a^2} \tag{1.11}$$

$$G_{others} = 0 \tag{1.12}$$

The stress-energy tensor in the right-hand side of equation 1.8 is extremely difficult to manage, indeed its form can be very complicated, especially in the case of inhomogeneity in the spatial energy distribution. A significant simplification can be obtained assuming a homogeneous Universe. In fact, in Cosmology, since many of the components of the Universe can be approximately described as perfect fluids, the stress-energy tensor to be considered is the one representing a perfect fluid — a fluid that is isotropic, with negligible viscosity and heat conduction. Considering this particular case, T^{μ}_{ν} can be written in the following way:

$$T^{\mu}_{\nu} = (\rho + P)U_{\mu}U_{\nu} + Pg_{\mu\nu}$$

where ρ is the energy density of the fluid, P its pressure and U_{μ} its four-velocity, with the normalization $U_{\mu}U_{\nu}$=1. According to Robertson-Walker's metric, the pressure P must be isotropic. Hence it can be written (with P and ρ only depending on time):

$$T^{\mu}_{\nu} = \begin{pmatrix} -\rho & 0 & 0 & 0 \\ 0 & P & 0 & 0 \\ 0 & 0 & P & 0 \\ 0 & 0 & 0 & P \end{pmatrix}$$

Combining this expression of the stress-energy tensor with the Robertson-Walker metric 1.6 we can obtain **Friedmann's equation** (Friedmann, 1922;

Ryden, 2003):

$$H^2 = \left(\frac{\dot{a}}{a}\right)^2 = \frac{8\pi G}{3c^2}\sum_i \rho_i - \frac{kc^2}{R_0^2 a^2} \tag{1.13}$$

where R_0 is the radius of curvature of the Universe and the summation is extended to all kinds of energy present in the Universe (which are weighted in different ways by the evolution of the scale factor with time). We have used $H = (\dot{a}/a)$, anticipating a result that will be shown in Section 1.2.3.

This equation is valid for any Universe which follows the Friedmann-Lemaître-Robertson-Walker metric and whose expansion or contraction is ruled by General Relativity. In fact a Universe that follows Friedmann's equation is an isotropic and homogeneous solution of Einstein's equations.

In a flat Universe (k=0), Friedmann's equation becomes a very simple expression. For any given value of the Hubble parameter, we can define the *critical energy density* as:

$$\rho_c = \frac{3H^2c^2}{8\pi G} \tag{1.14}$$

If the energy density is greater than ρ_c, the Universe is positively curved ($k = +1$). If the energy density is smaller than ρ_c, the Universe has a negative curvature ($k = -1$). We can then introduce the *density parameter* as the ratio of the total energy density and the critical energy density:

$$\Omega_{tot}(t) = \frac{\sum_i \rho_i}{\rho_c} \tag{1.15}$$

The density parameter binds the total energy density to the geometry of the Universe:

$$\Omega_{tot} \begin{cases} > 1 \longrightarrow k = +1 \\ = 1 \longrightarrow k = 0 \\ < 1 \longrightarrow k = -1 \end{cases}$$

Friedmann's equation can then be written:

$$1 - \Omega_{tot}(t) = -\frac{kc^2}{R_0^2 (a(t))^2 (H(t))^2}.$$

We can define the curvature component:

$$\Omega_k(t) = -\frac{kc^2}{R_0^2(a(t))^2(H(t))^2} \tag{1.16}$$

Considering the present time, we have

$$\Omega_{k0} = 1 - \Omega_0 = -\frac{kc^2}{R_0^2 H_0^2},$$

where it can be seen that the curvature of the Universe depends on the total energy density.

Knowing Ω_0, the sign of the curvature k can be found.

Friedmann's equation has got two variables: a and ρ. Another relationship is therefore needed that includes both of them as functions of time. The principle of energy conservation will allow us to find this relationship. It is expressed by the first law of thermodynamics:

$$dQ = dE + PdV$$

We consider a sphere of comoving radius r_s which expands as a result of the expansion of the Universe. If the Universe is perfectly homogeneous, for each comoving volume filled with any fluid, the expansion will be adiabatic. This means that the net heat flux dQ will be zero. The first law of thermodynamics can be applied to any fluid contained in a comoving volume; because of the cosmological principle, for each volume dV, dQ should be zero. The first law of thermodynamics can then be written: $\dot{E} + P\dot{V} = 0$. But we also have: $E(t) = V(t)\rho(t)$, hence we obtain the *flux equation*

$$\dot{\rho} + 3\frac{\dot{a}}{a}(\rho + P) = 0 \tag{1.17}$$

Combining this equation with Friedmann's equation we can derive the **acceleration equation** (Ryden, 2003) which gives the variation of acceleration with time:

$$\frac{\ddot{a}}{a} = -\frac{4\pi G}{3c^2}\sum_i(\rho_i + 3P_i) \tag{1.18}$$

For positive pressure, if the energy density is greater than zero this equation gives a negative acceleration, which means that the relative speed of two points decreases. If we consider as an additional variable P (the pressure of the matter that fills the Universe), we end up with three equations with three unknowns. However, these three equations are not independent, since the acceleration equation is obtained from Friedmann's equation.

We shall therefore introduce an equation of state to combine the pressure and the energy density of the matter that fills the Universe. Since the Universe is very diluted, it can be described as a perfect fluid. Under this assumption, the pressure and the energy density are bound through the *equation of state parameter* ω, which varies depending on the component being considered.

The relationship is: $P = \omega\rho$. Considering the relation for each component is a way of describing how the content of the Universe affects its evolution. This will be briefly reviewed in Section 1.3.1.

1.2.3 Distances

In the last Section I introduced the standard cosmological model and its three pillars: the redshift-velocity relation, the cosmological principle and the Friedmann-Lemaître-Roberston-Walker metric. Finally I described Friedmann's equations.

Another important point in Cosmology is the definition of distances. In the measurement of distances, there is a practical and conceptual issue: how can we define the distance between two points in an expanding Universe? The truth is that many different kinds of distances can be defined.

I will review the definitions and physical meanings of the following distances: comoving distance (line of sight and comoving), proper distance, Hubble distance, angular diameter distance and luminosity distance (an useful reference is Hogg (1999)).

Line of sight comoving distance

The Universe is expanding, distances between objects are affected by the expansion. It is then useful to consider a measure of distance that remains

unaffected by the expansion: the *comoving distance*. As anticipated in Section 1.2.1, one can consider a grid that expands with the Universe. If we define points in such comoving grid, we are using a comoving coordinate system. The distance defined in this system is the comoving distance.

The comoving distance to an object at redshift $z = a(t)^{-1} - 1$ is:

$$\chi(a) = \int_{t(a)}^{t_0} \frac{cdt'}{a(t')} \tag{1.19}$$

This distance is between us and another object (as given by the formula), or between objects at different redshift (and thus at a different time).

Transverse comoving distance

On the contrary, the transverse comoving distance is between objects at the same z. It is equivalent to the proper motion distance (Hogg, 1999) d_M (which is given by the ratio of the actual transverse velocity to its proper motion, in radians per unit time (Weinberg, 1972)). If the Universe is flat, the transverse comoving distance is equal to the line of sight comoving distance[10] χ.

Proper distance

I now consider the proper distance. In an expanding Universe, the distance between two points increases with time. I thus define the *proper distance* $d_p(t)$ as the length of the spatial geodesic[11] between two points at a fixed value of the scale factor, that is at constant cosmic time.

This distance thus changes over time due to the expansion of the Universe. More precisely, as defined by (Davis and Lineweaver, 2004), at a particular time t it is the distance that we can measure along the line of sight using a series of infinitesimal comoving rulers. An observer is placed near each ruler

[10] This explains why sometimes we only generally refer to the comoving distance without further specification.

[11] In fact, light travels along geodesics. These are curves with geodesic curvature equal to zero, where the geodesic curvature is a property of curves which reflects the deviance of the curve from following the shortest arc length distance along each infinitesimal segment of its length. In simplest terms, a geodesic is a curve that *locally* describes the shortest trajectory between points in a particular space. In the case of photons it must be $ds = 0$.

and measures its distance to the nearest observer; the proper distance is the sum of all distances. One would thus need synchronized comoving observers to measure proper distance.

To give a simplified expression of $d_p(t)$, we consider a fixed time ($dt = 0$); from equation 1.6, since the angles are constant over the spatial geodetic ($d\Omega$=0), we obtain $ds = a(t)dr$ (considering a flat Universe). The proper distance can be obtained integrating over the comoving radial coordinate r:

$$d_p(t) = a(t) \int_0^r dr = a(t)r \tag{1.20}$$

However the proper distance can also be defined in a different way. Considering Friedmann's equation in the case of a Universe composed of matter, radiation and a cosmological constant, we have:

$$\frac{H^2}{H_0^2} = \frac{\Omega_{r,0}}{a^4} + \frac{\Omega_{m,0}}{a^3} + \Omega_{\Lambda,0} + \frac{1 - \Omega_0}{a^2}$$

By considering the definition of the Hubble parameter $H = \dot{a}(t)/a$ and integrating, it is possible to obtain (Ryden, 2003):

$$d_p(t_o) = \frac{c}{H_0} \int_{a(t_e)}^1 \frac{da}{a(t')^2(\Omega_{r,0}a^{-4} + \Omega_{m,0}a^{-3} + \Omega_{\Lambda,0} + \Omega_{k,0}a^{-2})^{1/2}} \tag{1.21}$$

This distance is defined at a particular moment of time and, as the Universe is expanding, it is not measurable.

The definition of proper distance allows us to obtain a relationship between the scale factor and Hubble's parameter. Using the proper distance we can reformulate the redshift-distance relation:

$$v_p(t) = \dot{d}_p(t) = \dot{a}(t)r = \frac{\dot{a}(t)}{a(t)} d_p(t) = H(t)d_p(t)$$

which gives the relationship between the scale factor and Hubble's parameter:

$$H = \frac{1}{a}\frac{da}{dt} = \frac{\dot{a}}{a} \tag{1.22}$$

This definition is extremely important in Cosmology, this is the reason why we formulate it here. If we evaluate it now, it gives us H_0, the Hubble's constant.

Hubble distance

We define the *Hubble distance*:

$$d_H(t_0) = \frac{c}{H_0} \tag{1.23}$$

as the critical distance such that two points at a distance greater than $d_H(t_0)$ will have $v_p > c$.

The Hubble distance is not a distance that can be defined between any two objects, since it is the distance between us and the objects with super-luminar speed. There is some confusion related to these objects in an expanding Universe (Davis and Lineweaver, 2004): the super-luminous speed of objects refers to their relative motion inside an expanding Universe and therefore does not violate the law limiting the speed of massive objects at the speed of light. The redshift-distance relation thus gives super-luminar speed for objects. This is perfectly allowed in the framework of General Relativity, since faster than light motion occurs outside the observer's inertial frame. Galaxies receding from us super-luminally are at rest with respect to the cosmological frame (Davis and Lineweaver, 2004).

With H_0 obtained from the Planck mission (Planck Collaboration, 2013), and using the approximate redshift-distance relation, we have $d_H(t_0) = 4455$ Mpc. Galaxies farther than this distance are moving away from us at super-luminar speeds, along with the photons they emit.

We use the given definitions to find the relationship between the redshift z of a distant object and the scale factor at the moment of the emission of the light, $a(t_e)$. In the case of a distant galaxy, the light emitted at time t_e is observed at time t_o. During its path the light travels along a null geodesic, with $ds = 0$ and with constant angles θ and φ. Hence, along the null geodesic, we have: $c^2dt^2 = a(t)^2dr^2$ and so $ca^{-1}(t)dt = dr$. Integrating between t_e and

t_o and considering only one wavelength λ_e, we have

$$c\int_{t_e}^{t_o}\frac{dt}{a(t)} = \int_0^r dr = r$$

The forthcoming wavelength, emitted at the time $t_e + \frac{\lambda_e}{c}$, will be observed at time $t_o + \frac{\lambda_o}{c}$ and will get us to a similar integral with the same second term r, therefore:

$$\int_{t_e}^{t_o}\frac{dt}{a(t)} = \int_{t_e+\frac{\lambda_e}{c}}^{t_o+\frac{\lambda_o}{c}}\frac{dt}{a(t)}$$

Subtracting the integral between $t_e + \frac{\lambda_e}{c}$ and t_o from each side of this latter equation, we have:

$$\int_{t_e}^{t_o}\frac{dt}{a(t)} - \int_{t_e+\frac{\lambda_e}{c}}^{t_o}\frac{dt}{a(t)} = \int_{t_e+\frac{\lambda_e}{c}}^{t_o+\frac{\lambda_o}{c}}\frac{dt}{a(t)} - \int_{t_e+\frac{\lambda_e}{c}}^{t_o}\frac{dt}{a(t)}$$

$$\int_{t_e}^{t_e+\frac{\lambda_e}{c}}\frac{dt}{a(t)} = \int_{t_o}^{t_o+\frac{\lambda_o}{c}}\frac{dt}{a(t)}$$

We can compare the time between the emission and observation for the two wave crests with the age of the Universe. We obtain a rough approximation of the age of the Universe t_0 using Hubble's law:

$$t_0 = \frac{r}{v} = \frac{r}{rH_0} = H_0^{-1} \simeq (14.0 \pm 1.4)Gyrs$$

Since $t_0 >> \lambda/c$, we can assume that between two wave crests (regardless of whether we are considering emission or observation) the Universe has not expanded by a significant amount. Hence we can say that *a(t)* has remained constant during that time. Thus the integrals give:

$$\frac{\lambda_e}{a(t_e)} = \frac{\lambda_o}{a(t_o)} \tag{1.24}$$

and finally, since the redshift is defined as

$$z = \frac{\lambda_o - \lambda_e}{\lambda_e}$$

we obtain:

$$1 + z = \frac{a(t_o)}{a(t_e)} = \frac{1}{a(t_e)} \tag{1.25}$$

where the equation has been normalized with $a(t_o) = a_o = 1$. This equation gives the relationship between the redshift z of a distant object and the scale factor at the moment of the emission of the light $a(t_e)$. It shows that the redshift for a distant object depends only on the ratio of the scale factors at the times of emission and observation and not on the way in which the light passed between $a(t_e)$ and $a(t_o)$.

The distances we have introduced so far are distances that we cannot measure easily. A more directly measurable distance will be presented in the next section.

Angular diameter distance

A direct way to measure distances in Astronomy is through the angle[12] subtended by an object of known physical lenght l (Dodelson, 2003), assuming for simplicity that this object is disposed perpendicularly to the view line. We obtain the *angular diameter distance*:

$$d_A \equiv \frac{l_\perp}{\delta\theta} \tag{1.26}$$

The object size $l_\perp$ and its proper diameter r are related through $l_\perp = a(t_e) r \delta\theta$ (this can be shown using FLRW at a fixed time, in a flat Universe, considering the distance ds between the two sides of the object). Therefore, $\delta\theta = l_\perp / (a(t_e) r)$ (Peebles, 1993; Weinberg, 1972).

Thus, substituting $\delta\theta$ in 1.26, the angular diameter distance can be written as:

$$d_A = \frac{l_\perp a(t_e) r}{l_\perp} = a(t_e) r = \frac{a(t_0)}{1+z} r = \frac{r}{1+z} = \frac{D_M}{1+z} \tag{1.27}$$

where D_M is the transverse comoving distance, equal to the line-of-sight comoving distance χ if the Universe is flat. The generalisation for a non-flat

[12] Assuming a small angle.

Universe gives:

$$d_A = \frac{S_k(r)}{1+z}$$

The angular diameter distance has a maximum for a precise value of z, denoted by z_{max}. In a model with $\Omega_{m,0} = 0.3$ and $\Omega_{\Lambda,0} = 0.7$, z_{max} becomes 1.6, which corresponds to the angular distance $d_{A,max} = 1800$ Mpc. This is intuitively strange, because objects at redshift higher than z_{max} will appear to have smaller d_A, they will have a large angular size. We can explain this considering that when the light of the object was emitted, the Universe was much smaller (since it was in the past and the Universe is expanding), the object thus occupied a larger fraction of the Universe's size.

We will discuss this more extensively in Section 2.1. Before concluding the description of the angular diameter distance, we point out that some confusion might arise for the definitions used of the angular distance: some references call d_A the angular diameter distance, while others use the same symbol for the *comoving* angular diameter distance d_{Acom} (such as Weinberg et al. (2012)). To avoid confusion, we use different symbols and note that:

$$d_{Acom} = a d_A = \frac{d_A}{1+z} \tag{1.28}$$

The luminosity distance

Another intuitive way to measure distance is through the use of luminosity. If we have an object of known luminosity, it is possible to establish at which distance it is by the fading of its brightness. Measuring the energy flux f received on Earth and knowing the intrinsic luminosity of the object we can define a function called *luminosity distance*:

$$d_L = \left(\frac{L}{4\pi f}\right)^{1/2} \tag{1.29}$$

This function would correspond to the proper distance if the Universe were static and Euclidean. In reality, the expansion of the Universe results in a diminution of the photon energy flux by a factor $(1+z)^{-2}$. Let us consider the case of a photon emitted with energy $E_e = hc/\lambda_e$ when the scale factor

is $a(t_e)$. This photon would be observed now, when $a(t) = a(t_o) = 1$. Then, because of wavelength stretching, $E_0 = E_e/(1+z)$.

Moreover we can consider the case of two photons emitted in the same direction and separated by a temporal gap δt_e. At the beginning, their proper distance is $c\delta t_e$ and at time t_o, it will be $c\delta t_e(1+z)$. This means that the time interval between the emission of the two photons increases, as is shown by the equation:

$$\delta t_o = \delta t_e(1+z)$$

Therefore the frequency of the detection decreases.

Finally, in an expanding Universe governed by the Friedmann-Lemaître-Robertson-Walker model, the relationship between flux and luminosity is:

$$f = \frac{L}{4\pi S_k(r)^2(1+z)^2}$$

Hence the luminosity distance is $d_L = S_k(r)(1+z)$. The luminosity distance of an object with redshift z depends both on the geometry of the Universe and on its dynamics.

The latest observational data[13] seem to indicate a flat geometry for our Universe. We recall that the function $S_k(r)$ takes the following values:

$$S_k(r) \begin{cases} \sin(r) \Longleftrightarrow k = +1 \\ r \Longleftrightarrow k = 0 \\ \sinh(r) \Longleftrightarrow k = -1 \end{cases}$$

Since $k = 0$, the luminosity distance can then be written (Ryden, 2003):

$$d_L = r(1+z) = d_p(t_0)(1+z) \tag{1.30}$$

In a non-flat Universe, we have:

$$d_L = S_k(r)(1+z) = d_p(t_0)(1+z) \tag{1.31}$$

[13]BOOMERANG (de Bernardis et al., 2000) and the Planck satellite (Planck Collaboration et al., 2013)

Moreover, when $z << 1$, we have:

$$d_L \simeq \frac{c}{H_0} z \left(1 + \frac{1 - q_0}{2} z\right) \tag{1.32}$$

where we have used the *deceleration parameter*[14](Peacock, 1999).

Comparing distances

Using the definitions of d_L and d_A (equations 1.30 and 1.27 respectively), we obtain the following relation (Weinberg, 1972)[15]

$$d_L = (1 + z)^2 d_A$$

In the case of a flat Universe and assuming $z \longrightarrow 0$ (i. e. at low redshift), the following relations between distances can be established. As a start, the luminosity distance is a good approximation of the proper distance at the present time. Indeed, $d_p(t_0) \simeq d_L \simeq (c/H_0)z$.

Moreover, as $k = 0$, $d_A(1 + z) = d_L/(1 + z) = d_p(t_o)$, then

$$d_A = \frac{d_p(t_o)}{1 + z} = d_p(t_e)$$

Furthermore, if $z << 1$, the angular diameter distance can be approximated

[14]The deceleration parameter is defined as

$$q_0 = -\left(\frac{\ddot{a}}{\dot{a}^2}\right)_{t=t_0} = -\left(\frac{\ddot{a}}{aH^2}\right)_{t=t_0}$$

The deceleration parameter is adimensional and its value is negative if the expansion of the Universe is accelerating. It will be positive if the expansion is decelerating. It was called the "deceleration parameter" because it was introduced at a time when the Universe was believed to be dominated by matter and therefore undergoing a decelerated expansion. The deceleration parameter allows to approximate the scale factor:

$$a(t) \simeq a(t_0) + \left.\frac{da}{dt}\right|_{t=t_0} (t - t_0) + \frac{1}{2}\left.\frac{d^2a}{dt^2}\right|_{t=t_0} (t - t_0)^2 = 1 + H_0(t - t_0) - \frac{1}{2} q_0 H_0^2 (t - t_0)^2 \tag{1.33}$$

[15]Note that this relation, written in terms of the comoving angular diameter distance, becomes $d_L = (1 + z)(1 + z)d_A = (1 + z)d_{Acom}$.

using the deceleration parameter:

$$d_A \simeq \frac{c}{H_0} z(1 - \frac{3 + q_0}{2} z)$$

Thus as $z \longrightarrow 0$ we have:

$$d_A \simeq d_L \simeq d_p(t_0) \simeq \frac{c}{H_0} z \tag{1.34}$$

This can be understood thinking that at small distances the Universe seems Euclidean, even though the space-time is curved. Having introduced the basis of Cosmology and its history, we now describe the most recent model of Cosmology.

1.3 Recent developments in Cosmology

The Cosmological Constant

In 1917, two years after the publication in Annalen Der Physik of the article on General Relativity, Einstein considered applying his equations to the Universe as a whole. Since he had no experimental evidence about the expansion of the Universe and was unaware of the existence of the cosmic background radiation, Einstein was persuaded that the Universe was static. He imagined that much of the radiation in the Universe was provided by stars and that the main contribution to the energy density of the Universe came from non-relativistic matter. He therefore considered the approximation of a Universe without pressure (that is, more precisely, with positive energy density and negligible pressure).

However, he realised that a Universe that contained nothing but matter could not be static, so he inserted a factor Λ in his equations, which he called the *cosmological constant*, so that the equations would describe a static Universe filled with matter that was in accordance with his particular beliefs.

With the introduction of Λ, the Friedmann equation becomes:

$$\left(\frac{\dot{a}}{a}\right)^2 = \frac{8\pi G}{3c^2}\rho - \frac{kc^2}{R_0^2 a^2} + \frac{\Lambda}{3}$$

the fluid equation does not change and the acceleration equation becomes:

$$\frac{\ddot{a}}{a} = -\frac{4\pi G}{3c^2}(\rho + 3P) + \frac{\Lambda}{3}$$

It must be noted that adding Λ to the Friedmann equation is equivalent to adding to the Universe a component with negative pressure:

$$P_\Lambda = -\rho_\Lambda = -\frac{c^2}{8\pi G}\Lambda$$

In order to have a static Universe, both $\dot{a}$ and $\ddot{a}$ must be zero. Such solutions exist for a closed Universe, $k = 1$, and positive cosmological constant. Even then, the resulting model proposed by Einstein was unstable because the attractive force of ρ was in unstable equilibrium with the repulsive force of Λ. When the expansion of the Universe was discovered, Einstein, faced with experimental evidence, abandoned both the idea of a cosmological constant and his belief in a static Universe, calling the introduction of Λ his "biggest blunder". After having been reconsidered many other times, when the current value for H_0 was too small compared to the age of observed objects, the cosmological constant has finally been reintroduced on the basis of observational data that indicate that the expansion of the Universe is, indeed, accelerating.

2011: a Cosmology Nobel Prize

The observational data that led to reconsidering the cosmological constant[16] were obtained from a phenomenon exhibited by stars with very particular properties that can be used for the establishment of their distance, Type Ia supernovae (explosions of stars in binary systems that can be used as markers of the cosmic expansion). More details are given in Section 2.1.

[16]The case for observations favouring a cosmological model with large cosmological constant was discussed by Ostriker and Steinhardt (1995).

Recently, two research groups, the *Supernova Cosmology Project* (Perlmutter et al., 1999) and the *High-z Supernova Search Team* (Riess et al., 1998), have worked on type Ia supernovae in distant galaxies. With the aim of measuring the cosmological parameters (the Hubble constant and the deceleration parameter) the two groups have measured the redshifts and the light profiles of many Ia supernovae, obtaining results that are mutually coherent.

Both research groups have discovered that the absolute luminosity of these objects is smaller than it should be for a Universe only dominated by matter. The results are therefore consistent with a Universe dominated by the cosmological constant, in accelerated expansion. The responsible of the two projects, Saul Perlmutter, Brian Schmidt and Adam Reiss have been awarded in 2011 the Nobel Prize *"for the discovery of the accelerating expansion of the Universe through observations of distant supernovae"*.

Dark energy

The observation of luminosity distances to Type Ia supernovae larger than that expected for a Universe containing only matter results in an acceleration of the scale factor, which can be interpreted as evidence for a cosmological constant term in the Einstein equation. A hypothesized physical source of this contribution is labelled *dark energy*, though the detailed physics of this component remains a mystery and nowadays the terms is used for any model that explains the observed acceleration, up to and including models that modify Einstein's gravity itself.

In the standard model of Cosmology, dark energy accounts for 68% (Planck Collaboration, 2013) of the total mass-energy of the Universe. The cosmological constant is one of the proposed forms for dark energy and it is physically equivalent to vacuum energy (other forms include, for instance, quintessence, which is a dynamic quantity whose energy density can vary in time and space).

This leads to the mainstream cosmological model, called ΛCDM, that assumes homogeneity, isotropy and includes the existence of dark energy described by a cosmological constant.

1.3.1 Our Universe

Components

The study of the Universe is then based on this model defined by a set of cosmological parameters that describe the components of the Universe. In order to understand the structure and evolution of cosmos it is necessary to obtain constraints on these parameters from observational data. We have seen that the Universe contains many components.

The main components are photons, baryons, dark matter, neutrinos and dark energy. As they appear in the Friedmann equation and influence the cosmological evolution of our Universe, it is necessary to know the pressure and density of these components. Thus, for each component, we need to know the state equation and the evolution of its energy density with the scale factor.

We consider two kinds of matter: ordinary matter which can be observed directly and is (improperly[17]) called *baryonic matter*, and *dark matter*, whose existence can only be measured by its gravitational effect on baryonic matter, but whose nature is still unknown.

The existence of dark matter was first hypothesized in 1933 by the Swiss astrophysicist Fritz Zwicky, to account for evidence of "missing mass" in the orbital velocities of galaxies in galactic clusters. Studying the characteristics of the Coma cluster, Zwicky estimated the mass of the orbiting galaxies from their luminosity and compared it with the mass estimated from the measurement of the dispersion velocity of the galaxies. The estimate using velocity gave a mass ≈ 400 times greater than the mass obtained from the luminosity of the Coma cluster (Zwicky, 1933).

The gravity of the visible galaxies in the cluster would be far too small for such fast orbits, so extra mass was required. Based on these conclusions, Zwicky inferred that there must be some non-visible form of matter which would provide enough mass and gravity to hold the cluster together. This

[17] In Cosmology with the term "baryonic matter" we refer to the matter we usually know, i.e. protons, neutrons and electrons (the latter in fact are not baryons but leptons, and this is why the term is improper) as opposed to dark matter particles. The reason of this improper expression is that nuclei are so much more massive than electrons that virtually all the mass is in the baryons.

missing matter is the *dark matter*.

The comparison of the speed curve in spiral galaxies against the distance from the centre is another approach that has given irrefutable evidence of the existence of dark matter, thereby corroborating Zwicky's measurements. In 1954, in her doctoral thesis, Vera Rubin presented data regarding the orbits of stars in spiral galaxies. Her conclusions were largely ignored. In the late 1960s and early 1970s, she announced the astonishing discovery that most stars in spiral galaxies orbit at roughly the same speed. Her earlier conclusions were finally recognised.

Dark matter can also be revealed through its gravitational effect on other observed radiation sources. Unseen matter bends light from sources behind it. This phenomenon is called *gravitational lensing*. From the deviation of the light and the magnification of the source of light, the mass and the position of the object responsible for the deviation can be determined. The mass that causes the bending of light is the gravitational lens. The study of dark matter includes the development of dark matter maps of Universe.

However, even though dark matter appears to exist and its effects are measurable, its nature remains a mystery. This is because much of the dark matter in the Universe is believed to be non-baryonic and not subject to electromagnetic interactions. This fact makes dark matter extremely difficult to detect, as it can only be observed indirectly, through its gravitational effects and possibly other, non-electromagnetic, but presumably weak interactions.

Non-baryonic candidates for dark matter include neutrinos and possibly hypothetical entities such as axions, or supersymmetric particles. Dark matter has been divided into cold dark matter (CDM) and hot dark matter (HDM), depending on its speed at the moment of decoupling from baryonic matter (hot if the speed was relativistic, that is $kT_{dec} > mc^2$; cold if not). Most dark matter is believed to be CDM, as only non-relativistic matter would have allowed a sufficiently rapid halo gravitational collapse to explain the formation of structures such as galaxies in the available time.

Indeed in a Universe dominated by HDM, free-streaming of the relativistic dark matter particles suppresses the fluctuations that correspond to smaller

masses that would seed galaxies and the larger scale fluctuations will be the first to create clusters. In this scenario the galaxies would be created afterwards, as fragmentation of the bigger structures. This means that, in a Universe of HDM, clusters are older than galaxies.

This is absolutely in contrast with observations that establish a bottom-up scenario, where smaller structures collapse before and larger structures such as clusters are created by aggregation. This brought scientists to abandon the models dominated by HDM and consider that most dark matter is CDM.

Evolution

To briefly describe the role of each component in the evolution of the Universe, we need to consider how they affect the scale factor. The acceleration equation gives the variation for the acceleration with time and depends on the pressure P and the density ρ of each component. We shall therefore use the equation of state introduced in Section 1.2.2 to combine the pressure and the energy density of the matter that fills the Universe: $P = \omega\rho$, where the value of the state parameter ω depends on the considered component.

We evaluate the dependence of the different species from the scale factor. We have seen that the study of the evolution of the Universe is complicated by the presence of many components, each with a different equation of state. However, the energy density and the pressure can be summed for each component. The total energy density can then be written:

$$\rho = \sum_{\omega} \rho_{\omega} \tag{1.35}$$

where ρ_ω is the energy density of the component with the equation of state characterized by the parameter ω. The total pressure is:

$$P = \sum_{\omega} P_{\omega} = \sum_{\omega} \omega\rho_{\omega} \tag{1.36}$$

Assuming that there are no interactions between the different components,

the fluid equation can be written in the following way:

$$\dot{\rho}_\omega + 3\frac{\dot{a}}{a}(1+\omega)\rho_\omega = 0$$

Consequently we have

$$\frac{d\rho_\omega}{\rho_\omega} = -3(1+\omega)\rho_\omega \frac{da}{a}$$

and then, integrating with ω constant,

$$\rho_\omega(a) = \rho_{\omega,0} a^{-3(1+\omega)} \tag{1.37}$$

where we have normalized to the present time, when $a_0 = 1$ and the energy density is $\rho_{\omega,0}$.

We first consider the matter component.

For a gas of non-relativistic particles, it can be shown that $P_{nonrel} = \omega\rho_{nonrel}$ with $\omega \simeq (< v^2 > /(3c^2)) << 1$. Then ω can be approximated to 0.

Thus, from equation 1.37 it can be seen that the energy density associated with non-relativistic matter decreases with the expansion of the Universe, since using ω for matter it can be expressed as:

$$\rho_{mat}(a) = nE \propto a^{-3} \tag{1.38}$$

This result is logical because the energy density of matter is approximately proportional to the rest mass (which does not change if the Universe is expanding). The energy of matter ($\rho_m a^3$) is equal to the rest energy of matter, which remains constant with the expansion of the Universe. Then, as we have already anticipated, the energy density of matter is simply proportional to the inverse of the volume, that is a^{-3}.

We now consider the radiation component. A gas of massless particles, such as photons, is relativistic. Although photons have no mass, they do have momentum and consequently they exercise a pressure. Hence we have $\omega = \frac{1}{3}$ (as $< v^2 > \simeq c^2$), and so $P_{rel} = \frac{1}{3}\rho_{rel}$. Both these components, matter and radiation, cause deceleration.

We anticipated that the energy density of radiation decreases at a greater rate: $\rho_{rad}(a) = nE \propto a^{-4}$. This is in accordance with what we would expect. Indeed, since $\lambda \propto a$, the energy of photons and other relativistic particles can be expressed as: $E = \frac{hc}{\lambda} \propto a^{-1}$ and so $\rho_{rad}(a) = nE = n\left(\frac{hc}{\lambda}\right) \propto a^{-3}a^{-1} \propto a^{-4}$.

Finally we consider dark energy. For $\omega \leqslant -\frac{1}{3}$ this component results in a positive acceleration ($\ddot{a} > 0$ in the acceleration equation). A gas of ordinary matter has got a positive pressure due to the randomic thermal motion of the molecules of which it is formed. A positive pressure decelerates the expansion, while a sufficiently negative pressure accelerates the expansion. The cosmological constant is defined as a component of the Universe with $\omega = -1$ and so $P = -\rho$. Thus for the energy density of the Universe associated with the cosmological constant, we have $\rho_\Lambda(a) = \rho_{\Lambda,0}$. This means that the energy density associated with Λ does not depend on the scale factor and remains constant as time elapses.

The equations obtained for a Universe with different components show that, at the limit where $a \longrightarrow 0$, the component with greatest ω will be dominant. On the other hand, if the Universe is doomed to expand for ever, $a \longrightarrow \infty$ and the component with the smallest ω will be dominant.

The experimental evidence strongly suggests that in our Universe, radiation ($\omega = \frac{1}{3}$) dominated during the first phase, then our Universe passed to a period of matter domination. Only recently it has become a Universe dominated by the cosmological constant. At the present moment we have the following values (Planck Collaboration, 2013) $\Omega_{tot} \approx 1$, with $\Omega_m \approx 0.317$, $\Omega_\Lambda \approx 0.68$, $\Omega_r \approx 9.2 \times 10^{-5}$.

The Universe has expanded from an initial state of high density, so there must have been a moment when the energy density of matter and Λ were equal. This moment is called the *equivalent time for matter and* Λ and corresponds to the following value for the scale factor:

$$a_{m,\Lambda} = \left(\frac{\Omega_{m,0}}{\Omega_{\Lambda,0}}\right)^{1/3} \approx \left(\frac{0.3}{0.7}\right)^{1/3} \approx 0.75$$

which corresponds to the redshift $z_{m,\Lambda} \approx 0.33$.

Therefore, there were epochs of domination for each component of the Universe. Then, between each period of domination, there were periods of equivalence between components and this not only in the case of matter and Λ. For instance, even though matter is strongly dominant over radiation at the present time, there was a time when radiation and matter were equivalent. This can be obtained by setting equal the matter and the radiation densities:

$$\Omega_r a(t)^{-4} = \Omega_m a(t)^{-3} \tag{1.39}$$

from which we get

$$a(t) = \frac{1}{1+z} = \frac{\Omega_r}{\Omega_m} \tag{1.40}$$

Since $\Omega_r \simeq 9.2 \times 10^{-5}$ and $\Omega_m \simeq 0.32$, we have the time of equivalence for radiation and matter dominance at a redshift $z \simeq 3402$.

As in each period there is a dominant component, a simplistic approach can ignore the other components. Consequently the Friedmann equation can be considerably simplified in each case. Considering a flat Universe ($\Omega = 1$, k=0), we have (Ryden, 2003):

- Radiation-dominated era: $\Omega_r a^{-4} >> \Omega_m a^{-3} + \Omega_\Lambda$:

$$\left(\frac{\dot{a}}{a}\right)^2 = \Omega_r \frac{H_0^2}{a^4} \longrightarrow a(t) = \sqrt{\Omega_r}(H_0)^{1/2} t^{1/2} \tag{1.41}$$

- Matter-dominated era: $\Omega_m a^{-3} >> \Omega_r a^{-4} + \Omega_\Lambda$:

$$\left(\frac{\dot{a}}{a}\right)^2 = \Omega_m \frac{H_0^2}{a^3} \longrightarrow a(t) = \left(\frac{3}{2} H_0 \sqrt{\Omega_m}\right)^{2/3} t^{2/3} \tag{1.42}$$

- Dark energy-dominated era: $\Omega_\Lambda >> \Omega_m a^{-3} + \Omega_r a^{-4}$:

$$\left(\frac{\dot{a}}{a}\right)^2 = \Omega_\Lambda H_0^2 \longrightarrow a(t) = e^{\sqrt{\Omega_\Lambda} H_0 (t - t_0)} \tag{1.43}$$

However this simplification cannot always be used: during the times of equivalence we must consider both components that participate in the change of

domination. Then, in general, it can be seen that, in a Universe with many components, *a(t)* does not have a simple analytical form because, in the Friedmann equation, every term referring to each different component has a different dependence on the scale factor.

In a Universe with many components the Friedmann equation becomes:

$$(\dot{a})^2 = \frac{8\pi G}{3c^2}\sum_{\omega}\rho_{\omega,0}a^{-1-3\omega} - \frac{kc^2}{R_0^2}$$

A Universe constituted of matter, radiation and cosmological constant is the model that best fits with our Universe. In this case, using the density parameter and H from equation 1.16 we have:

$$\left(\frac{H}{H_0}\right)^2 = \left(\frac{\Omega_{r,0}}{a^4} + \frac{\Omega_{m,0}}{a^3} + \Omega_{\Lambda,0} + \frac{\Omega_{k,0}}{a^2}\right) \tag{1.44}$$

where $\Omega_{k,0} = (1 - \Omega_0)$ and $\Omega_0 = \Omega_{r,0} + \Omega_{m,0} + \Omega_{\Lambda,0}$ (as already mentioned, a flat Universe is favoured by current data, thus $\Omega_{k,0} = 0$).

Using this equation it is possible to show that the period of radiation domination[18] was much shorter than the typical time for a cosmic phenomenon. The radiation-dominated period is therefore insignificant in the estimation of the age of the Universe and it is in fact often neglected. Indeed the most general expression for the age of the Universe is:

$$H_0 t = \int_0^a \frac{da}{(\frac{\Omega_{r,0}}{a^2} + \frac{\Omega_{m,0}}{a} + \Omega_{\Lambda,0}a^2 + (1 - \Omega_0))^{1/2}}$$

In the case with $\Omega_{m,0} = 0.314$ and $\Omega_{\Lambda,0} = 0.68$, the present age of the Universe is $t_0 = 13.81 \pm 0.06\ Gyrs$ (with $H_0 = 67.4 \pm 1.4\ kms^{-1}Mpc^{-1}$, values from Planck Collaboration (2013)). We have shown that the scale factor at the time of matter-Λ equivalence was: $a_{m\Lambda} = \left(\frac{\Omega_m}{\Omega_\Lambda}\right)^{1/3}$, then the age of the equivalence matter-Λ is $t_0 = 9.8 \pm 1.0\ Gyrs$.

As a conclusion in the following table we show the principal density parameters relative to the standard cosmological model of our Universe, obtained

[18] A rough approximation gives 47000 yr for the radiation dominated period duration.

with different methods, such as the study of the CMB anisotropies (Planck Collaboration, 2013).

Density parameter		*Symbol*	*Value*
Matter	*All*	Ω_m	0.317
	Dark	Ω_{dm}	0.267
	Baryonic	Ω_b	0.049
Cosmological constant		Ω_Λ	0.68
Radiation		Ω_r	9.2×10^{-5}
Curvature		Ω_k	0.00

1.3.2 The most boring Universe?

Current measures for the cosmological parameters have reached an incredible level of precision. We refer to 1% precision Cosmology. Extremely stringent and recent constraints come nowadays from measures of the cosmic microwave background radiation, performed by the Planck satellite. The cosmic microwave background (CMB) radiation, that was created when the Universe became neutral and transparent, is an excellent instrument to obtain informations about the early Universe and its components. Indeed from the study of its anisotropies it is possible to understand the formation of structures and the evolution of the different components of the cosmos such as radiation, baryonic and non-baryonic matter. The phenomenon that brought to the creation of the CMB radiation is called *recombination*[19] and consist in the moment when free electrons became bound into hydrogen and helium atoms, ending their interactions with photons and allowing photons to propagate freely. The Universe became transparent and neutral. The spectrum of the CMB is the radiation constituted by these photons that have been travelling ever since, and give us a window into the past of the Universe.

[19]The term recombination might be misleading: in fact, before this time, electrons and protons had never combined into electrically stable neutral atoms, then the "re" is not correct, as more precisely it is a "combination".

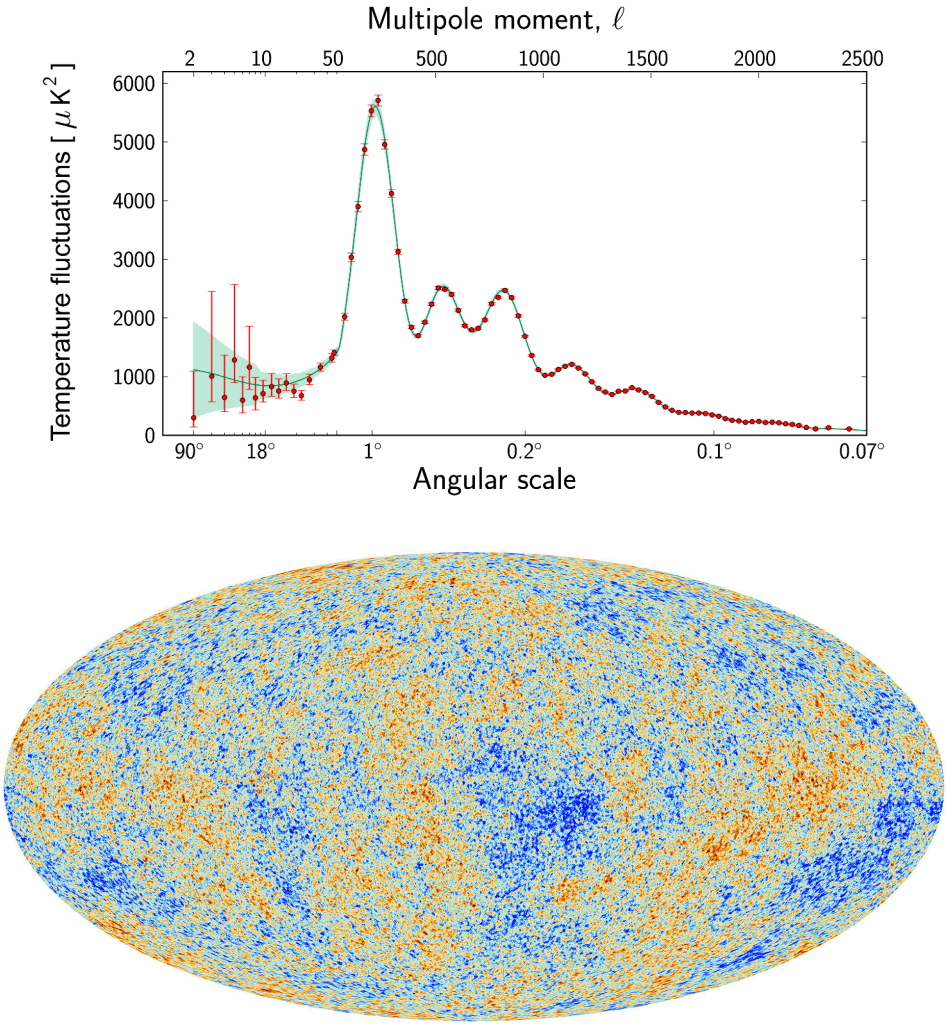

Figure 1.8: The Planck results: top panel illustrates the perfect agreement of the standard model of Cosmology with the observational data from the temperature release of the Planck satellite; bottom panel shows the cosmic microwave background radiation map (Planck Collaboration, 2013).

The photons that became free had at that time a temperature of about 3000 K. However, as the Universe was expanding, they had to fill a larger Universe. Consequently they became fainter and less energetic. These photons form the CMB radiation, which was serendipitously discovered by Arno

Penzias and Robert Wilson in 1964. They were awarded a Noble Prize for their discovery in 1978.

The CMB was the evidence of the theory of the hot Big Bang, formulated for the first time by Gamov in 1948. In fact, Gamow realised that if the Universe is now expanding and cooling, it must once have been extremely hot and dense. By extrapolation, it expanded from a gravitational singularity with infinite temperature and density.

The CMB has a blackbody spectrum with an average temperature of 2.725 K and its spectrum peaks in the microwave range frequency of 160.2 GHz, corresponding to a wavelength of 1.9 mm. The temperature is no longer 3000 K because it has been redshifted. It is possible to show that a blackbody spectrum at time t is still a blackbody spectrum at the present time but with a temperature $T_0 = aT$, where T_0 is the temperature at the present time and T the initial temperature when the scale factor was a. The temperature T_{CMB} of the CMB as a function of redshift, z, can be shown to be proportional to the temperature of the CMB as observed at the present day (2.728K):

$$T_{CMB} = 2.728(1 + z) \tag{1.45}$$

On April 23, 1992 the satellite COBE research team announced an even more important discovery: the satellite had detected some tiny fluctuations in the CMB. The extreme importance of these fluctuations was evident when it was hypothesized that the small temperature anisotropies in the CMB could be responsible for the formation of the structures of matter that we now see in our Universe. The temperature of the CMB is isotropic and homogeneous down to variations of 10^{-5} and in those minuscule variations is written the origin of all the structures of the Universe: they are the seeds of clusters, voids, sheets and filaments.

The Wilkinson Microwave Anisotropy Probe (WMAP) satellite, a NASA Explorer mission launched in June 2001 gave the first fundamental measurements of cosmological parameters establishing some of the basis of the standard model.

More recently, high-precision data from the Planck satellite confirm a sce-

nario where ΛCDM is strongly favoured. Results from this satellite are — to say the least — amazing. The CMB power spectrum illustrates the match between the most accepted current model for Cosmology ΛCDM and observational data, as presented in Figure 1.8 (from Planck Collaboration (2013)).

Thus with such a perfect agreement between theory and observations, can we say that Cosmology came to an end?

The real status of Cosmology is actually far from that. There is still more than 90% of the Universe which is not well understood — the dark sector is the next mystery to uncover. Furthermore, as pointed out by Verde et al. (2013), in light of the recent results from the Planck satellite and of the slight tension risen with data from Type Ia supernovae, a local cosmological-independent measurement of the Hubble parameter (potentially accessible with cosmic voids) assumes great importance.

Indeed, in a framework were the CMB analysis has reached its apex, the use of the large-scale structures of the Universe to constrain Cosmology has just began to show its power. The era of large-scale surveys produces a huge amount of data, allowing the development of new approaches to constrain Cosmology. The next Chapter presents the use of cosmic voids as an extremely powerful tool to shed light into the nature and behaviour of dark energy and constrain the cosmological model and the evolution of the Universe.

Chapter 2

Understanding the Universe with Voids

The first Chapter showed the importance of tools able to measure the expansion of the Universe. Although the ΛCDM model seems to be well established many mysteries remain to be elucidated about the dark sector. Focussing on dark energy, we know that it is responsible for the accelerated expansion of the Universe and we know the amount we should expect of such component, but our understanding of it does not go much farther. Measuring the acceleration of the Universe is thus both a way to confirm the ΛCDM accepted scenario and to eventually grasp information about the properties of this elusive component.

The use of different tools to measure the expansion of the Universe narrows the constraints on dark energy, since different probes explore the parameter space[1] in different ways. The first Section of the Chapter will present the tools to measure the expansion of the Universe, standard objects. The second Section of the Chapter will focus on cosmic voids, present their use for Cosmology through the Alcock-Paczyński test and, finally, discuss the main challenges when working with voids.

[1]For a model describing a phenomenon, the parameter space is defined as the set of all combinations of values for all the different parameters of the model.

2.1 Standard objects

The so-called *standard objects* are a powerful tool to constrain the expansion of the Universe. We can consider three families of objects: standard candles, standard rulers and standard spheres.

Standard candles

The discovery of the acceleration of the Universe has shown the importance of the use of standard candles. Their use is based on the theory that predicts the exact value of their luminosity.

The 2011 Nobel Prize established the expansion rate of the Universe using a particular kind of supernovae, the type Ia supernovae, which have very a precise value for their luminosity. Type Ia supernovae were double stars that became supernovae only when the mass of one of them, absorbing mass from the other, exceeded the Chandrasekhar limit of 1.4 $M_{\odot}$.

The mass involved in the explosion is then very similar for each star, and, consequently, so is the luminosity. This particular property allows a very precise estimate of the distance of the galaxy in which the phenomenon is observed. Standard candles allow the measure of the acceleration for the expansion of the Universe through their *known luminosity*. They permit us to measure the luminosity distance and consequently they are measures of the integral of $H(z)$.

Standard rulers

A tool based on a similar idea are standard rulers. These are astronomical objects of *known length*. By measuring the variation of their length, cosmologists can obtain information about the expansion of the Universe. An example of standard rulers are baryon acoustic oscillations (BAO).

Before recombination (which we recall to be the moment when, because of the cooling of the Universe, photons stopped their interaction with baryons and decoupled) the Universe could be described as a plasma where baryons and photons were coupled. The presence of small primordial density fluctu-

ations allowed the formation of structures in this homogeneous and isotropic scenario. Thus, in an overdense region of the primordial plasma, the pressure of radiation (photons) is a restoring force acting against gravity.

The potential well generated by dark matter tends to make the photo-baryonic fluid collapse, while the increase in the density of radiation during the collapse makes the radiation pressure increase, counteracting gravity. The continuous balancing of these two forces leads to *oscillations of the photo-baryonic fluid*. The fluid will be subject to compression and expansion until the moment when photons and baryons separate.

When recombination happens, photons and baryons decouple. Photons are thus free to diffuse away, thus the pressure ends. This leaves an imprint in the distribution of baryonic matter: at fixed radius around the perturbation it is possible to measure a shell of baryonic matter, the baryon acoustic oscillations (BAO).

Theory determines the scale of BAO, which makes them the most powerful and reliable standard ruler ever used in Cosmology. This BAO scale roughly measures 150 Mpc.

When we observe an object such as the BAO feature in the Universe, we can determine the angle subtended by the object $\Delta\theta$. The correspondence between what we observe and the size of the object in the transverse direction (the direction perpendicular to the line-of-sight direction) is Cosmology-dependent — and embodied in the definition of the angular diameter distance.

We have defined the angular diameter distance as the ratio of the comoving (physical) size of the object over its angular size, and we showed that d_A is also related to Cosmology:

$$d_A = \frac{c}{1+z}\int_0^z \frac{dz}{H(z)} = \frac{\Delta\chi}{\Delta\theta} \tag{2.1}$$

Thus the BAO measure the angular diameter distance and consequently they are measures of the integral of $H(z)$. If, as for BAO, we know the size of the object $\Delta\chi$ (from theory, for instance), we can measure $\Delta\theta$ and obtain d_A.

Furthermore, in a completely independent way (as pointed out by Bassett and Hlozek (2010)) we can constrain $H(z)$ if the standard ruler aligns with

the line of sight, rather than across the line of sight. We can directly measure Δz, the extent of the object along the line of sight in redshift space. This extent is related to the Hubble parameter:

$$H(z) = \frac{c\Delta z}{\Delta \chi} \tag{2.2}$$

where $\Delta\chi$ is the size of the ruler. We have to keep in mind (for a discussion in the following section) that we had to assume that we knew the physical size of the object *both* in the transverse direction and in the direction along the line of sight. This is true for BAO in an isotropic universe, though peculiar velocities will affect the measured extent in redshift space. Up to this point, BAO are then also a direct way to measure $H(z)$ (unlike the measure of the transverse size of the ruler, or the measure with standard candles both of which give the integral of $H(z)$).

With transverse and line-of-sight standard rulers we obtain independent constraints on d_A *and* $H(z)$, which is a powerful way to shrink the allowed parameter space.

As pointed out by Bassett and Hlozek (2010), BAO are a statistical standard ruler, defined as a statistically preferred scale for the clustering of galaxies. For reference, more details about BAO can be found in Cooray et al. (2001), Blake and Glazebrook (2003) and Seo and Eisenstein (2003); the first detection of the BAO peak was in 2005 by Eisenstein et al. (2005) using data from the Sloan Digital Sky Survey and by Cole et al. (2005) using data from the final 2dF Galaxy Redshift Survey. The BAO measurement is considered today one of the most robust tests of Cosmology.

Standard spheres: the Alcock-Paczyński test

Finally, a similar idea to standard rulers is the use of standard spheres. Imagine that we were able to populate the Universe with spheres. We could then observe these objects and measure their angular size $\Delta\theta$ and their size in redshift space, along the line of sight Δz. Again, as with standard rulers, the way these measures relate to the physical sizes of objects depends on Cosmology.

We know that the object is a sphere, thus the radial over transverse size[2] needs to be one. When we convert this into cosmological observables, it means that a standard sphere is an object of known ratio between its redshift size and its angular size.

If this is not the case, it means the wrong cosmological model has been assumed to relate the measured quantities (angular size and along-the-line-of-sight size) with the physical quantities (transverse size and radial size). The basis of this important idea were laid down by Charles Alcock and Bohdan Paczyński in 1979 (Alcock and Paczynski, 1979).

Labelling as $\Delta r_\perp$ the size of the object in the transverse direction and as $\Delta r_\parallel$ the physical size along the line of sight, the Alcock-Paczyński test essentially imposes:

$$\Delta r_\perp = \Delta r_\parallel \tag{2.3}$$

Each of these two sizes can be related to observable quantities through Cosmology:

$$\Delta r_\perp = d_A(z)\Delta\theta \tag{2.4}$$

$$\Delta r_\parallel = \frac{c\Delta z}{H(z)} \tag{2.5}$$

Thus, imposing the equality of the two diameters of the sphere we get:

$$d_A(z)\Delta\theta = \frac{c\Delta z}{H(z)} \tag{2.6}$$

We measure, as usual, Δz and $\Delta\theta$. Thus, isolating on the left-hand side of the equation the measured quantities and on the right-hand side the cosmological quantities that we would like to constrain, we obtain:

$$\frac{c\Delta\theta}{\Delta z} = H(z)d_A(z) \tag{2.7}$$

The Alcock-Paczyński test constrains the *product* $H(z)d_A(z)$ through the measure of $\Delta\theta$ and Δz. It is less powerful than a standard ruler in constraining

[2]Both are *physical* sizes

Cosmology, since exploring separately $H(z)$ and $d_A(z)$ better constrains the parameter space (Bassett and Hlozek, 2010). Nevertheless is also requires less: it is probably more simple to find a spherical object of whatever size than to find a quantity of which we know with absolute certainty the radius from theory.

Furthermore even though the use of standard spheres could be less constraining than standard rulers, it still explores the parameter space in a different way, through a different combination of observables, thus excluding other areas and shrinking the range where parameters can vary and thus adding information.

I also point out that, as we have seen, BAO have been used to constrain $H(z)$ and $d_A(z)$ independently, through the use of the physical size of the object *both* in the transverse direction and in the direction along the line of sight. Since we know the length, this use of BAO could be thought of as the application of an *absolute* Alcock-Paczyński test.

With standard spheres, where we do not know the length, we can perform a relative Alcock-Paczyński test. This differentiation is introduced by Bassett and Hlozek (2010), and I find it particularly enlightening, since it shows that we are using the exact same equations in both cases. One could say that, if known, the diameter of the sphere in the relative Alcock-Paczyński test can be used as a standard ruler, in which case we would perform an absolute Alcock-Paczyński test.

I have presented the three main methods to obtain measures of the expansion of the Universe using standard objects (Figure 2.1). While the first one (candles) has been the most used in the past, the second and the third are perhaps gaining upon it nowadays — with the advent of large-scale surveys — because of the enormous amount of data available and the great reliability they offer.

In this scenario, a new, powerful cosmological probe is emerging: the use of cosmic voids to constrain Cosmology. The next Section will present these objects.

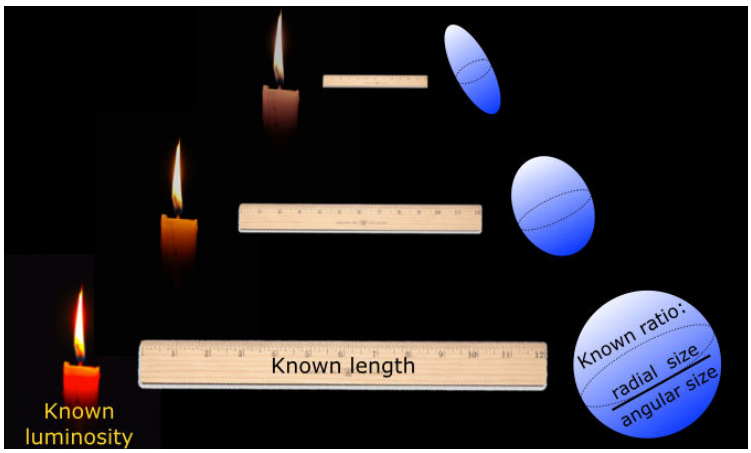

Figure 2.1: Standard objects: candles, rulers and spheres

2.2 Cosmic voids

We have seen in the first Chapter of this thesis how the discovery of the cell structure of the Universe showed the presence of unexpected empty regions: voids. For many years the under-dense regions of the cosmic web remained unexplored due to the lack of information and the inability of surveys to measure great portions of the sky with sufficient depth in magnitude.

This is changing nowadays. The era of large-scale surveys is giving us an incredible amount of data to deal with and, along with it, the possibility to extract information using statistical average of quantities in the sky. We will see that both these features are essential to transform voids into a potentially powerful tool to constrain Cosmology.

Some early work with voids considered the possibility of using them to constrain cosmological models. Among them, examples are Melott (1987), which showed that the size of voids was sensitive to the matter in the Universe (and to the matter's nature: voids in hot dark matter models are twice the size of voids in cold dark matter models); Martel and Wasserman (1990), that considered a pressureless matter and non-zero cosmological constant model; or Goldwirth et al. (1995) who looked for a characteristic scale related to voids and studied how the abundance of voids in surveys could differ in different cosmological models.

One of the first scientists to reconsider the use of cosmic voids as a direct geometrical tool to measure the expansion of the Universe was Barbara Ryden (although works such as Dekel and Rees (1993) had considered the use of voids to infer the amount of dark matter). In 1995, she considered the idea of applying the Alcock-Paczyński test to cosmic voids (Ryden, 1995). The clever idea proposed to observe the elongation of voids along the line-of-sight direction (i. e. in redshift space) due to the expansion of the Universe — supposing that voids were spherical (Icke, 1984) in real space. Her interest in voids started relatively soon, in 1984, with a paper where she compared voids in simulations and in galaxy surveys (Ryden and Turner, 1984).

Nevertheless, it is not before 1995[3] that, through the use of simulations in real and redshift space, she looked for the Alcock-Paczyński signal with voids.

In her two papers (Ryden, 1995; Ryden and Melott, 1995), she concludes that the shape of voids changes when going from real space to resdhift space but the accuracy in the measure of the deceleration parameter is mainly affected by the shape (and size) of voids. Indeed the shape of an individual cosmic void is highly complicated and far from being perfectly spherical, leading to high systematics errors undermining the extraction of the cosmological signal with the Alcock-Paczyński test.

Barbara Ryden also mentions peculiar velocities as a possible source of incertitude in using voids as Cosmology probes (although the shape of voids is the strongest source of systematics in her analysis). Despite pointing out these sources of systematics, Ryden's work considers the statistical properties of voids, thus opening the way to their use in Cosmology: she introduced the use of voids as a probe of models and established the nature of the main systematics that Cosmology with voids is facing nowadays. The following years brought pioneering studies about voids from many groups (e. g. van de Weygaert and van Kampen (1993), Fairall (1998) and Hoyle and Vogeley (2002)). The use of voids for Cosmology through the study of their shape was not reconsidered before 2012, when Lavaux and Wandelt (2012) introduced

[3]A year before, in 1994, Barbara Ryden had also written another paper on voids, but this was more focused on the density profile than on constraining Cosmology with the Alcock-Paczyński test (Ryden, 1994).

the idea of extracting cosmological information from *stacked voids*[4]. The simple but powerful idea of stacks solved many issues that had prevented the previous use of voids to extract Cosmology: find voids in a given redshift bin and stack them in size bins allowed *to average their shape*. In a homogeneous and isotropic Universe there is no possible reason that could ever give to the void an average shape following preferred directions.

Thus voids are, on average, *spherical*. The application of the Alcock-Paczyński test is then not only possible, but can be done with reduced systematics. Voids are the standard spheres distributed in the whole Universe needed for the test. The work of Lavaux and Wandelt (2012) presents the method to stack cosmic voids and perform the Alcock-Paczyński test, it tests it with a dark matter particles simulation and establishes a forecast of voids constraints that could be achieved with the Euclid survey (Laureijs et al., 2011).

A shape for the stacked void emerges from this work: an underdensity in the center, the density then rises, to reach a maximum at the wall of the void. The wall is made by a stack of filaments, clusters and sheets. After the wall, the density goes back to the mean density of the Universe.

As an additional advantage, the stacking greatly reduces the impact of sparsity of data in underdense regions: the small amount of galaxies present in each void adds up, leading to a well defined density profile.

For what concerns the definition of voids, Lavaux and Wandelt (2012) decided to consider a particular approach: with the main aim of extracting cosmological information from voids, they chose a definition of voids (described in Section 6.1) and investigate cosmological information under that definition. It is reasonable to consider that, if Cosmology is affecting the shape of voids, the effect should be present in all definitions of voids — although to differing degrees. Thus it makes perfect sense to choose one and look for the cosmological signal with it, taking care that the definition washes out the lowest possible amount of information. As an example, a void finder that uses the

[4]Other studies had considered the statistical study of voids (in a certain way "stacking" their properties, e. g. Padilla et al. (2005); Ceccarelli et al. (2006), nevertheless, this statistical study was not aimed to extract constraints for cosmological models.

spherical prior might not be adapted, since voids shapes taken on a one-to-one basis are known to be highly irregular. Section 6.1 will discuss the technical details about the void finder `VIDE` used for this work (Sutter et al., 2014b).

The next Subsections describe the use of voids to constrain dark energy and the application of the Alcock-Paczyński test to voids.

2.2.1 Voids as a tool for dark energy

Stacked voids are the standard spheres needed for an application of the Alcock-Paczyński test. Measuring their shape we can infer the expansion of the Universe. Nevertheless, this is not the only reason to consider cosmic voids as a promising tool for Cosmology.

Matter is missing in cosmic voids, which means that the main component of these objects is dark energy. Cosmic voids are then dark-energy-dominated objects. In a framework where the efforts of cosmologists are focussing on the understanding of this mysterious component, it would be unwise to neglect *places in the Universe where dark energy rules*. Until very recently, due to the difficulty of extracting data from low density zones, the potential of voids has been under-explored. Voids constitute a large volume of the Universe: the amount of volume fraction might depend on the void definition, but remains in any case significant (see e. g. Kauffmann and Fairall (1991), El-Ad et al. (1997), Hoyle and Vogeley (2002), Bos et al. (2012a) and Pan et al. (2012)).

Since voids are made of dark energy, their evolution is particularly sensitive to its properties (Bos et al., 2012a,b). This is especially true for the evolution of the inner part (excluding the overdense wall), where matter is the sub-dominant component and dark energy dominates.

Dark energy affects the large-scale tidal force field, the shape of voids is modelled by the force field. Thus the shape and evolution of voids keeps an imprint of the effect of dark energy. With a first simplistic analysis, voids appear to be expanding (Icke, 1984; Fujimoto, 1983), however high-resolution simulations show that some voids might collapse into overdense regions (Gottlöber et al., 2003; Colberg et al., 2005).

The work of many groups tried to understand such evolution, such as

Sheth and Van De Weygaert (2004), which considered the excursion set theory to explain the void-in-cloud phenomenon, where voids can collapse into halos. Other groups used the properties of the cosmic web (which includes voids, filaments, sheets and clusters) to constrain the properties of dark energy (van de Weygaert et al., 2011). So both the inner evolution of voids and their statistical properties as members of the cosmic web are sensitive to dark energy.

The evolution of voids depends on the properties of this elusive component, but dark energy with a cosmological constant is not the only model able to explain the acceleration of the expansion of the Universe: models describing a modification of gravity itself are a valuable alternative to this unknown component accounting for ~ 70 % among the Universe components.

Voids can thus constrain these alternative models: Spolyar et al. (2013) and Belikov and Hu (2013) showed that a detailed study of cosmic voids is promising to directly probe a density-dependent equation of state. It seems logical that, if we consider models where massive gravity induces a density-dependent change in the equation of state, we should be able to infer the properties of the modified gravity model from the regions that are extreme in density.

These would include high density and low density regions. In high density regions, however, we do not expect gravity to be different from General Relativity predictions: for massive gravity, the change in the potentials is negligible for high-density zones, but becomes considerable for low density zones (Spolyar et al., 2013). Similarly, Li (2011) shows that in coupled scalar field Cosmology models, voids should start developing at an earlier time and would end up having bigger sizes. This can be explained considering that the scalar field coupling would produce a fifth force able to enhance the clustering of structures at earlier times.

Cosmic voids evolution can thus shed light on models of dark energy and modified gravity, but this is not the only field of Cosmology in which they can be considered innovative probes. Since voids are mildly non-linear, non-virialized structures, they better preserve memory of initial conditions — they

have evolved less, and in a simpler way, than high density regions. The study of their density profile and its evolution is thus a window into the early Universe.

Cosmology with cosmic voids appears as a promising area to explore, starting with its first application, the Alcock-Paczyński test. In the next Section I review the formalism to apply this test to voids.

2.2.2 Alcock-Paczyński test with voids

The formalism to apply the Alcock-Paczyński test to voids is slightly different and deserves a description of notation that allows comparison with conventional notation used in other applications of the test (e. g. BAO). Although the formalism is slightly different, we still wish to use the ratio of a void size along the line of sight to its size in the transverse direction. We need:

$$\frac{\Delta z}{\Delta d} \tag{2.8}$$

where Δz is the extent of the void along the line of sight in redshift space and Δd is the projected angular extent of the void (different from both angular length in real space $\Delta r_\perp$ used in our previous description of the Alcock-Paczyński test, and from the angular extent $\Delta\theta$, which is an angle).

The projected extent in the angular direction Δd is related to the angular extent $\Delta\theta$:

$$\Delta d = \frac{cz\Delta\theta}{H_0} \tag{2.9}$$

The physical size of the object in the transverse direction $\Delta r_\perp$[5] is related to the angle $\Delta\theta$ through the angular diameter distance (equation 2.4):

$$\Delta r_\perp = d_A(z)\Delta\theta \tag{2.10}$$

Thus, from equations 2.10 and 2.9 we obtain:

$$\Delta d = \frac{cz}{H_0}\frac{\Delta r_\perp}{d_A(z)} \tag{2.11}$$

[5]Corresponding to δr_v in papers applying the Alcock-Paczyński test to voids, such as Sutter et al. (2012b); Sutter et al. (2014d).

In a flat Universe, the comoving line-of-sight distance corresponds to the comoving angular diameter distance. We need to obtain the redshift extent of the object, thus we express the comoving line-of–sight distance as a function of z (from equation 1.19):

$$d_A(z) = \chi(z) = \frac{c}{H_0}\int_0^z \frac{dz'}{E(z')} \tag{2.12}$$

where we have defined $E(z) = H(z)/H_0$ (Ryden, 1995). Using the definition of d_A we obtain the redshift extent of the object Δz:

$$\Delta z = \frac{\Delta r_\parallel}{d(d_A)/dz} = \frac{H_0 E(z)}{c}\Delta r_\parallel \tag{2.13}$$

Thus from equations 2.9 and 2.13 we obtain the ratio of the redshift extent to the projected transverse extent:

$$\frac{\Delta z}{\Delta d} = \frac{H_0 E(z)\Delta r_\parallel}{c}\frac{H_0}{cz}\frac{d_A(z)}{\Delta r_\perp} \tag{2.14}$$

Using the Alcock-Paczyński test main relation (equation 2.3): $\Delta r_\parallel = \Delta r_\perp$, we obtain

$$\frac{\Delta z}{\Delta d} = \left(\frac{H_0}{c}\right)^2 \frac{E(z)d_A(z)}{z} = \frac{H_0}{c^2}\frac{H(z)d_A(z)}{z} \tag{2.15}$$

So, again, we are constraining the *product* $H(z)d_A(z)$, as we expect for an Alcock-Paczyński test. Common notation defines the *void stretch* as:

$$e_V(z) = \frac{c}{H_0}\frac{\Delta z}{\Delta d} = \frac{H(z)d_A(z)}{cz} \tag{2.16}$$

The measure of the void stretch is thus an Alcock-Paczyński test (relative, following the distinction introduced in Section 2.1). The cosmological model is telling us $H(z)d_A(z)$, which means that it is telling us the expected void stretch in an expanding Universe following the ΛCDM Cosmology. Any departure from such expected stretch would be a deviation from fiducial Cosmology (ΛCDM). The original description of the Alcock-Paczyński test with voids

has been done in Ryden (1995) and has been recently reformulated by Lavaux and Wandelt (2012); Sutter et al. (2012b); Sutter et al. (2014d).

After having focussed on the Alcock-Paczyński test and on the use of voids for cosmological purposes, I discuss the main systematics affecting void measurements for Cosmology.

2.2.3 Questions and challenges

Recent developments of surveys provide us with huge datasets, as discussed in Section 1.1.4. The use of voids is becoming an important tool for Cosmology. As with any new probe of Cosmology, one of the main concerns is to build a thorough understanding of the tool as well as the systematics that can arise.

Although cosmic voids are now used for many different applications, we do not yet understand them fully. Particularly, apart from the problem of a definition, which can be set once a definition is chosen and maintained (see the discussion in the previous Section), we lack of an insight on the behaviour of voids in real space.

When observing galaxies in the Universe, we do not have real-space images. Surveys such as the SDSS measure the position in redshift space. Since our Universe is expanding, all galaxies are redshifted due to the expansion of space. To this is added the redshift caused by the peculiar motion of the galaxies. Only the line of sight component of velocity affects the galaxy redshift (Hamilton, 1998).

Stacks of cosmic voids, the under-dense regions of the Universe, have a density profile with a general shape, as described previously: an under-density on the center; the density then increases towards its maximum value, reached at the over-dense stacked wall enclosing the void (which consists of clumps, filaments and sheets). Logically, a density profile of a stacked void in a homogeneous and isotropic Universe is spherically symmetric, and can be expressed as a function of radius.

When we find and stack voids in galaxy catalogues, however, the position of galaxies is measured in redshift space. This modifies the shape one would expect for the stacked void: the real-space spherical shape of voids is distorted

in redshift space (as it emerges from Lavaux and Wandelt (2012) and Sutter et al. (2012b).

Redshift space distortions affect the density profile of cosmic voids obtained until now (both in simulations and observations). To fully understand voids — and use them for Cosmology — it is of crucial importance to recover the shape of the density profile *without redshift distortions*. Unfortunately getting free from redshift space distortions is one of the most difficult and crucial points of the extraction of Cosmology from the large-scale structure of the Universe.

The goal of this thesis is to find a way to extract the density profile of voids in real space, in a way independent from Cosmology. Before discussing how we can attempt to solve this challenging problem, I point out what would be the applications of such results, thus giving a strong motivation for our work.

A first motivation is the improvement of the Alcock-Paczyński test. The test with cosmic voids can be performed starting from the spherical profile of the void and distorting it to reach the distorted void that we have in observations. To perform such test, we need the profile of the void in real space. Until now, there has been no way to obtain the real space shape of voids from real data.

Furthermore, the major systematics in applying the Alcock-Paczyński test is the effect of peculiar velocities. The distortion of voids in redshift space is a combined effect of the expansion of the Universe and of the peculiar velocities of galaxies. The determination of the density profile of stacked cosmic voids in real space is the first step to a model of the effect of peculiar motions and promises to improve the application of the test.

The Alcock-Paczyński test is not the only application for cosmic voids: I have discussed the relevance of the density profile of the void to constrain alternative models such as modified gravity models. The theoretical work able to constrain such models needs a reliable real-space density profile, which observations cannot provide without assuming a model for redshift distortions and a cosmological model. Also, voids are particularly sensitive to diffuse components such as neutrinos, that could affect the real-space shape of voids and their evolution.

Finally, when knowing the density profile of voids in real space, the compensation of the mass can be checked. Indeed, integrating the density profile, it is possible to obtain the mass inside the void. Mass compensation in voids could shed light into the evolution of structures and eventually allow the definition of a static ruler (as discussed by Hamaus et al. (2014), using simulations). At this point this static ruler has only been identified from the real-space profiles (see discussion in Section 5.3.1).

For the following discussion, it is important to specify the purpose of using cosmic voids. While interesting work focuses on defining the properties of voids as objects standing by themselves — thus not needing to use cosmology independent methods, but on the contrary, assuming a Cosmology — we chose to focus on a different decision, namely the use of voids for cosmological purposes. While this approach is potentially powerful, caution must be taken to avoid any assumption. The necessity of a model independent approach is one of the main challenges of this work.

Finally understanding and defining the density profile of voids in real-space can shed light on the initial conditions. Voids evolve far less chaotically than overdense structures. We have evidence that certain aspects of void behaviour are well-described by linear theory Hamaus et al. (2014), which strongly simplifies their use. With simulations and cosmology independent methods, voids can be studied and used to constrain cosmological models.

A further probe of cosmology using cosmic voids, is the abundance of voids of a certain size and at a certain redshift. This number function depends on the cosmological model and can therefore be a powerful probe of Cosmology, analogous to cluster counts (Majumdar and Mohr, 2004). The abundances depend on both theoretical constraints and on details of the surveys used to observe voids; a model of both is thus necessary to use the abundances as probes, as described in Section 7.2.

I have discussed the important implications of understanding voids in real space. As mentioned previously, the leading systematic effect when working with cosmic voids (and with large-scale structures in general) is the presence of redshift space distortions caused by the peculiar velocities of galaxies. The

next Chapter will discuss the method to beat redshift space distortions within the framework of cosmic voids in a model independent way.

Chapter 3

Redshift space distortions: To real space and beyond

In this Chapter I present the method to obtain real-space density profiles of cosmic voids in a model independent way.

3.1 Redshift-space distortions

The study of the large-scale structure of the Universe is based on the positions of galaxies in the Universe. As mentioned, when observing galaxies in the Universe, we do not have real-space images. Galaxies are redshifted due to the expansion of space and due to the presence of the peculiar motion of the galaxy. Only the line-of-sight component of velocity affects the galaxy redshift (Hamilton, 1998). The large-scale structures are thus distorted in redshift space. When studying voids, for all the reasons mentioned in the previous Chapter, we would like to access the real-space information in a cosmological independent way.

Since the redshift-space distortions are the major source of uncertainty when inferring cosmological parameters from the large-scale structure of the Universe, two possible approaches are possible.

The first is to model redshift-space distortions, through the use of simulations. Since the redshift-space distortions are also are a source of information,

this approach certainly has its advantages. However the modelling of the redshift-space distortions is particularly difficult and relies on the use of simulations.

The second approach consists in finding a way to extract the real-space information without any modelling of the redshift-space distortions. While this can seem extremely difficult, since data will always be measured in redshift space, in a few cases it might lead to a simpler and more direct result.

For cosmic voids the second approach can be extremely powerful. Before illustrating the idea at the basis of the extraction of real-space information from cosmic voids, I briefly introduce redshift-space distortions.

For the purpose of our work, a full treatment of redshift-space distortions is not necessary, since we have chosen the second approach, that namely beats the redshift-space distortions without any modelling. The description I give of redshift distortions is thus simplistic. I consider approximations valid at low redshift ($z \ll 1$) and low curvature for an isotropic and homogeneous Universe. The redshift distance is obtained considering the real distance plus the effect of peculiar velocities along the line of sight.

Following the notation in Hamilton (1998), along the line-of-sight direction we have: $s = r + v cos\theta$, where s is the redshift distance in velocity units, equal to cz; r is the true distance; and v is the peculiar velocity, projected along the line-of-sight direction by defining the angle θ between the line-of-sight direction and the velocity. We then have

$$cz = H_0 d + v cos\theta \tag{3.1}$$

where c is the speed of light, z is the redshift of the galaxy, H_0 is Hubble constant, and d is the distance of the galaxy.

While we define how velocities affect the position of galaxies in redshift space, we need to understand a crucial point for our method to obtain the real-space shape: *the redshift-space distortions only affect the line of sight component*. If we found a way to remove the distortion along the line of sight we would be able to obtain the real-space shape of voids.

The next Section illustrates the method to reach this goal and lays the

basis for the reconstruction of the real-space shape of voids.

3.2 To real space

3.2.1 Using sphericity

The reconstruction method uses the fact that the redshift-space distortions only affect the line of sight component for the galaxies composing the void. The two components in the plane perpendicular to the line of sight remain unaffected by redshift-space distortions. Thus, the *projection* of the void stack along the line of sight does not depend on redshift-space distortions.[1]

If we are then able to reconstruct the void from the projection, we will have the density profile in real space, that is without redshift distortions.

In case a void had a non regular shape, this would be impossible. Nevertheless, considering that *the stacked void ought to be spherical in real-space*, by imposing sphericity we can reconstruct the 3-dimensional density profile of the void from its 2-dimensional projection.

The idea is shown in Figure 3.1.

The steps of the method can be stated as follows:

- project the *distorted* 3-dimensional density profile of the redshift-space stacked void,
- assume sphericity and,
- from the projection (which is *not* affected by redshift-space distortions), reconstruct the real space density profile of the void.

We note that this can be done for voids of reasonable size (smaller than 100 h^{-1}Mpc) and at low redshift ($z \ll 1$).

In the next Section we define some notation useful to the discussion of the method.

[1]By projection, we define the number count of galaxies in bins, projected along the line of sight. It can be thought as a column density.

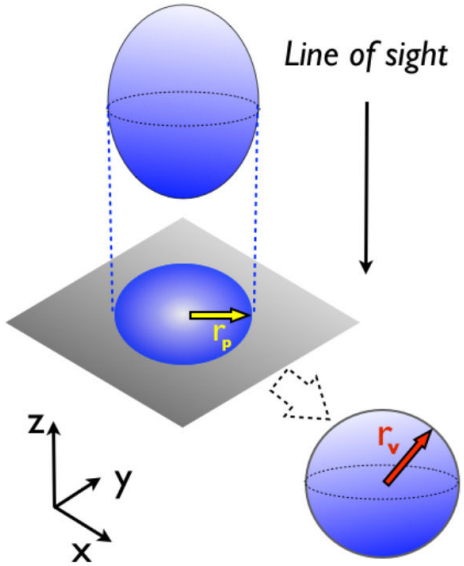

Figure 3.1: Representation of the method to obtain the sphere in real space from the distorted sphere in redshift space: the distorted void is projected along the line of sight (velocities do not affect the projection). From the projection we reconstruct the sphere in real space. The red arrow represents $r_{\rm v}$, the radius of the void in real space; the yellow arrow $r_{\rm p}$, the radius of the projection.

3.2.2 Notation

We consider the density of the void, where by density we mean the number of galaxies per volume element (a number density).

First, a spherical void has a spherically symmetric density function. This is the density that we aim to reconstruct. We notice that the density profile for a stacked void will simply be a function of the radius, since the void is spherically symmetric in real space.

We write it as $g(r_\mathrm{v})$, where r_v is the radius of the void (see Figure 3.1), given by:

$$r_\mathrm{v} = \sqrt{x^2 + y^2 + z^2}$$

Second, for a distorted void the density is not spherically symmetric, since the void is distorted along the line of sight direction, z. For an isotropic structure, the coordinates x and y are invariant if we consider a rotation around the axis of the line-of-sight direction. We can then define the radius of the projection onto a plane perpendicular to the line of sight: $r_\mathrm{p} = \sqrt{x^2 + y^2}$ (see Figure 3.1). The distorted density is written: $\rho(r_\mathrm{p}, z)$.

Finally we write the projected density as $I(r_\mathrm{p})$, only depending on the radius of the projection r_p. This density can be thought as a column density. We obtain the projected density by summing galaxies in each r_p bin at all z (and normalized in the bin). After having defined the necessary notation, I will now describe the reconstruction.

3.2.3 The inverse Abel transform

The most difficult step of the method is the reconstruction of the spherical real-space density profile of the stacked void $g(r_\mathrm{v})$ from the projected profile $I(r_\mathrm{p})$.

The densities $I(r_\mathrm{p})$ and $g(r_\mathrm{v})$ are related by the Abel transform, that cylindrically projects $g(r_\mathrm{v})$ to obtain $I(r_\mathrm{p})$ (Abel, 1842, reprint 1988; Bracewell,

1999):

$$I(r_\mathrm{p}) = 2\int_{r_\mathrm{p}}^{1} \frac{g(r_\mathrm{v})r_\mathrm{v}}{\sqrt{r_\mathrm{v}^2 - r_\mathrm{p}^2}} dr_\mathrm{v} \tag{3.2}$$

By inverting this relation, it is possible to obtain the spherical density $g(r_\mathrm{v})$ from $I(r_\mathrm{p})$. The formula used for the reconstruction is known as the inverse Abel transform (Abel, 1842, reprint 1988; Bracewell, 1999):

$$g(r_\mathrm{v}) = -\frac{1}{\pi}\int_{r_\mathrm{v}}^{1} \frac{I'(r_\mathrm{p})}{\sqrt{r_\mathrm{p}^2 - r_\mathrm{v}^2}} dr_\mathrm{p} \tag{3.3}$$

Using the inverse Abel transform, the real-space density profile of the void seems now accessible: the reconstructed 3D profile will not include the distortions in the line of sight direction. Unfortunately, the matter is not so simple as it appears.

The problem is that the Abel inverse transform, although well mathematically defined by the formula, is strongly *ill-conditioned*: if there is some noise in the input function $I(r_\mathrm{p})$ (of which $I'(r_\mathrm{p})$ is the derivative with respect to r_p), the reconstruction will be dominated by noise. In physics, one often deals with inverse problems, that relate measurements from observations to the physical properties we want to infer. Because of noise in real data, inverse problems often are ill-conditioned, thus smalls errors in the input data can result in error-dominated outputs.

For real data from voids this is obviously the case: when we consider a stacked void obtained by running a void finder on a galaxy survey, the cosmic void density profile in redshift space will be affected by noise, and so will its projection in a 2-dimensional plane.

The noise in the projection $I(r_\mathrm{p})$ of the void in redshift-space will strongly affect the reconstruction through the Abel inverse transform. The obtained profile in real space $g(r_\mathrm{v})$ will be noise-dominated: the physical features of the profile would be overwhelmed by noise, making impossible any use of the information to constrain Cosmology.

To obtain the real-space density profile it is thus necessary to overcome the ill-conditioning of the inverse. This is the subject of the next Section.

3.3 Fighting ill-conditioning

The simple and powerful idea of exploiting spherical symmetry of void stacks to beat redshift-space distortions is unfortunately thwarted by ill-conditioning. To overcome such a problem and extract the real-space shape of stacked cosmic voids, we have to regularise the inverse in such a way that the ill-conditioning is controlled in the reconstruction.

To reach such an objective, we have considered two different approaches, that we describe in the following subsections.

3.3.1 Polynomial regularisation

The first method follows the idea proposed in Abel (1842, reprint 1988) (see also Li et al. (2007)): a polynomial regularisation of the inversion. I have adapted this method to the particular case of cosmic voids.

The polynomial regularisation method approximates the Abel inversion through integrals of the input function $I(r_\mathrm{p})$, directly using data. The method allows to manage noise in the inversion and gives good results in the case of voids, where the profile $I(r_\mathrm{p})$ is noisy and the reconstruction could be ill-conditioned.

We summarize the method as follows:

1. expand the spherical density to be obtained $g(r_\mathrm{v})$ as a polynomial series;
2. using the polynomial expansion of $g(r_\mathrm{v})$, re-write the Abel equation relating the 2-dimensional projection $I(r_\mathrm{p})$ and the spherical reconstruction in order to obtain a system of equations with solution $g(r_\mathrm{v})$;
3. solve the system of equations.

The polynomial expansion of $g(r_\mathrm{v})$ is characterized by an order, n. The choice of the order n allows to manage noise and control the precision of the reconstruction. To determine the order that gives the best reconstruction we use the reprojection of the reconstructed profile: we consider the order that minimizes the difference between the $I_\mathrm{exact}(r_\mathrm{p})$ from which we reconstruct and the $I_\mathrm{reprojected}(r_\mathrm{p})$ from the reconstruction.

For the application of the algorithm to real data, this test will also be possible: as we will discuss in Section 4.3.2, the $I_{\rm exact}(r_{\rm p})$ is the projected density from data. Generally, for increasing n the precision of the reconstruction increases and the only limitations are numerical (Li et al., 2007).

In order to avoid over or under fitting, we implement a bootstrap analysis to choose the order. Bootstrap analysis is more appropriate in a case where noise strongly affects data (as suggested by Andrae et al. (2010)). For each profile we create bootstrap samples from the sample to reconstruct. We implement the reconstruction and choose the order that gives the best fit for each one of the samples. We then take the model chosen by the different bootstrap samples.

Also, to test if the choice of the order is robust, we exclude one point at a time in the profile to reconstruct and check if the chosen order is stable when repeating the analysis. Finally we additionally calculate the AICc information criteria (Akaike, 1974; Burnham and Anderson, 2002) to test the order, which validates the result from the bootstrap analysis.

The Akaike information criterion (AIC) allows to test the quality of a statistical model to represent the data. It gives a good trade-off between increasing too much the complexity of the model by using too many parameters and maintaining the goodness of the model. Following Burnham and Anderson (2002), it gives an estimate of the information lost when using a determinate model for the data. In the case of finite samples n and k parameters, defining L as the maximized value of the likelihood function; the criteria to be used is the corrected Akaike criterion (AICc), defined as:

$$AICc = 2k - 2\ ln(L) + \frac{2k(k+1)}{n-k-1} \tag{3.4}$$

While having used the AICc criteria to validate the procedure, for the reconstruction of voids the bootstrap method remains the most adapted to choose the order: it accounts for all the sources of errors such as the ill-conditioning of the inversion procedure and the errors present in the data.

The method of Li et al. (2007) assumes the boundary condition $I(1) = 0$ and is described for values of the radius between 0 and 1. This is the case of

the test function for the toy model (see next Chapter), but is not the case of voids: the density is not zero outside the void. We had to adapt the method for voids by rescaling the void and considering that, if $I(r_{\rm v})$ is different from 0 in $r_{\rm v} = 1$, the mean density must be subtracted from the reconstruction.

As a further validation for the polynomial reconstruction method we control that $I(r_{\rm p})$ and $g(r_{\rm v})$ have the same value at the edge of the void, where the projection is equal to the value of the 3D function (since the projection is done along a line tangent to the void, it considers only the point at the very edge of the void). Finally, as discussed in Section 4.3.2, a sanity check for the reconstruction of the void is the reprojection of the spherical reconstructed profile: the reprojection must match the projection of distorted density profile.

3.3.2 Singular value decomposition

I now illustrate the second method for the reconstruction, using the singular value decomposition approach to overcome the ill-conditioning of the Abel inverse. The singular value decomposition relies on the consideration that, if we discretize the integration of the inverse, projecting is like computing a matrix operation. We call M the matrix of the projection. We can write:

$$I = MG \tag{3.5}$$

where I is the projected density (that is our data, with noise), G is the spherical density and M is the matrix allowing for the transformation between I and G. We use singular value decomposition to decompose M into U (a unitary matrix), W (a diagonal matrix) and V (a unitary matrix).

The Abel inverse can then be written as:

$$G = VW^{-1}U^{T}I \tag{3.6}$$

The use of singular value decomposition allows to drop the noisiest singular values, which are the smallest in matrix W. The number of singular values that we keep must be discussed: we need to drop enough to control noise, but not too much or we will lose information.

The way we manage the choice of the number of dropped singular values is the same as the way we used to choose the order in the polynomial regularisation method: we reproject the reconstructed profile and consider the order that minimizes the difference between the $I_{\text{exact}}(r_{\text{p}})$ from which we reconstruct and the $I_{\text{reprojected}}(r_{\text{p}})$ from the reconstruction. We use the calculation of AICc to determine the number of dropped singular values for the reconstruction.

In a certain way the singular value decomposition method is the generalization of the first method without the assumption of the polynomial form for the spherical density profile to reconstruct $g(r_{\text{v}})$.

3.3.3 Differences between the methods

The main difference between the two methods is conceptual. The singular value decomposition method determines the basis that gives the best reconstruction using all the points of $I(r_{\text{p}})$ to calculate the spherical density. Thus it gives a more regular reconstructed density profile for the first points. The determination is however strongly dependent on data and might be more sensitive to noise.

On the other hand, the method with polynomial regularisation of the Abel inverse enforces polynomial smoothness and calculates the values of the density $g(r_{\text{v}})$ at each point, considering for the calculation only the points of $I(r_{\text{p}})$ from the considered radius r_{p} to the edge of the sphere (see Li et al. (2007) for details).

A separate reconstruction for each point of $g(r_{\text{v}})$ gives a less regular profile for the first points of the profile (due to the higher difficulty of disentangling the 3D structure from a projection when considering all the radii from the center to the edge, as it is for the inner points) but might be useful to control noise for the reconstruction of voids, where the presence of clumps in the wall and noise in data is likely to affect the quality of the reconstruction.

3.3.4 Technical details

After presenting the methods for the reconstruction, I briefly discuss technical details about the algorithm.

- *Normalisation*: The original data are divided in slices of different redshift and in each slice are stacked voids of different radius. The projected density $I(r_\mathrm{p})$ is a number density, i. e. the total number of galaxies divided by the area of the bin. The spherical density is normalised to the mean density of the sample. Furthermore, as the algorithm works for a radial profile, normalisation factors are taken into account to refer to the whole void. Additionally, the number of voids in the stack is necessary for the normalisation. The normalisation is automatically done by the algorithm.

- *Binning*: An advantage of the algorithm is that the binning can be chosen by the user. While the reconstruction does not change when changing the binning (as expected), a too frequent binning would overfit the data (that is the projected profile from which we reconstruct) and enhance the noise of the projection, thus leading to a noisy profile for the $g(r_\mathrm{v})$. A wide binning on the contrary would wash out details of the void profile (such as the compensation wall).

- *AICc*: The Akaike criterion introduced in Section 3.3.1 and used to check the order of the reconstruction obtained with the bootstrap procedure is the most adapted for the case of voids. Another possibility would have been the use of the Bayesian information criterion (BIC), which penalizes the number of free parameters in a less severe way. Nevertheless, as Burnham and Anderson (2002) discuss, the AICc criteria is more reliable, as it is based on principles of information theory and is asymptotically optimal.

In this Chapter I have presented the method for the reconstruction of real-space density profiles of stacked voids. Due to the ill-conditioned nature of the problem, it is important to widely test the algorithm and check that noise

in the reconstruction is correctly dominated. The next Chapter presents tests of the algorithm in the ideal case with no-noise, with a toy model, with a stacked void from a dark matter simulation and — finally — with voids from a mock catalogue of galaxies.

Chapter 4

Testing void reconstruction

4.1 The ideal case: no-noise

A preliminary test of the algorithm is based on the reconstruction of a particular kind of functions that can be inverted analytically. For such functions, we can calculate the expected reconstruction and thus test the algorithm reconstruction. I performed a first analysis without noise in the input function $I(r_{\rm p})$.

The following functions are used[1], where $I(r_{\rm p})$ is the 1-dimensional projection on the plane and $g(r_{\rm v})$ is the analytical 1-dimensional profile of the 3-dimensional density, that must be compared with the profile obtained from the algorithm. By increasing the degree of the approximation n of the reconstructed profile $g(r_{\rm v})$, the reconstruction is more precise, as expected (Li et al., 2007). The only case in which this might not be true is when n becomes too high; because the calculation for the reconstruction of $g(r_{\rm v})$ reaches high rounding errors related to numerical computation. The choice of the degree n allows to enhance the precision of the reconstruction, as discussed in Section 3.3.1.

Some examples of the functions used to test the reconstruction are:

[1] We actually tested the algorithm with a wider range of functions, but choose to represent only a selection.

- Example 1

$$I(r_{\mathrm{p}}) = \frac{8}{105}\sqrt{1-r_{\mathrm{p}}^2}(19 + 34r_{\mathrm{p}}^2 - 125r_{\mathrm{p}}^4 + 72r_{\mathrm{p}}^6) \tag{4.1}$$

$$g(r_{\mathrm{v}}) = \frac{1}{2}(1 + 10r_{\mathrm{v}}^2 - 23r_{\mathrm{v}}^4 + 12r_{\mathrm{v}}^6) \tag{4.2}$$

- Example 2

$$I(r_{\mathrm{p}}) = \frac{\sqrt{\pi}}{1.1\sqrt{1-r_{\mathrm{p}}^2}} e^{1.1^2(1-\frac{1}{1-r_{\mathrm{p}}^2})} \tag{4.3}$$

$$g(r_{\mathrm{v}}) = (1-r_{\mathrm{v}}^2)^{(-3/2)} e^{1.1^2(1-\frac{1}{1-r_{\mathrm{v}}^2})} \tag{4.4}$$

- Example 3

$$I(r_{\mathrm{p}}) = \sqrt{1-r_{\mathrm{p}}^2}(1 - 2.5r_{\mathrm{p}}^2) + 1.5r_{\mathrm{p}}^4 \ln\frac{1+\sqrt{1-r_{\mathrm{p}}^2}}{r_{\mathrm{p}}} \tag{4.5}$$

$$g(r_{\mathrm{v}}) = 1 - 3r_{\mathrm{v}}^2 + 2r_{\mathrm{v}}^3 \tag{4.6}$$

- Example 4

$$I(r_{\mathrm{p}}) = r_{\mathrm{p}} - 1 \tag{4.7}$$

$$g(r_{\mathrm{v}}) = -\frac{1}{\pi}\log|1 + \sqrt{1-r_{\mathrm{v}}^2}| - \log|r_{\mathrm{v}}| \tag{4.8}$$

- Example 5

$$I(r_{\mathrm{p}}) = r_{\mathrm{p}}^2 - 1 \tag{4.9}$$

$$g(r_{\mathrm{v}}) = -2\frac{\sqrt{1-r_{\mathrm{v}}c^2}}{\pi} \tag{4.10}$$

From the results obtained without noise it can be checked that increasing the order of approximation, the reconstruction is more precise (see Figure 4.1, the example 1 will be used for the toy model)[2]. Furthermore. as discussed in

[2]The precision increases except for too high n, for which the calculation of the determinant of the matrix might have great rounding errors because of numerical analysis.

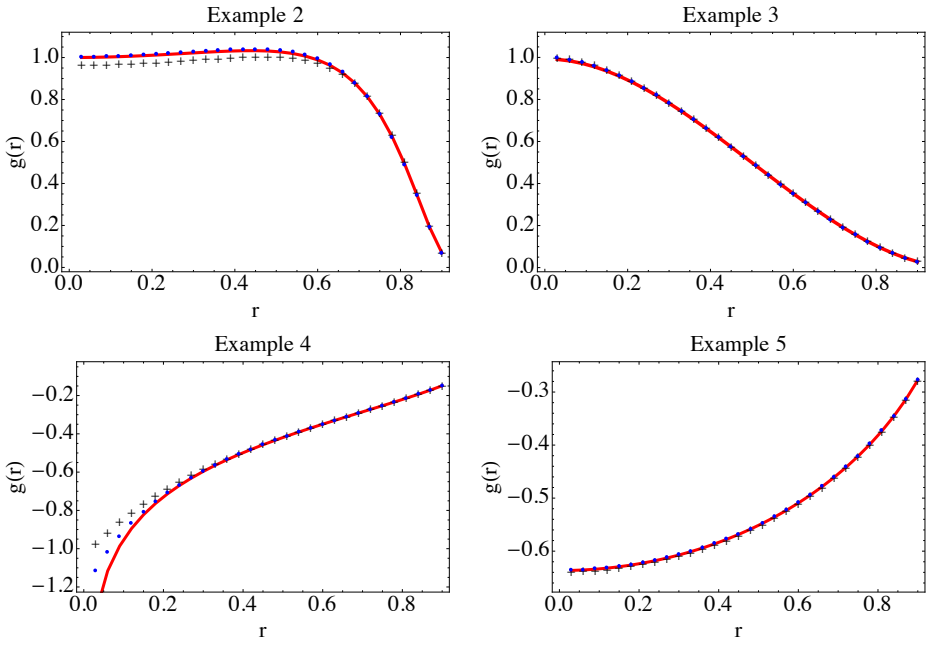

Figure 4.1: Examples 2, 3, 4, 5: theoretical profile of the 3D density (red line) and reconstruction for the different examples. Black symbols (crosses) show the reconstructed profile with order 3 for the reconstruction, blue symbols (dots) with order 5. We note that in some cases the lower order already reaches a good reconstruction, for others, increasing the order improves the quality of the result.

Section 3.3.2, the result is more precise at higher radii, while losing precision at smaller radii (this effect is more evident in the examples when diminishing the order of the reconstruction, because the Abel pairs examples[3] are more regular cases for the inversion).

To assess the functionalities of the algorithm in reconstructing the real-space density profile of a void distorted in redshift space, I create a toy model of the void — the next Section illustrates this simple benchmark and the test of the algorithm.

4.2 The toy model: constructing and using a simple benchmark

In order to test the feasibility of the method and the algorithm, we can simulate a distorted profile by artificially adding a velocity along the line of sight to a spherical profile. Since we know the initial spherical profile, we can test our algorithm by trying to recover the correct initially spherical density from the distorted one. I use the simplicity of this toy model to illustrate the full method for the reconstruction of the spherical density profile.

From the presentation and explanation of the method in previous Sections, it can be understood that the following steps are necessary:

- create a distorted profile;
- project it along the line of sight and
- reconstruct the sphere from the projection.

To construct an efficient test, I choose one of the example functions for which we can calculate the exact Abel inverse through mathematical integration, namely the function of equation 4.1. These kinds of functions are called *Abel pairs* (Bracewell, 1999; Abel, 1842, reprint 1988). I test all the steps of the algorithm with this function, considering that we know through analytic calculation $g_{\rm exact}(r_{\rm v})$ if $I_{\rm exact}(r_{\rm p})$ is known; they are related through Equation

[3]Defined in the next Section.

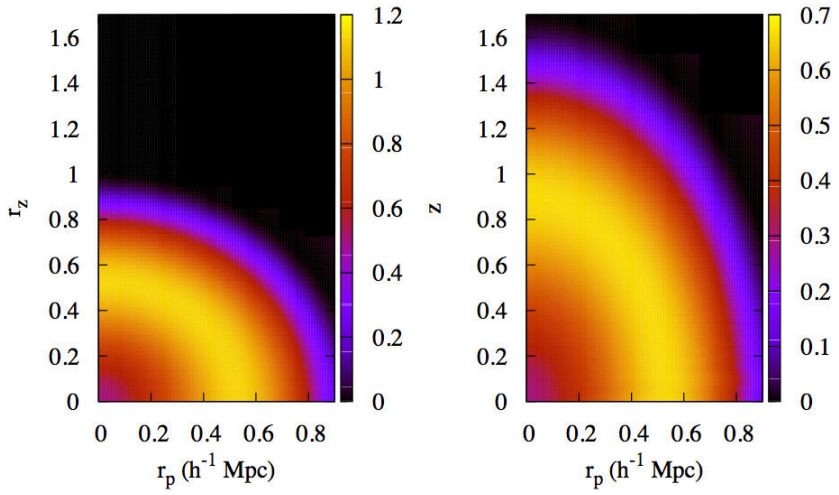

Figure 4.2: Density spherical profile (right) as a function of radius and distorted density profile (left) for the test function. Units for the density are arbitrary in the toy model, since we use a test function.

(3.3). The function for the toy model needs to have an exact mathematical inversion, this is the only important constraint for its choice. Additionally, it has a shape whose features roughly match those of a void profile.

I use the function to simulate a stacked void in redshift space: the first step is to create a distorted profile from the spherical profile $g_{\rm exact}(r_{\rm v})$. I show the results of the distortion in Figure 4.2 (right plot), along with the spherical profile (left plot). The void is distorted by adding an artificial velocity component to the line of sight coordinate (as described in Equation 3.1), which, as expected, changes the value of the density.

The next step is the projection of the distorted profile. Peculiar velocities contribute to redshift and distort the density profile; but, since the distortion is along the line of sight, velocities do not affect the projection. As a sanity check, I control that the projection of the distorted density is the same as the projection $I_{\rm exact}(r_{\rm p})$ from the non-distorted profile $g_{\rm exact}(r_{\rm v})$, even when using different kinds of velocity to distort the profile (such as $v(r_{\rm v}) = ar_{\rm v}$, or $v(r_{\rm v}) = ar_{\rm v}^2$). The left panel of Figure 4.3 shows the result of the comparison: the profile matches perfectly.

Once we have the projection, we can reconstruct the spherical density

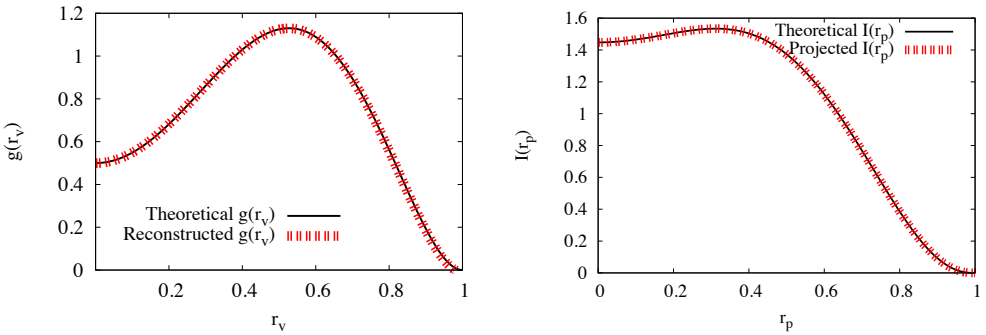

Figure 4.3: *Left panel*: Theoretical profile of the 3D density $g(r_\mathrm{v})$ (black line) and reconstructed profile (red bars) in the case without noise (using the method of polynomial regularisation). *Right panel*: Projection from a 3D simulated distorted profile (red bars) and theoretical projection (black line). As a sanity check: the projected profile from the distorted sphere matches the profile from the theoretical projection (the projection of the spherical profile), the projection cancels the deformation of the density profile.

profile of the stacked void, $g(r_\mathrm{v})$ and compare it with the known function. We show in Figure 4.3 an example of the reconstruction of $g(r_\mathrm{v})$ from the test function $I(r_\mathrm{p})$ without noise. After taking into account the case without noise, I consider the presence of noise in the input to the reconstruction algorithm, $I(r_\mathrm{p})$. The algorithm allows to add a gaussian noise to the input function. The noise I considered is a 1%, 3% and 5% gaussian noise. In such cases with noise, the ill-conditioning is well dominated: because the function can be inverted analytically, the function is particularly regular, both the singular value decomposition and the polynomial reconstruction method lead to good results (the reconstruction overlaps with the theoretical profile). To illustrate the ability of the algorithm to reduce noise in the reconstruction, I show the reconstruction in the case of a 1% Gaussian noise in the input function and compare this to the direct calculation of Abel inverse, without methods to reduce the noise[4] (see Figure 4.4).

The reconstruction with regularisation matches the theoretical $g_\mathrm{exact}(r_\mathrm{v})$

[4]It must be noted that the effect of noise is generally even worse than in this case, since for the considered example the function is an Abel pair and is therefore a particularly regular function. While this gives a rough idea of the effect of noise, cases with real data present an even more noise dominated reconstruction if no method for the regularisation of the inverse is considered.

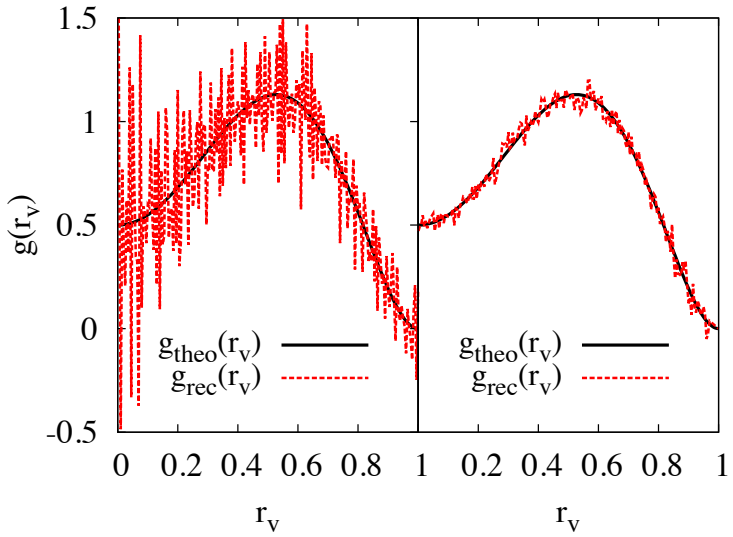

Figure 4.4: Theoretical profile of the 3D density $g(r_\mathrm{v})$ (black line) and reconstructed profile (red) in the case with 1% Gaussian noise in the input function. The left plot shows the Abel inversion without regularisation, the right plot shows the reconstruction obtained with the polynomial regularisation of the inversion.

also in the presence of noise. An additional check that we can do is the following: at the edge of the void $I(r_\mathrm{p})$ and $g(r_\mathrm{v})$ should have the same value because the projection has the same value of the density function (the projection is done along a line tangent to the void, the projection thus considers only a single value, the point at the very edge of the void).

In the case of the toy model, I assessed the capability of the algorithm to overcome noise in the reconstruction with an arbitrary percentage of noise.

Nevertheless, despite of its capacity to show noise reduction in the inverse and while being useful to describe the features of the algorithm, the toy model cannot account in a realistic and physical way for the complex sources of noise that would be present in a full simulation. The main source of noise in the density profiles is due to the sparsity of data, specifically Poisson noise on galaxy counts in the bins for the projected $I(r_\mathrm{p})$. The use of the stacking procedure allows to obtain well populated stacks, thereby permitting the extraction of cosmological information, however sparsity remains the major responsible for a projected profile affected by noise.

So, while the simpler case of the toy model is a proof of concept to assess the capability of the algorithm to control noise in the reconstruction procedure, the use of a simulated stacked void accounts for a more complex and realistic situation, where noise is implicitly taken into account. Furthermore, the use of a simulated void from a full dark matter particle simulation naturally takes into account the clustering of structures, serving the purpose of testing the reconstruction algorithm and show its first application as a proof of concept.

As discussed in the next section, the simulation will provide us with a robust test for the reconstruction algorithm and for the impact of noise in the reconstruction.

4.3 Dark matter particles

We will now compare the reconstruction methods in a more realistic case: a stacked void from a full dark matter simulation. We test the reconstruction in the case of a full simulation (by comparison with the known spherical profile from the simulation) and we show the consistency between results from the two reconstruction methods.

The simulated stacked void contains voids with radii between 10 and 12 h^{-1}Mpc from a dark matter particle simulation in a 500 h^{-1}Mpc box with 512^3 particles used in Lavaux and Wandelt (2012). The void finder is also the same, based on Neyrinck (2008) (`ZOBOV`). To show the realistic aspect of the void in resdhift space, we plot the density as a function of the radius of the projection r_p and of the z component. We clearly see the void profile (Figure 4.5, left plot) in redshift space, with a low density at the center and a wall at 10-12 h^{-1}Mpc. As expected, the distortion is along the line-of-sight direction.

The aim of this Section is the reconstruction of the real space density profile of this stacked void.

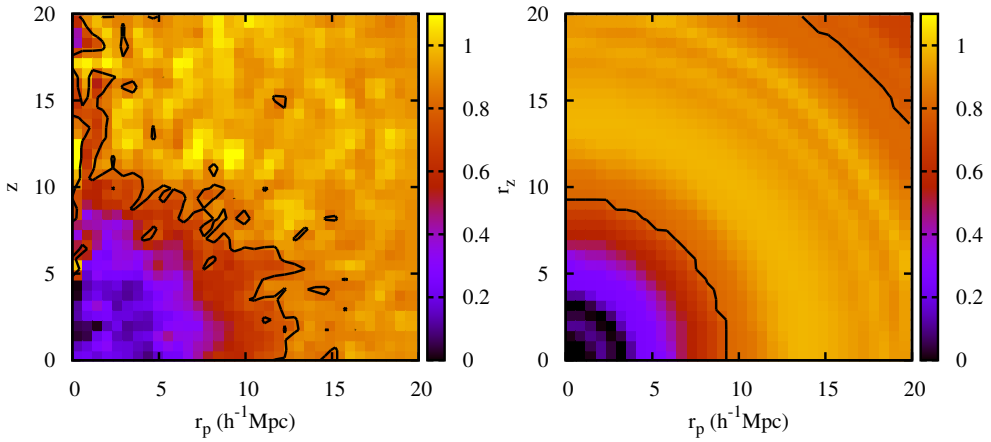

Figure 4.5: Distorted density profile of stacked void (left) from simulation and reconstructed spherical void in real space (right), both normalized to the mean density. Black contours in both images are density contours at 0.8 (where we have normalized to mean density).

4.3.1 Reconstructed density profile of a stacked void with the polynomial regularisation method

The spherical reconstructed profile is shown in Figure 4.5 (right). To test the quality of the reconstruction we use the known spherical profile from the real-space position of the particles.

Figure 4.6 shows the result of the reconstruction: it matches the spherical profile from simulation, validating the reconstruction. It must be noted that the reconstruction is obtained from a subsample of 200,000 dark matter particles of the total (about 10^9 particles). Real stacked voids do not have 10^9 galaxies as the simulated stacked void and, by taking only 200,000 of 10^9, we crudely simulate the effect of sub-sampling due to the fact that we are not able to observe all the galaxies that shape voids.

We also show in Figure 4.7 a reconstructed profile obtained from a sample of 100,000 particles in the same void stack: the reconstruction is noisier and with higher errors, but we are still able to reconstruct the void shape despite the more severe subsampling. This shows the capability of the algorithm to

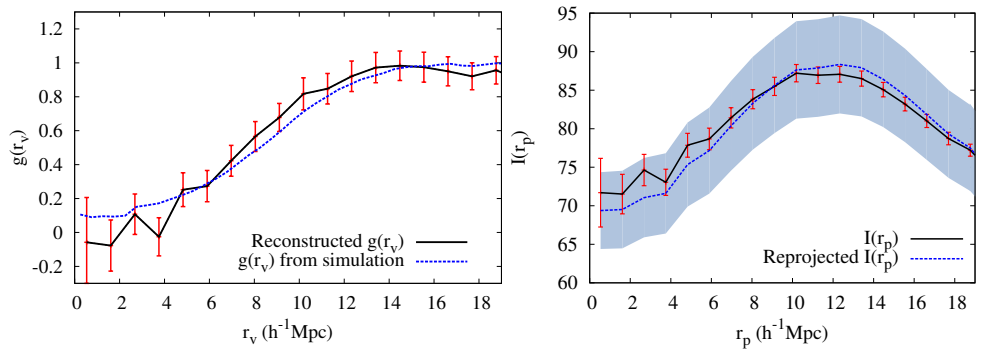

Figure 4.6: *Left panel:* The polynomial reconstruction matches the spherical profile from simulation within the error bars (except for the inner part of the profile, as discussed in Section 4.3). The reconstruction is obtained from a subsample of 200,000 dark matter particles of the total (about 10^9 particles). The error bars are correlated. *Right panel:* For the simulated void, I show the match between the $I(r_\mathrm{p})$ from simulated data and the reprojection from the reconstructed profile from a subsample of 200,000 dark matter particles of the total (about 10^9 particles). The light-blue bands are the errors on the reprojected $I(r_\mathrm{p})$ (that is obtained by projecting the reconstructed spherical density profile $g(r_\mathrm{v})$).

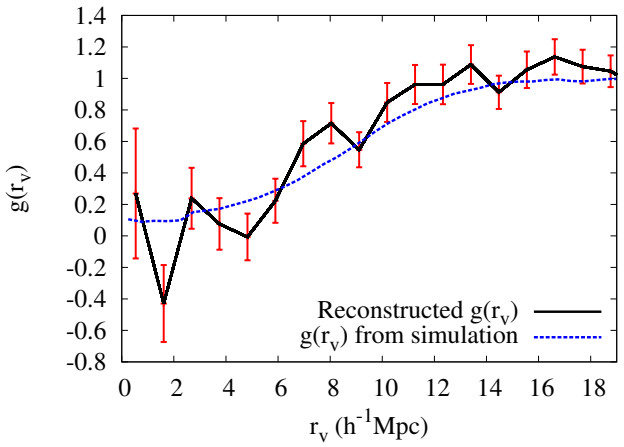

Figure 4.7: Reconstructed density for the simulated void from a smaller subsample (100,000 dark matter particles of the total, about 10^9 particles).

work with a subsampled number of galaxies, as in the case of real stacked voids. Furthermore the quality of the reconstruction can be assessed by checking the reprojection of the profile (as discussed in the next Section).

We compute error bars for the polynomial reconstruction method considering Poisson noise on galaxy counts in the bins for the projected $I(r_{\rm p})$ and use the bootstrap method to obtain the errorbars in the reconstruction and in the reprojection. The bootstrap error analysis gives a realistic estimation of errors due to the finite number of galaxies. We show in Figure 4.8 the choice of the order for the simulated void reconstruction (following the procedure discussed in Section 3.3.1). The order selected by the bootstrap method is the most realistic to choose, since the bootstrap analysis takes into account all the errors affecting the reconstruction.

The estimates for the density profile reconstruction are correlated. The errorbars are higher at small radii of the void because the algorithm of polynomial regularisation is less precise for inner points: the reconstruction is more complicated at the center, where the projection gets a major contribution from the outer shells of the sphere.

Before concluding this Section, I briefly comment the differences between

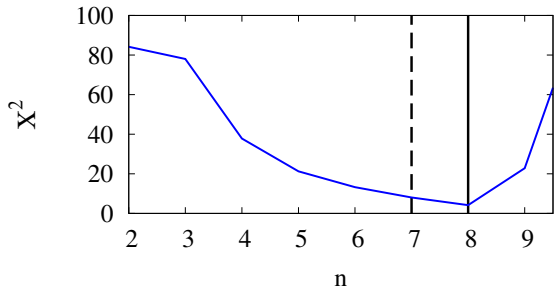

Figure 4.8: Choice of the order for the polynomial regularisation method of the Abel inverse, in the case of a simulated void. The solid black line is the order chosen by bootstrap method, which also coincides with the order chosen by the AICc information criterion and minimization of chi-squared. The dashed black line shows the order chosen by minimizing the reduced chi-squared.

the toy model and the simulation reconstructions. In the toy model the simplicity of the function used to roughly represent a density profile of a void gives rise to regular contours even after the distortions due to the added peculiar velocities. The contours in Figure 4.2 remain symmetric. On the contrary, the simulated stacked void has all the complexity of a real stacked void, including realistic noise in the projected shape of the void that we use to reconstruct the spherical density profile in real space. The presence of noise results in contours that have a slightly different extent in r_p compared to the corresponding redshift profile (see Figure 4.5).

Despite the presence of this kind of effect, arising in the realistic case of the simulation, the reconstruction algorithm still dominates the ill-conditioning of the inverse and is able to manage noise, obtaining a profile that is coherent (as discussed in this and in the next Section) with the profile from the simulation, used to test the reconstruction.

4.3.2 The reprojection, a quality test for the reconstruction

To check for consistency we reproject the reconstructed spherical void (right panel of Figure 4.6). This is an important sanity check for the reconstruction algorithm. In ill-conditioned problems, noise can easily blow up and completely dominate the results. In such case, the shape resulting from the reconstruction would lose any physical sense, since it would represent noise. The reprojection is a powerful tool to recognise noise-dominated reconstruction.

For this particular problem of reconstruction, we indeed have the possibility to re-invert the procedure by projecting the reconstructed density profile to check if its reprojection matches the projected profile $I(r_{\rm p})$ from which we made the reconstruction. The reconstruction of density profiles of voids is thus a fortunate case in which we are able to directly test the results of the reconstruction with data, using the reprojection.

In the case of data with noise, the consistency test allows to check results: the match of the reprojection can be used to validate the reconstruction for the profiles when applying the algorithm to real data, where the ill-conditioning due to noise must be dominated. The projection test would fail if noise dominated the reconstruction, thus it is a powerful sanity check for the algorithm to validate the reconstruction. So, in addition to the robustness of the method (that uses chi-square, AICc criteria and also bootstrap analysis to obtain a profile acceptable within the errorbars), we have here an independent quality test for the reconstruction.

Right plot of Figure 4.6 shows the result of this test for the simulated void: the reprojection matches the initial projection $I(r_{\rm p})$ (within the error bars), validating the reconstruction. The $I(r_{\rm p})$ is obtained from the simulation, by projecting the positions of galaxies and counting galaxies in radial bins on the plane of the projection. While the inner points of the profile are noisier as expected, we get high quality information for the part of the void where the density rises from low to high values near the wall.

I have presented the reconstruction with the polynomial regularisation method and discussed the role of the reprojection. The next Section shows the reconstruction with the singular value decomposition method.

4.3.3 The singular value decomposition method for the simulated void

We also show in Figure 4.9 the reconstruction with the singular value decomposition method, in order to check for consistency.

As discussed, the profile obtained in the case of the singular value decomposition method is more sensitive to the presence of clumps in the wall, because it considers all the points together to obtain the profile $g(r_v)$. This might affect the quality of reconstruction.

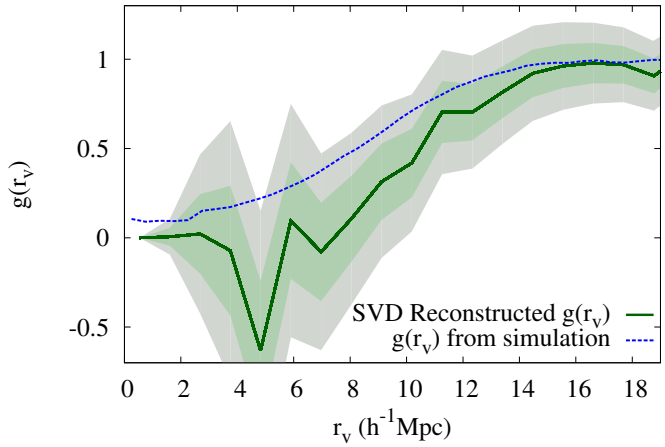

Figure 4.9: The singular value decomposition reconstruction matches the spherical profile from simulation within the error bars (green bands correspond to 1σ, grey to 2σ), but is more affected by noise than the polynomial regularisation method. The reconstruction is obtained from a subsample of 200,000 dark matter particles of the total (about 10^9 particles). The error bars are correlated.

Furthermore, the singular value decomposition method has larger error bars since it does not use prior information (except the truncation of the ma-

trix of singular values); while the polynomial regularisation method enforced polynomial smoothness. For this reason the singular value method is less precise than the polynomial method.

As a conclusion, apart from the mentioned difference, both methods (polynomial regularisation and singular value decomposition) allow to manage noise in the Abel inverse transform and show similar reconstructed profiles. For practical purposes we have chosen the polynomial regularisation method, that is more adapted in the case of voids, and use the second to check for consistency in the reconstruction.

The reconstruction of the spherical profile for stacked voids in the case of a dark matter particle simulation (left panel of Figure 4.6) is completely implemented and tested. As a further test of the quality of the reconstruction and capability of the algorithm, we describe in the next Section a test with stacked voids from a mock galaxy catalogue.

4.4 Galaxy mocks

To further test the capability of the reconstruction algorithm, we use a mock galaxy catalogue matching the properties of the Sloan Digital Sky Survey DR7. The mock catalogue is sourced from a high resolution N-body dark matter simulation with 1024^3 particles and 1 $h^{-1}Gpc$ side (also used in Sutter et al. (2013)) and part of the Public Cosmic Void Catalog[5].

The cosmological parameters of the simulation assume a WMAP 7-year Cosmology, the initial conditions of the simulation were obtained through a power spectrum calculated with `CLASS` (Blas et al., 2011) and realized with a modified version of `2LPTIC` (Crocce et al., 2006). The simulation is used as a source for an Halo Occupation Distribution model (Tinker et al., 2006; Zheng et al., 2007) to produce the galaxy catalogue. The model assigns to each dark matter halo of mass M a central galaxy and satellite galaxies, the mean number of central galaxies and satellites is described by:

[5]http://www.cosmicvoids.net

$$\left\langle N_{\rm cen}(M)\right\rangle = \frac{1}{2}\left[1+{\rm erf}\left(\frac{\log M-\log M_{\rm min}}{\sigma_{\log M}}\right)\right] \tag{4.11}$$

$$\left\langle N_{\rm sat}(M)\right\rangle = \left\langle N_{\rm cen}(M)\right\rangle\left(\frac{M-M_0}{M_1^{'}}\right)^{\alpha} \tag{4.12}$$

where we have $\sigma_{\log M}$, $M_{\rm min}$, M_0,$M_1^{'}$ and α as free parameters which are set to match the properties of a given galaxy population. Namely, we match the galaxy population to the main sample of SDSS DR7 (Strauss et al., 2002; Zehavi et al., 2011).

This allows us to have a mock galaxy catalogue exactly matching the real data to which we will apply the reconstruction algorithm. We thus run the void finder `VIDE` described in Sutter et al. (2014b) (and explained in Section 6.1) and obtain void stacks on which we run the reconstruction with polynomial regularisation.

With the methodology described in the previous Section, we apply the algorithm to stacked voids obtained from the mock galaxy catalogue matching the properties of the SDSS DR7. To assess the capability of the algorithm, we compare the reconstructed profile with the real-space profile of the stacked void from the mock catalogue. Furthermore, we use the reprojection of the profile as a quality test for the reconstruction, as described in Section 4.3.2. This independent test is a further validation of the reconstruction.

We show in Figures 4.10 and Figure 4.11 the reconstructions for stacked voids of respectively 10-15 h^{-1}Mpc and a 40-45 h^{-1}Mpc radii from the mock galaxy catalogue: in both cases the reconstructed real-space stacked void profile matches the profile of the stacked void from the mock catalogue. The sanity check of the reprojection serves as an additional consistency check for the quality of the reconstruction.

We notice that the first points are less precise: the errorbars are higher at small radii. As discussed in the previous Section, the reconstruction with the algorithm is more complicated at the center, where the projection gets a major contribution from the outer shells of the sphere, resulting in an increased precision for the profile when the radius increases. As expected, this

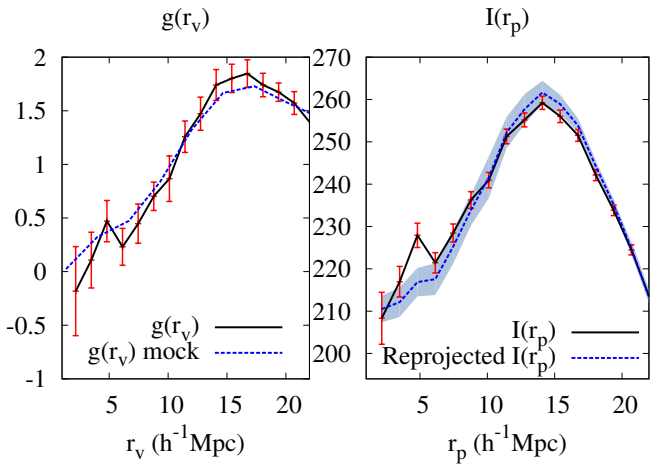

Figure 4.10: Reconstruction for a 10-15 h^{-1}Mpc stacked void from the mock galaxy catalogue: left plot shows the match between the profile in real space from the mock catalogue (dashed blue line) and the reconstructed profile $g(r_v)$(black line); right plot shows the match between the $I(r_p)$ from the mock catalogue (black line) and the reprojection from the reconstructed profile $g(r_v)$ (dashed blue line). The light-blue bands are the errors on the reprojected $I(r_p)$ (that is obtained by projecting the reconstructed spherical density profile $g(r_v)$). Here we have normalised to mean density for g (while $I(r_p)$ units are number of galaxies per $(h^{-1}Mpc)^2$).

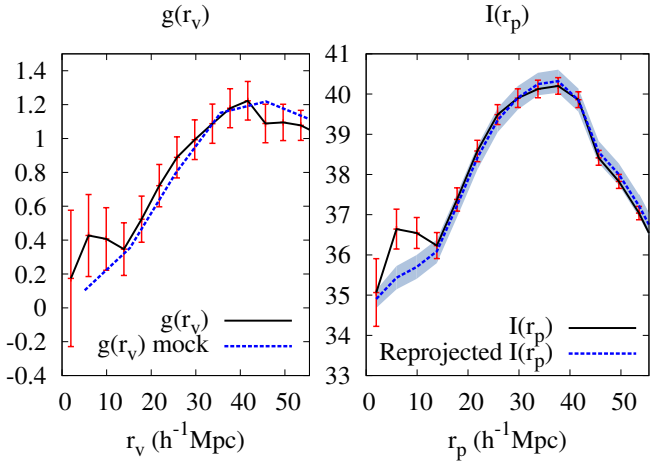

Figure 4.11: Reconstruction for a 40-45 h^{-1}Mpc stacked void from the mock galaxy catalogue. Construction and coloring is identical to Figure 4.10.

is correctly captured by the test with the reprojection, which also shows that the reconstruction is able to overcome the ill-conditioning and to recover the real-space density profile of the stacked voids.

The reconstruction of the spherical profile of stacked voids obtained from a mock galaxy catalogue targeted to match the properties of the SDSS DR7 sample (Figures 4.10 and 4.11) has been successfully tested — the set is now ready for a first application to real data: reconstruct spherical density profiles of stacked voids from the SDSS.

Chapter 5

Results: real space density profiles for stacked voids from SDSS DR7

The Chapter presents the first application of the algorithm to reconstruct density profiles of real cosmic void stacks in real space from the Sloan Digital Sky Survey.

5.1 Results

The algorithm is applied to the most recent real stacked voids catalogue from Sutter et al. (2012a). The catalogue is divided in datasets based on redshift and radius of stacks. More precisely, the datasets are: dim1 (z=0.0-0.05), dim2 (z=0.05-0.1), bright1 (z=0.1-0.15), bright2 (z=0.15-0.20), lrgdim (z=0.16-0.36) and lrgbright (z=0.36-0.44). The first application shows that consistent results can be obtained from real data, I focus on showing the general shape of real space profiles in a subset of the datasets of stacked voids.

It is clear that a good reconstruction requires void stacks with a large number of voids (to converge to an isotropic stack) and galaxies (to lower Poisson noise). I present a few first examples of real-space void profile reconstructions where these conditions hold at least approximately.

At first glance, considering the need of many voids and galaxies in the stack, we might think that stacked voids including a large range of radii for the void sizes would give better results. This is not the case: if the range of radii for voids in the stack is too large compared to the size of the smallest voids in the stack (for example a stacking of 5-25 h^{-1}Mpc), the wall of the stack is very thick, and the density profile noisy, since we are stacking voids with very different wall sizes and with a small common volume. Very large bins would then be undesirable since they would mix too many void scales, the lack of rescaling in these cases would result in a very broad profile.

Nevertheless, even if, on average the shape of voids is spherical, each void of the stack can have a different shape and a different wall thickness. Depending on the use to be done for the stacked void, it might be preferable to consider a range of radii for voids when stacking voids (instead of normalizing at the void radius). The rescaling could indeed distort the profiles and affect their use, it might thus be necessary to check whether the rescaling changes or not the properties of the stack (as discussed in Sutter et al. (2012b), where the rescaled and the non-rescaled case are compared).

For such cases we want to assess the capability of the algorithm to reconstruct the real space shape even with extreme cases — which means larger and possibly unscaled bins — in case one wanted to avoid rescaling that can affect the use of stacks for some applications. As we will further discuss, the example of the 5-15 h^{-1}Mpc stack in Figure 5.1 shows that the reconstruction works well even in this more extreme case: the reconstructed void has, as expected, a prominent wall — the physical properties are preserved in the reconstruction.

We finally point out that, in the eventuality of choosing to work with a range of radii for the stacks, the reconstruction algorithm continues to perform well, but a balance is generally needed between too large radii stacks (to avoid mixing too many scales) and too small radii stacks (to avoid poorly populated voids).

Indeed, choosing a range of radii that is too small (for example 10-12 h^{-1}Mpc) will not be adequate in the case of real data. In such small ranges

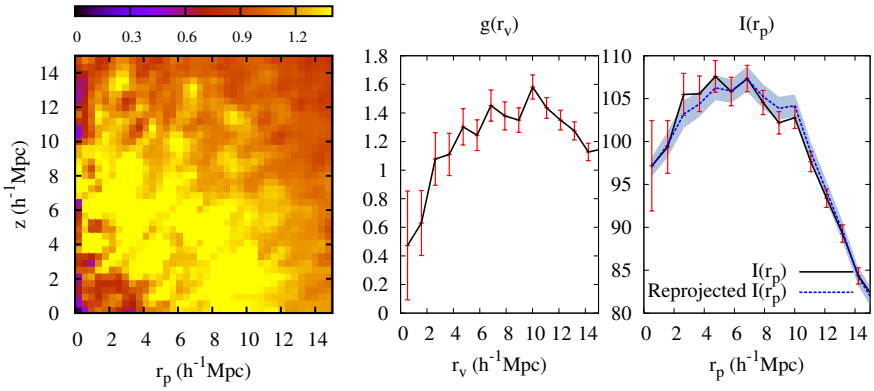

Figure 5.1: Results for a 5-15 h^{-1}Mpc stacked void of dataset dim2: from left to right we represent the density in redshift space $\rho(r_p, z)$, the reconstructed density $g(r_v)$ as a one dimensional plot, and finally the comparison between initial $I(r_p)$ (column density) and the reprojected $I(r_p)$ from the reconstruction. The light-blue bands on the right plot are the errors on the reprojected $I(r_p)$ obtained by projecting the reconstructed spherical density profile $g(r_v)$. Here we have normalised to mean density for g and ρ (while $I(r_p)$ units are number of galaxies per $(h^{-1}\text{Mpc})^2$).

the number of voids would be very limited, the noise on projection high and the reconstruction poor. This radius range is acceptable only for the simulation, where we have enough particles and can get a sample of 200,000 particles in a void stack with radius range of 10-12 h^{-1}Mpc.

Globally, datasets with more galaxies have lower error, so for datasets of voids with small radius (that have more voids) the error is smaller in the $I(r_p)$ and consequently also in the reconstruction $g(r_v)$. The projections of large voids have higher noise because there are less voids (and less galaxies). Furthermore, datasets at large redshift have higher noise, because less galaxies are detected at larger redshift.

So we limit the choice to low redshift and to small voids: we exclude datasets lrgbright, lrgdim and large sizes of voids (larger than 45 h^{-1}Mpc) since they have noise-dominated projected densities.

Finally, from the analysis of the full dataset, it empirically emerges that even datasets with many voids need to have an average of at least 1000 galax-

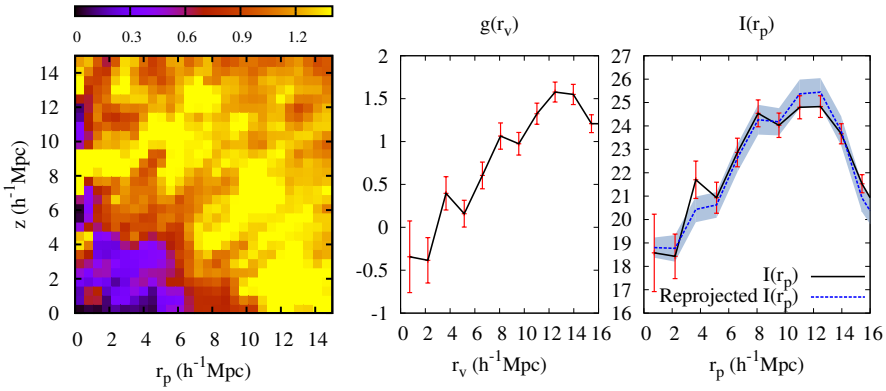

Figure 5.2: Results for a 10-15 h^{-1}Mpc stacked void of dataset dim2: from left to right we represent the density in redshift space $\rho(r_p, z)$, the reconstructed density $g(r_v)$ as a one dimensional plot, and finally the comparison between initial $I(r_p)$ (column density) and the reprojected $I(r_p)$ from the reconstruction. The light-blue bands on the right plot are the errors on the reprojected $I(r_p)$ obtained by projecting the reconstructed spherical density profile $g(r_v)$. Here we have normalised to mean density for g and ρ (while $I(r_p)$ units are number of galaxies per $(h^{-1}\text{Mpc})^2$).

ies for each void to have an acceptable signal-to-noise. We found that both datasets with many low populated voids and datasets with few highly populated voids have noise-dominated profiles. Only datasets well populated in *number of voids* and in *number of galaxies per void* can give acceptable profiles.

Following these considerations, to illustrate a first application of the method we have chosen stacked cosmic voids with an average of 1000 galaxies per void and (for some of them) at least 35 voids per stack. The number of voids in the stack must indeed allow the assumption of sphericity, this is why it can not be too low. For the considered cases the algorithm controls noise in the reconstruction and gives an acceptable spherical density profile.

We consider the stacked voids in table 5.1.

In this first application we show for each stack the distorted density profile of the stacked void in the plane (r_p, z), the reconstructed spherical profile in real space (as a function of the radius of the void r_v, since the profile is

Stack radius	Redshift	Dataset	Galaxies	Voids
5-15	0.05-0.10	dim2	173929	173
10-15	0.05-0.10	dim2	43527	41
20-25	0.10-0.15	bright1	21241	17
25-45	0.15-0.20	bright2	51913	37

Table 5.1: Stacked cosmic voids from SDSS data.

spherical) and the projection from which the reconstruction is done.

We also show, for each reconstructed profile, the reprojected density obtained from the reconstruction. In each plot of the reprojected density (right plot of Figures 5.1, 5.2, 5.3 and 5.4), the light-blue bands represent the errors on the reprojected $I(r_{\rm p})$ obtained by projecting the reconstructed spherical density profile $g(r_{\rm v})$. As discussed, we compute errors using bootstrap samples, in order to fully take into account the effects contributing to errors. The shape of the reconstructed profiles generally reaches gently the mean density.

The reprojected density shown in Figures 5.1, 5.2, 5.3 and 5.4 generally peaks at the radius of voids since it sums all the galaxies along the line of sight, which at that radius includes the wall. As pointed out in Section 4.3.2, the comparison of the reprojected density with the initial $I(r_{\rm p})$ from data allows to check the quality of the reconstruction, so we use the reprojected $I(r_p)$ as a diagnostic.

The reconstructions show the capability of the algorithm to obtain the spherical profile in real space even in the case of real — noisy — projections. All the profiles show the characteristic shape of the void: under-density in the center, wall and then return to mean density of the stack. As noted in the simulated stacked void, the first few points are noisier. After those initial points, the reconstruction is acceptable.

The fact that a good reconstruction can be obtained even in the case of very noisy data is an important asset of the algorithm. The noise reduction of the Abel inversion is critical in the case of high noise in the initial projection of the stacked void, *i. e.* for real stacked cosmic voids. The reconstruction also validates the stacking radius, since it is now possible to check the radius

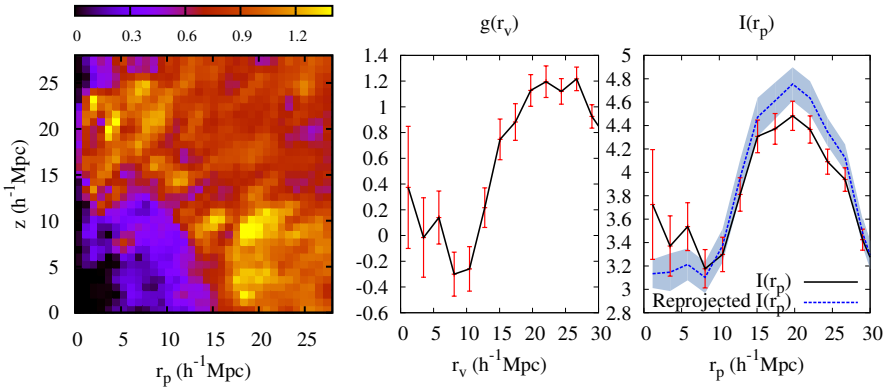

Figure 5.3: Results for a 20-25 h^{-1}Mpc stacked void of dataset bright1: from left to right we represent the density in redshift space $\rho(r_p, z)$, the reconstructed density $g(r_v)$ as a one dimensional plot, and finally the comparison between initial $I(r_p)$ (column density) and the reprojected $I(r_p)$ from the reconstruction. The light-blue bands on the right plot are the errors on the reprojected $I(r_p)$ obtained by projecting the reconstructed spherical density profile $g(r_v)$. Here we have normalised to mean density for g and ρ (while $I(r_p)$ units are number of galaxies per $(h^{-1}\text{Mpc})^2$). Low sampling leads to biases at small radii.

of the void stacks in real space.

We now briefly comment on the profiles. For dataset dim2 (Figure 5.1 and 5.2) we choose to represent stacks with two different radii ranges for the stacking, in order to show the effect of the different, overlapping ranges on the reconstruction. The first (see Figure 5.1) is a stacking of voids with radii in the range 5-15 h^{-1}Mpc, the second is a stacking of voids with radii in the range 10-15 h^{-1}Mpc. We immediately see in the reconstruction that the wall for the stack 5-15 h^{-1}Mpc (see Figure 5.1) is thicker and the slope of the density profile is higher compared to the 10-15 h^{-1}Mpc stacked void (see Figure 5.2). This is because for the 5-15 h^{-1}Mpc stack we include very small voids (with 5 h^{-1}Mpc of radius), so the wall starts at smaller radius. The stacking with larger bins will contain more galaxies, but the resolution for the shape of the wall will be lower and will result in a different shape. If we consider the stacking of voids with radii in the range 10-15 h^{-1}Mpc, the compensation in the profile is narrower, since the wall does not include the wall of the voids with 5 h^{-1}Mpc radius.

From this we can get two conclusions. The first is that the reconstruction of the density profile in real space correctly reflects the physical properties of the stack: we recover a thicker wall if we also consider small radii voids in the stack. The second is that, if we want to extract cosmological information from stacked voids, it is necessary to be cautious in taking reasonable radius ranges for the stacks and understand well the effects of the stacking on the density profile for each application. This affects the shape of the void (and the thickness of the wall, that is the compensation). Further work with density reconstruction in real space and stacking of reconstructed profiles might help to understand the dynamics of voids and eventually study the existence of a universal profile in real space with real data (while the existence of a universal profile has been studied with simulations by Hamaus et al. (2014); Sutter et al. (2013)).

We also note that the 10-15 h^{-1}Mpc stacked void has slightly negative values for the first points of the profile. We did not use any prior assumption for the density to be positive, and, as observed in the case of the simulated void,

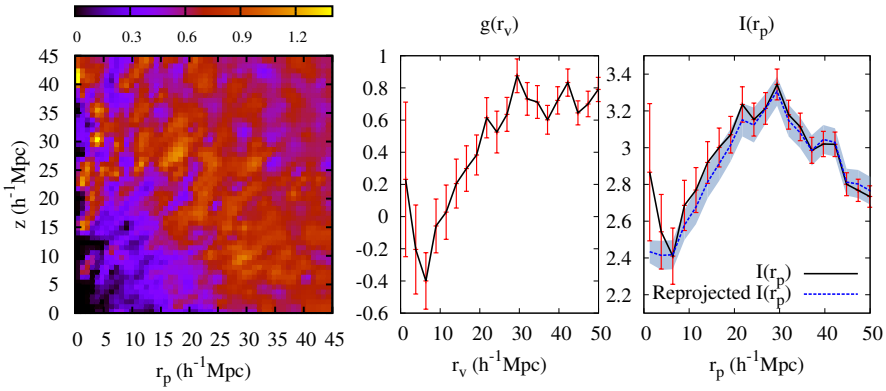

Figure 5.4: Results for a 25-45 h^{-1}Mpc stacked void of dataset bright2: from left to right we represent the density in redshift space $\rho(r_p, z)$, the reconstructed density $g(r_v)$ as a one dimensional plot, and finally the comparison between initial $I(r_p)$ (column density) and the reprojected $I(r_p)$ from the reconstruction. The light-blue bands on the right plot are the errors on the reprojected $I(r_p)$ obtained by projecting the reconstructed spherical density profile $g(r_v)$. Here we have normalised to mean density for g and ρ (while $I(r_p)$ units are number of galaxies per $(h^{-1}\text{Mpc})^2$). Low sampling leads to biases at small and large radii.

the first points of the reconstruction are less precise, while the reconstruction gains in precision when the radius increase (both because more galaxies are present at higher radii, and because of the feature of the algorithm of being more precise at high radii, discussed in Section 3.3.2). As expected, with less galaxies the profile loses precision in the center: the 5-15 h^{-1}Mpc stack is less affected by errors because of the high number of galaxies considered (173929 galaxies, see Table 5.1). The match within the errors of the reprojected $I(r_p)$ with the density $I(r_p)$ from data (right plot in Figure 5.1 and 5.2) is a consistency check for the reconstruction of both profiles from dataset dim2.

We now analyse the results for bigger voids. The stacked void from dataset bright1 with radius in the range 20-25 h^{-1}Mpc (see Figure 5.3), is more affected by noise, as expected because of the small number of voids. The reconstruction is noisier at small radii (lower than 10 h^{-1}Mpc), but the algorithm still manages to reconstruct the profile. The density starts increasing after 10

h^{-1}Mpc, and its slope is higher. We observe that the inner part of the profile has density values higher than expected. This might depend on the feature of the algorithm (that gains in precision at a few points from the center) and — in this case — on the assumption of sphericity: in the case of large voids, the low sampling of galaxies might result in large asymmetries and explain the observed higher densities in the center of voids.

Finally the profile of the stacked void of 25-45 h^{-1}Mpc of dataset bright2 (Figure 5.4) shows a lower density for the wall compared to other datasets.

I have shown as a proof of concept the first application of the algorithm to real stacked voids. The use of the reconstruction algorithm with well-populated stacks of well-populated voids in the case of real data allows to control noise in the reconstruction and to obtain the expected profile of stacked voids in real space. In the next Section I discuss limitations and future applications of the algorithm.

5.2 Discussion

I have presented a model-independent non-parametric algorithm to reconstruct spherical density profiles of stacked voids in real space. I have tested the algorithm in the case of a simplistic toy model in order to illustrate the method.

I computed the density profile in real space for a simulated stacked void. I used different methods to implement the Abel inverse with the aim of checking for consistency. The reconstruction of the density profile for the stacked void matches the profile in the simulation, showing the capability of the algorithm to obtain a reliable profile. Furthermore I have tested the algorithm with a realistic mock galaxy catalogue mimicking data from the Sloan Digital Sky Survey DR7. The mocks provide a validation of the algorithm in the case of scenarios with realistic signal-to-noise ratio, further enhancing its reliability for the application to real data.

Finally I showed a first application of the algorithm to real data and obtained the spherical density profile of real, well populated stacked voids from

the catalogue of Sutter et al. (2012a). I empirically set some constraints on the number of galaxies needed for each void of the stack (at least 1000 galaxies per void) and on the number of voids of the stack necessary to allow the algorithm to overcome noise (35 voids) and I showed that the reprojection is a valid consistency check to assess the quality of the reconstruction. I have shown the capability of the algorithm to control noise in the reconstruction of the void density profile in real space solely assuming sphericity, *i. e.* without introducing a prior on cosmological parameters, a dynamical model of voids or a model for redshift-space distortions.

The main limitation of the algorithm remains the high noise in the projection for datasets at high redshift and for large voids. Introducing reasonable priors may improve the reconstruction at the expense of giving up some of the explicit model independence. In the reconstructed stacked void density profiles, the shape and value of the over-density of the wall (the compensation) has an important role in understanding the physics of the void and is another factor to be investigated. The reconstructed density $g(r_{\rm v})$ might allow in future to discriminate between different cosmological models.

This first application of the algorithm on real voids is a proof of concept, the first step to a better understanding of the shape of voids. It is important to determine the reason of these differences in the shape of voids, that might depend on many factors (on the radius, physics and evolution of the stacked void). Lavaux and Wandelt (2012) and Sutter et al. (2012b) suggested the presence of a common profile for stacked voids of different radii and Hamaus et al. (2014) introduced an empirical function for the average density profile. The reconstruction of density profiles in real space offers the possibility to analyse this claim in observations. A future possible improvement of the algorithm would be the rescaling of the reconstructed profile for different sizes of voids to obtain statistical properties of profiles, although caution must be taken in this framework and further work is necessary to test whether the rescaling could change the properties of the stack and affect the use of voids for Cosmology.

As for future applications, since the Alcock-Paczyński test relies on the

shape of voids in redshift space to measure the expansion of the Universe, the cosmology-independent shape of the voids density profile in real space can help to reduce the systematic error in the test (Sutter et al., 2012b): it would give the shape of the void to compare with the distorted shape of the void in redshift-space data. Furthermore a complete knowledge of the real-space density profile of voids will allow to study their evolution without being affected by redshift distortions.

Finally, Verde et al. (2013) argued that a local cosmological-independent measure of the Hubble parameter (i. e. from the Alcock-Paczyński test) may help understanding the discrepancy suggested by recent data for the value of H_0 (see Planck Collaboration (2013), Riess et al. (1998) and Perlmutter et al. (1999), but also discussions in Fleury et al. (2013) and Marra et al. (2013)). Models of modified gravity (such as fifth force models) and dark energy (e. g. Spolyar et al. (2013), Clampitt et al. (2013) and Sutter et al. (2014d)) could be constrained with our algorithm: comparing the shape of the density profiles on simulations with the models and the real-space shape of profiles obtained applying our algorithm to observational data, we could discriminate between such models.

The reconstruction method does not make any cosmological assumption about the model, thus the density profile reconstruction of stacked voids in real space opens the way to better constrain the value of the Hubble constant and eventually cosmological models and new physics on current and future datasets such as the Euclid survey (Laureijs et al., 2011).

The next Section describes two possible direct applications using the reconstructed real-space density profiles.

5.3 Possible direct applications

In this Section I discuss two applications of the real-space profile reconstruction: we can use the real-space profiles to obtain information about the mass compensation and the velocity of cosmic voids.

5.3.1 Mass compensation and theoretical prediction of velocity profile

Using the density profile of voids in real space and defining $\Delta g = g(r) - \bar{g}(r)$ it is possible to obtain the mass included in the void:

$$\delta M(r) = 4\pi \int_0^r \Delta g r'^2 dr' \tag{5.1}$$

A measure of the mass as a function of radius permits to verify if the stacked void is *compensated*. A void is compensated when the mass present in the wall balances the lack of mass inside the void[1]. In such case the mass as a function of radius for $r \to \infty$ is zero, in other words the uncompensated mass is 0. Otherwise, if the uncompensated mass is lower than 0 the void is undercompensated; if the uncompensated mass is higher than 0 the void is overcompensated.

While with real data it is difficult to check for a compensation for each stacked void of different size and at different redshift because of Poisson noise, by considering all the stacks together it is possible to obtain an average void profile in real space. This is of course a strong assumption, that we will drop as soon as new surveys provide us with more galaxies, but meanwhile it allows us to show the potential of having a real space density profile of the void for such analysis.

Furthermore, the assumption is physically motivated by the universality of void density profiles shown by Hamaus et al. (2014) with simulations. Future surveys will allow the measurement of redshifts for a higher number of galaxies, giving highly populated stacks of voids. It will thus be possible to measure the mass for stacked voids at different redshift and of different size from real-space density profiles.

For the moment, we consider the average of the reconstructed density pro-

[1] I note that the compensation of voids must not be confused with the presence of the overdensity in the wall: a void can be under-compensated but still have an overdense wall. Thus it is difficult to decide whether a void is compensated or not just looking at the density profile, it is necessary to calculate the mass included in the void, or eventually look at the theoretical velocity profile.

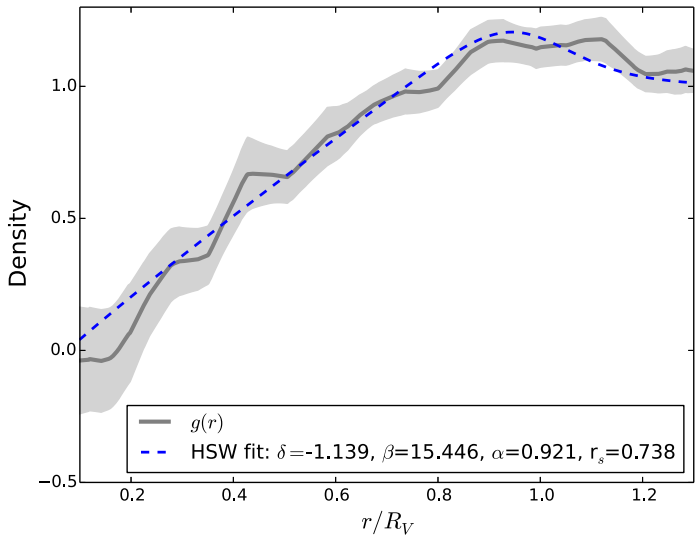

Figure 5.5: Average real-space reconstructed void fitted with the HSW profile. The parameters of the fit are shown in the plot. The averaging washes out some features of the profile, but it is still possible to describe the profile with the same functional form.

files of stacked voids in real space. The average stack considered for the calculation of mass is reproduced in Figure 5.5. For the average I have considered the reconstruction of all the voids with radii from 10 to 35 h^{-1}Mpc for which the ill-conditioning can be overcome (see discussion in Section 5.1). Interestingly, the real space reconstruction of the density profile provides us with an average profile of voids following the universal density profile functional shape found by Hamaus et al. (2014) and Sutter et al. (2013) in simulations. At small radius the profile I reconstruct has slightly negative density, but positive within the errorbars, it must be noted that at small radii the errorbars are higher. As discussed in Section 5.1, this is a feature of the reconstruction algorithm which gains in precision as the radius increases. I use the functional form from Hamaus et al. (2014) to fit the average real-space density reconstruction.

The HSW (Hamaus et al., 2014) profile is defined as:

$$\frac{\rho}{\bar{\rho}} = \delta_{\rm center}\frac{1-(r/r_s)^{\alpha}}{1+(r/R_{\rm v})^{\beta}} + 1 \tag{5.2}$$

where $\delta_{\rm center}$ can be identified as the underdensity in the central core (relative to the mean density), r_s is the scale radius at which $\rho_{\rm v} = \bar{\rho}$ and α and β are respectively the inner and outer slopes of the void's compensation wall. I note that since we are averaging on all voids, we are losing some properties of the profile, namely the compensation wall is made shallower by large voids. The average of independent stacks is more robust than stacking all the voids in one stack, since it avoids washing out the properties of the voids in an excessive way by rescaling all voids. The use of many stacks, while being an acceptable assumption at this stage (as discussed above), is nevertheless the reason why the average profile does not match some of the scaling relations found by Hamaus et al. (2014). The average profile used here as an example thus needs to have all four parameters proposed by the HSW universal profile.

I now use the average real-space profile obtained using the reconstruction algorithm to analyse the mass compensation of voids in real space with real

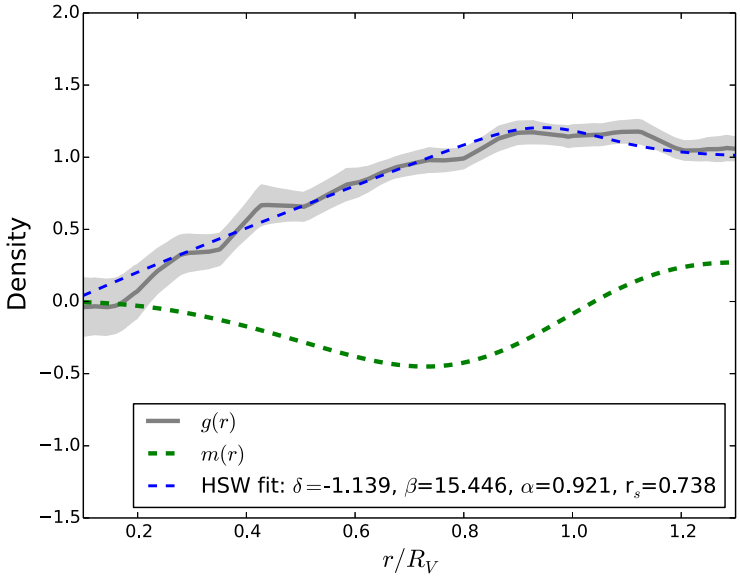

Figure 5.6: Average mass as a function of radius, the considered void is overcompensated.

data. This is just a proof of concept since ideally one should avoid averaging profiles; future highly-galaxy-populated datasets will allow a measure of the mass compensation per stack. Properties such as the ones derived for dark matter and HOD models by Hamaus et al. (2014) and Sutter et al. (2013) will be tested for cosmic voids from real data and in real space, thus promising to shed light into the compensation of voids.

Figure 5.6 shows the $\delta M(r)$ for the average real-space density profile from real data. For the average we obtain an overcompensated void, probably due to the fact that we are stacking mostly small voids (the average radius is lower than 17 h^{-1}Mpc, according to Hamaus et al. (2014), lower than the radius scale at which voids are compensated, 17.6 h^{-1}Mpc).

From the density profile it is also possible to obtain a theoretical prediction for the velocity profile of voids in real space, considering linear theory and assuming a cosmological model. As discussed in the next Chapter, the determination of velocity without any assumption about the cosmological model

is more interesting as well as more challenging. Nevertheless, with the idea of comparing to tests with simulations, we can compute the theoretical prediction for the velocity profile within a model consistent with ΛCDM. The formula to obtain the velocity profile[2] Peebles (1993) is:

$$v_{\rm v}(r) = -\frac{1}{3}\Omega_m^{\gamma} H(z) \frac{3}{r^2 \bar{g}} \frac{\delta m(r)}{4\pi} \tag{5.3}$$

where $H(z) \simeq 67.4\ km\ s^{-1}\ Mpc^{-1}$ is the Hubble constant[3], $\Omega_m \simeq 0.314$ [4] is the matter content in the Universe and $\gamma \simeq 0.55$ is the growth index of matter perturbations. Figure 5.7 shows the obtained velocity profile. Consistently with the mass compensation, the velocity becomes negative, which is coherent with an infall velocity from the outside towards the wall for an overcompensated void.

To push the proof of concept further, we can also study the differences between small and big voids cases and the high and low redshift cases with the density profiles in real space. This shows the possibility of using the density profile of voids of different sizes and at different reshift from real data to test mass compensation. The mentioned recent works on simulations (Hamaus et al., 2014; Sutter et al., 2013) analysed these differences.

The real space density profiles allow to test such claims on real data for the first time, in a model independent framework. With the limited statistics available from real data, we group stacks of voids smaller and bigger than 15 h^{-1}Mpc. A scaling of voids is necessary, where we scale stacks by the mean radius of the wall range, thus preserving the features of the average shape for each group. Figure 5.8 shows the average real space density profile comparison of stacked voids of different size (smaller and bigger than 15 h^{-1}Mpc) from real data, as well as their fit with the HSW profile.

The plot shows some interesting features for the profiles. First I note that, as expected, the reconstruction algorithm lacks in precision for the inner

[2]The formula is used by Hamaus et al. (2014) in a slithly different form, as a function of the integrated density contrast, but the two are equivalent.

[3]Using values from the Planck collaboration (Planck Collaboration, 2013)

[4]See footnote 3.

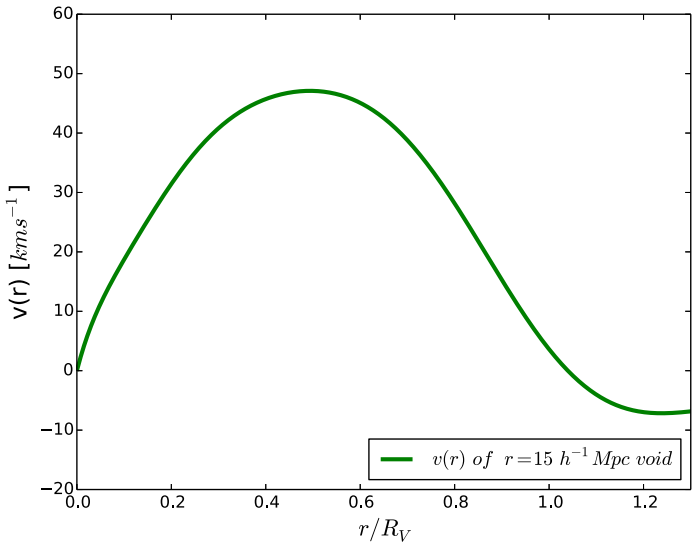

Figure 5.7: Theoretical prediction for the velocity profile as a function of radius, computed using linear theory and assuming a ΛCDM cosmological model.

points, resulting in a central density lower than 0 for large voids. While the resulting profile are too noisy to reach precise conclusions, generally larger voids appear to be more underdense (although, as discussed in the previous Chapters, the reconstruction in the inner part of the profile is less precise). This is consistent with the fact that larger voids have emptied more. While this feature has been suggested through the use of density profiles in redshift space and simulations in real space, the real-space reconstruction has the power to validate it.

Furthermore, using the HSW fit, I can study the mass compensation and the theoretical prediction for the velocity profiles (assuming a cosmology) for the two cases of small and large voids. The result is shown in Figure 5.9. Small voids are overcompensated, and big voids are undercompensated. The velocity profiles are coherent with this interpretation, since small voids have a negative infall velocity denoting a flow of galaxies from outside the voids towards the wall of the void; while big voids maintain a positive velocity

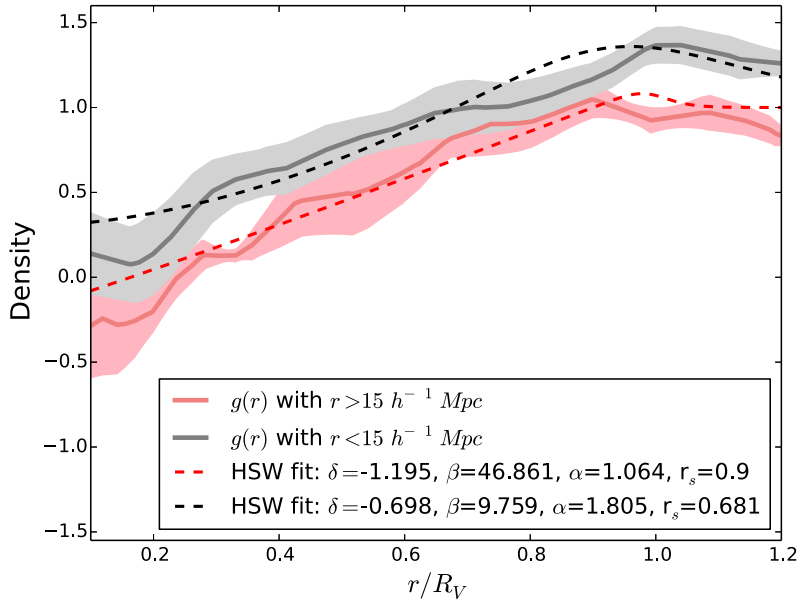

Figure 5.8: Average real-space reconstruction of stacked voids of different size (smaller and bigger than 15 h^{-1}Mpc) fitted with the HSW profile. The parameters of the fit are shown in the plot for both cases.

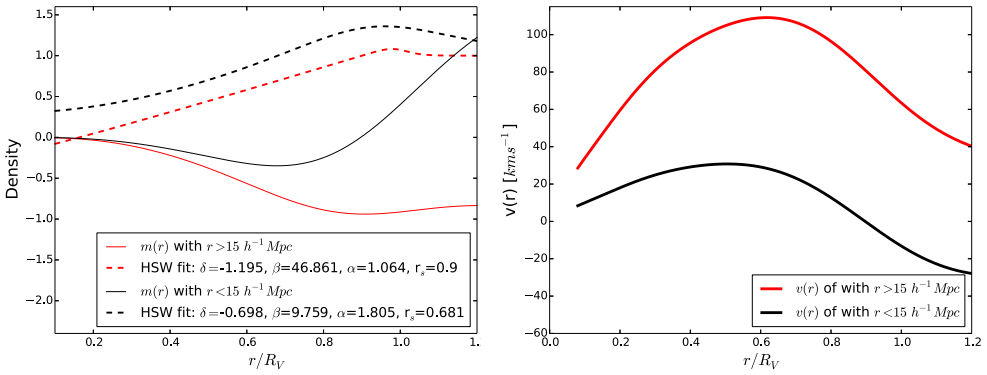

Figure 5.9: Mass compensation and velocity profiles (assuming a cosmology) for the two cases of small and large voids.

denoting an outflow, the velocity will eventually reach zero at large distances. Furthermore the amplitude of velocities is larger for large voids. These real data results match surprisingly well the results from simulations found by Hamaus et al. (2014).

Similarly, real space profiles allow to look at variations in the shape of voids with time, since they give us profiles independent from redshift distortions, but at different redshift. With the limited statistics available from real data, we group stacks of voids at redshift lower and higher than $z = 0.15$.

Figure 5.10 shows that voids at higher redshift appear to be more underdense and shallower. While this seems contradictory with the previous analysis, since voids at higher redshift should be less evolved (younger) — with higher compensation walls, steeper profiles and less underdense — this does not seem the case. Such behaviour can be understood considering that at higher redshift we are capturing less galaxies, which means that we are more sensitive to big voids, because the cosmic web and its void-subvoid structure is only captured smoothly, thus erasing small voids.

Being sensitive to larger voids, it makes sense to expect voids at high redshift to be shallower and emptier. So for voids at high redshift there is a selection effect preferring big voids, thus impacting the density profile. For this reason, when considering the mass compensation and the velocity profiles,

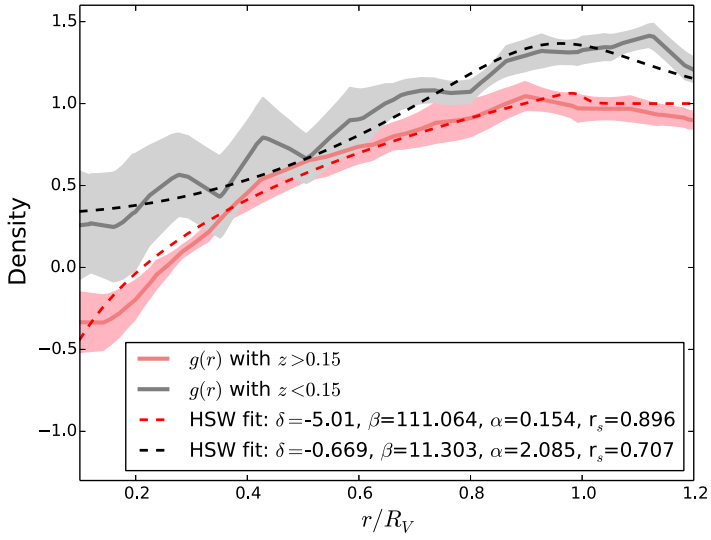

Figure 5.10: Average real-space reconstructed of stacked voids at different redshift, lower and higher than $z = 0.15$, fitted with the HSW profile. The parameters of the fit are shown in the plot for both cases.

we see a similar difference to the one observed between average shapes of voids of different sizes. When more data are available, real-space density profiles will allow to disentangle the selection effect from the physical differences and will permit us to analyse voids at different redshift with varying size, thus shedding light into the evolution of voids.

In this Section I showed as a proof of concept an analysis of void density profiles in real space at different redshift and of different size. I have as well analysed the compensation of mass for the same cases and obtained a theoretical prediction for the velocity profiles from linear theory, when assuming a cosmological model consistent with ΛCDM.

The analysis of real-space density profiles will extensively profit of future surveys, which promise to increase the quality of void density profiles through an improvement of statistics. As it is discussed in previous Chapters, it is possible to relate the density profile of voids to a constrain of models of modified gravity (Spolyar et al., 2013). Eventually, the understanding of the differ-

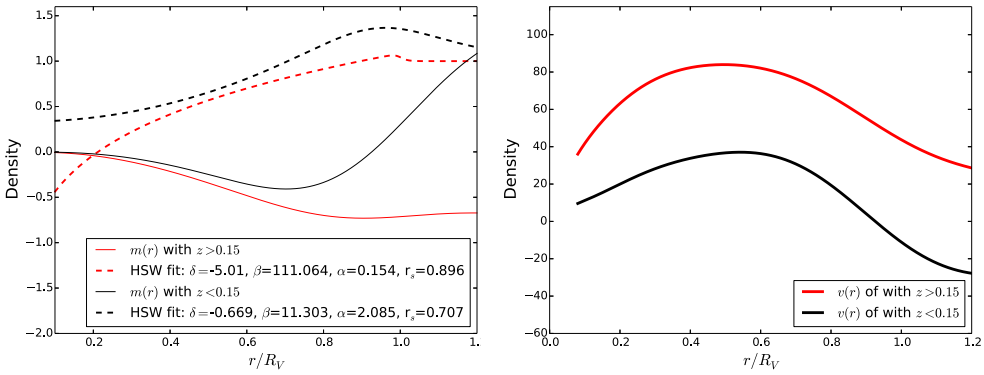

Figure 5.11: Mass compensation and velocity profiles (assuming a cosmology) for the two cases of high and low redshift stacked voids.

ences between the mentioned cases can shed light into the evolution of voids — directly related to dark energy.

5.3.2 Velocity reconstruction

A further application based on the real-space density profile of voids is its use to infer properties of the peculiar velocity field around voids without any assumption (except the sphericity of stacked voids in a homogeneous and isotropic Universe). Extreme caution must be taken for this application, to maintain the cosmological model independence. This approach is different compared to the one used in the previous Section, where, *assuming a cosmological model* it is possible to infer a prediction for the velocity profile within the framework of linear theory. The tool to reach the velocity information is the comparison between the real-space shape that we obtained from the reconstruction and the redshift-space shape that we directly obtain from finding and stacking voids.

But there is a problem: what distorts the void in redshift-space is *both* the effect of peculiar velocities *and* the expansion of the Universe (*i.e.* the Hubble flow). Thus the two effects are partially degenerate.

This is particularly unfortunate, since one of the motivations to study the velocity field within voids is its use to correct the Alcock-Paczyński test for

the effect of peculiar velocities and to extract cosmological information non affected by systematics (which is the reason why a model independent approach is particularly interesting compared to the method used in the previous Section). While obtaining the real-space density profiles stands as a first step towards a modelling of velocities, it is non trivial to separate the two effects in a model independent way — allowing to correct cosmological measurements for the effect of peculiar velocities.

Usually, the more non trivial is the step, the more difficult the challenge and promising the result: a cosmology-independent model for the evolution of voids is, without any doubt, a challenging goal to focus on. In our case, we can consider two approaches. The first is the use of simulations with and without the addition of peculiar velocities: the comparison of voids in both cases might allow us to estimate the effect of velocities on void's shape. This approach is promising, but relies on simulations, which — being based on our models — could fail in capturing all the effects of the evolution of the cosmic web. It is nevertheless a valid approach to reach a first insight towards the understanding of velocities. The simulation approach is described in the next Chapter.

A second approach — potentially extremely powerful, but difficult — is to consider that there might be a way to extract independent information about the velocity field of voids from the comparison of the real and redshift density profiles of voids. Considering a stacked void, we can assume spherical symmetry (in a homogeneous and isotropic Universe). Thus the velocity field can be expressed as function of the radius of the void $r_{\rm v}$. The velocity field departs from the center and expands radially (if the void is expanding, otherwise it contracts, but still radially). On the contrary, the Hubble flow can be assumed parallel to the line of sight and is *the same* for each point of the void which is at the same distance from us. The redshift distortion of the void due to peculiar velocities has an angle dependence — which the Hubble flow has not. A possibility to extract velocity could be to consider a joint fit of the Hubble parameter and the peculiar velocities for each point of the void.

To reach such goal, we consider a stacked void in redshift space and in real

space. The coordinate along the line of sight of the galaxies belonging to the void will be distorted because of the two mentioned effects: peculiar velocities and the expansion of the Universe. The line-of-sight coordinate of a galaxy is written:

$$z_{\rm m} = z_{\rm c} + H_0 r_{\rm z} + v\cos\theta \tag{5.4}$$

where $z_{\rm m}$ is the *measured* redshift of the galaxy, $z_{\rm c}$ is the redshift of the center of the stacked void, $r_{\rm z}$ is the projection along the line of sight of the distance of the galaxy from the center of the void and v is the peculiar velocity of the galaxy. The angle θ is the angle between the line of sight and the direction from the center of the void to the galaxy. If we consider the center of the void, we write the redshift of the galaxy relative to the void center as $z = z_{\rm m} - z_{\rm c}$. Thus we obtain the following expression:

$$z = H_0 r_{\rm z} + v\cos\theta \tag{5.5}$$

It is then possible to write a relationship between the real-space density g and the redshift-space density ρ:

$$\rho(z, r_{\rm p})dz = g(r_{\rm z}, r_{\rm p})dr_{\rm z} \tag{5.6}$$

Both densities are expressed as functions of the radius of the projection $r_{\rm p}$, and of the radius along the line of sight: $r_{\rm z}$ in real space and z in redshift space. It is possible to calculate $dz/dr_{\rm z}$, the exact calculation is described in the Appendix B. I obtain:

$$\frac{dz}{dr_z} = H_0 + v'(r_{\rm v})\cos^2(\theta) + \frac{v(r_{\rm v})}{r}\sin^2(\theta) \tag{5.7}$$

Thus I can write:

$$\rho(z, r_{\rm p})\left[H_0 + v'(r_{\rm v})\cos^2(\theta) + \frac{v(r_{\rm v})}{r}\sin^2(\theta)\right] = g(r_{\rm z}, r_{\rm p}) \tag{5.8}$$

In principle, I have a relation for each angle θ. It is an inhomogeneous linear first-order differential equation. It is important to notice that I have

assumed spherical symmetry to describe peculiar velocities, I described them as a function of the radius of the void $r_{\rm v}$. This assumption is a direct consequence for voids stacks in a homogeneous and isotropic Universe, thus it is not particularly constraining.

A possible use for the equation relating the real- and redshift-space voids is the assumption of H_0, such that the peculiar velocity can be calculated directly solving the equation. Nevertheless, with the wish of keeping a velocity reconstruction *independent* from the cosmological model, a different method can be considered.

I assume a polynomial form for the velocities: $v(r_{\rm v}) = ar_{\rm v}^3 + br_{\rm v}^2 + cr_{\rm v} + d$. The choice of the analytical form is not particularly important to describe the method, as long as it is able to approximate the shape of the velocity profile; it is always possible to obtain a higher order polynomial estimation of the velocity profile, without any change in the logic of the method. With this assumption and considering the distorted density $\rho(z, r_{\rm p})$ from data and the reconstructed $g(r_{\rm v})$, it is possible to find the best combination of coefficients H_0, a, b, c and d.

The cosmological component is thus only degenerate with some part of the velocity function, namely the part of the velocity which scales with $r_{\rm v}$ (i. e. for our example c). Thus, in principle, the real-space density profile reconstruction of stacked voids permits to reach an independent constraint on the higher order terms of the peculiar velocity.

While I leave for future work the exploration of this powerful independent method to extract information about the peculiar velocities around void stacks, I constructed a first test using the toy model described in Section 4.2. With this model and assuming the value of H_0, I reconstructed the input peculiar velocity used for the model (namely a linear function of the void's radius) (see Figure 5.12).

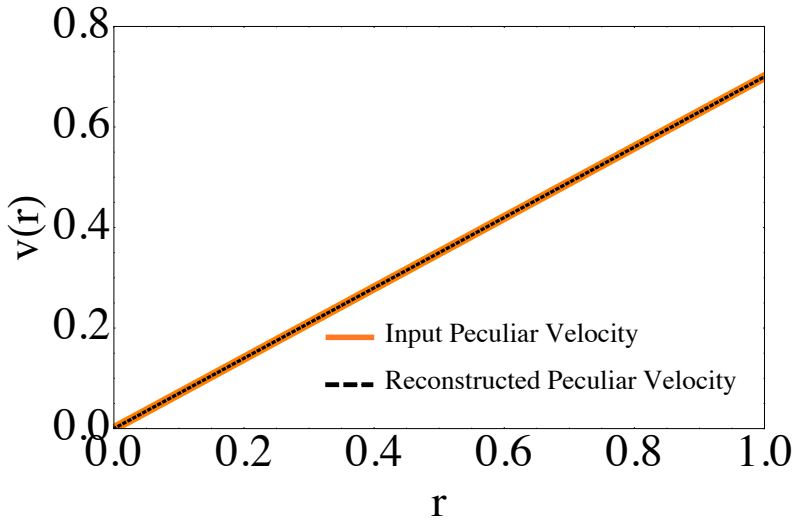

Figure 5.12: The test of the velocity reconstruction with the toy model: assuming the value of H_0, the Figure shows the reconstructions of the input peculiar velocity used for the model.

The model independent velocity reconstruction is an interesting challenge and will be considered as a future application for the algorithm.

The use of the real-space density profiles of stacks to constrain higher order terms of peculiar velocities around voids promises to be crucial to reach the level of precision requested to cosmological probes in the 1% precision Cosmology era.

I have discussed in this Section the possible approaches to obtain the velocity information; in the next Chapter I follow the first approach described above and I investigate the effect of peculiar velocities by finding voids in a simulation with and without peculiar velocities.

Chapter 6

The effect of peculiar velocities and VIDE

> The results presented in this Chapter will soon be submitted in Pisani, Sutter and Wandelt (2014) *"Mastering the effects of peculiar velocities on voids"* (Pisani et al. (2014c), in prep.), thus are part of a work done in collaboration with Paul M. Sutter and Benjamin Wandelt.

To understand the effect of peculiar velocities it is necessary to analyse what difference they make for the physical features of voids *and* for the way the void finder selects and defines voids. We want to assess the impact of both processes.

The two processes are distinct: when considering a field with and without peculiar velocities, this will affect the shape of voids on a one-to-one basis. Thus voids in the density field will *change* both in shape — their density profile and geometrical shape could be affected — and in number (for example small voids can be smeared out by the effect of velocities, thus disappearing, or can become part of a bigger void). This is a physical process that we wish to understand.

Furthermore, the physical effect of peculiar velocities will affect the way the void finder selects (i. e. defines) voids in a non trivial way: the motion of

galaxies will result in a change of voids, and it is difficult to establish if — and how — this will affect the way the void finder selects empty regions.

While the physical differences between voids with and without peculiar velocities cannot be dissociated by the differences introduced in the way the chosen void finder selects voids, it remains extremely useful to assess the impact of velocities for both effects together. Indeed, when using the void finder on real data, both these effects — affecting voids — should be understood to take into account the systematics for the extraction of cosmological information from voids.

By comparing voids in simulations with and without peculiar velocities it is possible to understand the effect of velocities on the shape of voids, on their size, on their number and on their position when using a particular void finder, in our case `VIDE`. One of the features of `VIDE` is to take into account the foam-like aspect of the cosmic web through the use of the Voronoi tessellation (introduced in the study of the large-scale structure of the Universe by Icke and van de Weygaert (1987) and explained below), thus being particularly sensitive to the physical features of voids.

This study is thus based on `VIDE`, but since many void finders use similar methods, it can provide general guidelines to treat with peculiar velocities. Numerous studies use Voronoi-watershed-based void finders, thus with this analysis we assess the impact of velocities for many works using voids to extract physical information (e. g. ISW and Alcock-Paczyński test). This work also provides guidelines on how to account for such effects.

Basically I provide an answer to the following question: how do peculiar velocities affect observed voids? To simulate a dense galaxy survey with and without peculiar velocities, I use Halo Occupation Distribution models with an N-body simulation. I run the watershed-based void finder in both cases and I analyse the differences between the resulting voids catalogues: how is void ellipticity affected by peculiar velocity in our surveys? To what extent can we reliably extract cosmological information from voids in surveys — affected by peculiar velocities — and what corrections need to be done to consider the effect of peculiar velocities?

I focus particularly on the variation of the average ellipticity due to peculiar velocities. This value should allow improving estimates of cosmological parameters from the application of the Alcock-Paczyński test on voids. It is important to use HOD catalogues to have a realistic estimate that can be used to correct applications with void catalogues based on real data.

So far I have considered the use of void stacks, without worrying about how we find voids and stack them. A high performance tool has been used — and sometimes modified, depending on the purpose — to obtain the stacks: the public void finder VIDE.

To understand to what extent the void finder and peculiar velocities might affect void research, I first need to describe VIDE; this is the subject of the next Section.

6.1 VIDE

VIDE[1] (Void IDentification and Examination), a widely tested improved version of ZOBOV[2], is the void finder used in this work to identify voids. For a detailed description see Sutter et al. (2012a); Sutter et al. (2014b)[3].

Improvements include a pipeline able to handle data from real surveys through a reliable consideration of survey masks. As a brief description, the void finder tessellates the tracers into Voronoi cells and creates basins and ridges though the use of the *watershed transform* (Platen et al., 2007).

The idea of using *Voronoi tessellation* to describe the large scale structure has been introduced in pioneering papers (Icke and van de Weygaert, 1987; van de Weygaert and Icke, 1989; van de Weygaert, 1994) and is now widely used, resulting particularly adapted to describe the foam-like feature of the cosmic web.

An alternative to the use of Voronoi tessellation is the use of the Delaunay tesselation field estimator (DTFE), based on the dual of the Voronoi diagram, called Delaunay tessellation. For an extensive and pedagogical description, see

[1] The french word for *void*.
[2] ZOnes Bordering On Voidness, see Neyrinck (2008).
[3] Details can also be found at http://www.cosmicvoids.net .

Schaap and Van De Weygaert (2000); van de Weygaert and Schaap (2007); van de Weygaert and Schaap (2009) and for a recent application and comparison of the methods see Platen et al. (2011), which uses magnitude-limited and volume-limited mocks of the SDSS redshift survey from the Millennium simulation (Springel et al., 2005) to compare different reconstruction methods. Another project aiming to compare different techniques to find voids is the Void Finder Comparison Project (Colberg et al., 2008).

For the sake of clarity, I add some details on the functioning of the process allowing to go from a field of particles (would the particles be dark matter particles, halos or galaxies — basically any tracer the user chooses) to the definition of voids. This is the process computed by the void finder `VIDE`.

The process can be described through the following steps:

- *The void finder tessellates the tracer field into cells.* The tessellation is done by means of the **Voronoi tesselation**[4] (see Figure 6.1). Taking the tracer as a seed, this tessellation considers all the points closer to that seed. This allows to define a volume around each tracer. The volume around each tracer defines the cell. A local density is thus defined for each cell:

  $$\rho_{\text{cell}} = \frac{1}{V_{\text{cell}}}$$

  where V_{cell} is the volume of the cell. This definition gives a logical result: in places of the tracer's field where there are few tracers, the volumes around each tracer will be bigger, thus corresponding to a lower density; on the contrary, where there are many tracers, the volume around each tracer will be small, resulting in a high density for the cell. Figure 6.1 shows a Voronoi tessellation in 2D; it can be noticed that, where the density of tracers is higher, cells are smaller and vice-versa.

- *It creates basins from cells.* Cells are merged into basins, which center is the cell only surrounded by higher density cells. This merges basins around the local minima in the cell density field.

[4]When defining a Voronoi tessellation, the possibility of degeneracies must be taken into account to ensure the robustness when computing the diagram.

- *It uses the* ***watershed transform*** *to further merge basins into zones.* Basins are merged in one void if, looking at the density along borders, the border with lower density (compared with other borders of the basin, not with the center of the basin) is common between the two basins. A density-based threshold is added preventing basins to merge if the density of the wall between them is higher than $0.2\,\overline{\rho}$, the mean density of the whole field (a simulation box or a survey). This cut preserves the voids to be in average overdense, only adding together cells if the ridge density if low. This cut is prior to the proper void finding.

- *Each zone is a void.* Here, a second cut imposes that the density within $0.25R_{\rm eff}$ of the void is lower than $\overline{\rho}$. This cut guarantees that the void has a true underdensity in its barycenter, excluding voids that are very large but with only a mild underdensity. The effective radius $R_{\rm eff}$ is defined below. This cut is posterior to the proper void finding

- *The ridges represent the void walls.* Because of this definition of voids, the entire volume will eventually be filled with voids, only leaving the ridges separating the underdensities. Thus the borders of voids will include the high density walls.

The void definition used by `VIDE` presents numerous advantages. First it does not assume any *a priori* shape for voids (since is makes use of the Voronoi diagram to tessellate the density field), which is important to characterise these structures in the correct way. Second, it considers the void hierarchy through the basin definition: voids are made of subvoids, preserving the multi-level hierarchical structure of the cosmic web.

Finally, `VIDE` takes into account the surveys boundaries and masks, which is extremely useful, as it allows application to real data. The volume V of the void is defined as the total volume of the Voronoi cells contributing to the void, and the effective radius $R_{\rm eff}$ of the void as the radius of a sphere with volume V. It is also important to define the void center: it is the volume-weighted

[5]Image created by the author using a modified version of the `Mathematica` notebook publicly available at http://mathworld.wolfram.com/notebooks/ComputationalGeometry/VoronoiDiagram.nb

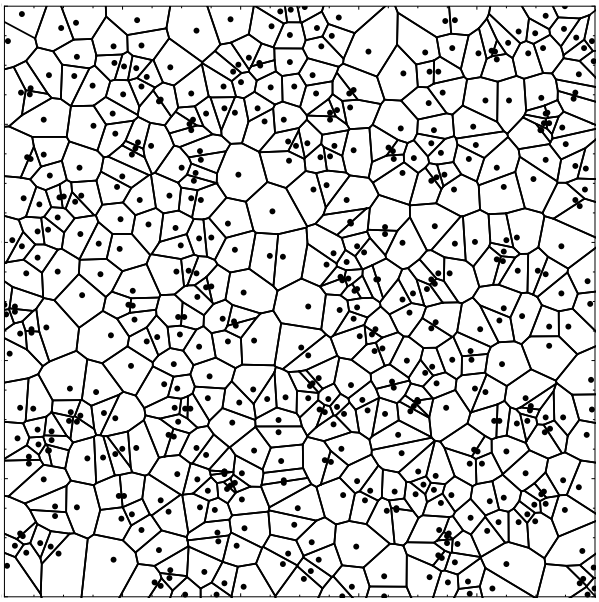

Figure 6.1: Example of Voronoi tessellation.[5]

center of the void Voronoi cells. A final consistency criterion for voids is to exclude voids with effective radii lower than the mean particle separation, since they are an effect of Poisson fluctuations in the tracer population.

Now that I have described what `VIDE` does, I introduce in the next Section the simulations used for the analysis of the effect of peculiar velocities.

6.2 Peculiar velocities affect voids and VIDE

In this Section I first describe the simulation used for the comparison, then I present the matching algorithm and finally I illustrate the one-to-one comparison of voids.

6.2.1 Simulation and HOD details

The simulation we use in this work is a 1 h^{-1}Gpc box size dark matter N-body simulation, for which accuracy and error behaviour have been improved for

cosmological volumes. It contains 1024^3 particles and has a particle resolution of $7.36\times10^{11}h^{-1}M_{\odot}$. We used `2LPTIC` and `CLASS` to generate initial conditions. The `2HOT` code operation scales as $N\log N$ in the number of particles. More details on the simulation can be found in Sutter et al. (2014c).

To obtain two mock catalogues, we apply the `Rockstar` halo finder and use it as an input for an HOD code. Thus we produce two galaxy catalogues, to mimic a high- and a low-resolution galaxy sample. We use the HOD model to assign to each galaxy its peculiar velocity. We then use these galaxy samples to study the effects of peculiar velocities on the finding of voids in a realistic situation by comparing mocks with and without the presence of velocities.

6.2.2 The matching algorithm

To analyse the effects of peculiar velocities on the void detection, we use a matching algorithm able to compare two voids catalogues in the most efficient way for our purposes.

A simple but crucial point for our analysis is the choice of *the catalogue with peculiar velocities as a base catalogue* for the comparison. This choice is instrumental, since it considers the correct perspective for the void finding: when we find voids in real surveys we observe them *with* peculiar velocities. Thus any study of peculiar velocities has to use the information we have as a starting point, so that the results of the analysis can be applied to a real galaxy survey, where we only have voids with peculiar velocities.

For each void in the peculiar velocity catalogue, the matching algorithm selects all possible matches with centres lying in the Voronoi volume of the void. The matching method uses the unique cells ID to find matches; it takes as the best match the one with major overlap in number of cells.

The analysis needs to consider two approaches: first we will use the matching algorithm to check which voids found in the peculiar velocity mock correspond to voids in the mock without velocities, and we will look at their properties. This procedure tells us which voids we are correctly matching, i. e. voids that are well detected in real surveys despite the effect of peculiar velocities.

As a second approach, we will look at the number of unmatched voids. The unmatched voids are highly affected by peculiar velocities, at the point that they actually do not exist in real space[6], they are created by the effects of peculiar velocities. Finally we disregard voids that are in the catalogue without peculiar velocities but not found in the catalogue with peculiar velocities, because in any way we will never be able to detect them — the fact that we do not find them in the peculiar velocity mock means that velocities have erased them.

For the groups working on the cosmological analysis of voids, which could be affected by peculiar velocities, we give a measure of the dynamical effects affecting the measured voids, and give some guidelines to exclude the most affected voids from the analysis. Using such guidelines, the signal-to-noise ratio for cosmological measurements such as the Alcock-Paczyński test can be improved, thus leading to a better detection.

6.2.3 One-to-one comparison

To obtain a high quality one-to-one void comparison I use the matching routine of `VIDE` described above. Nevertheless, it is very beneficial to obtain a good visualisation of voids, to check the behaviour of the matching algorithm and to understand the behaviour of voids when peculiar velocities are added.

A previous visualisation of voids shows them as circles overlapped to the density field, with the area of the circle defined by the effective volume of the void and its center by the barycenter.

While this technique has proven to be particularly effective to match properties of voids in the dark matter and galaxy distribution (Sutter et al., 2014c), to assess the effect of peculiar velocities we need a more detailed visualisation. Indeed velocities change the shape of voids, we thus need to check their effect looking at the shape of each void with a more detailed representation.

An idea to reach such result is to represent the cells constituting the void.

[6]With the void definition we are using. Of course, with a different definition of voids, such as the one proposed by Lavaux and Wandelt (2010), that is based on a Lagrangian orbit reconstruction, the situation might change.

Each cell is represented as a sphere, its area is related to the volume of the cell, and the center of the sphere is defined by the barycenter of the cell. I have developed an algorithm able to represent voids following this idea[7].

Although the cells are not spherical, this constitutes an approximation that allows to observe the shape of voids in a particularly effective way. Figure 6.2 shows its ability to represents the results of the matching: it gives a visual impression of the effect of peculiar velocities on individual voids[8]. It is possible to actually see the effect of peculiar velocities for each void on a one-to-one basis. While this allows checking the quality of the matching algorithm, it also shows the amount of shape variation of voids, thus serving as a guide for the analysis of the peculiar velocities effect.

I have presented the simulation and the method for comparison. The next Section shows the results of the analysis.

6.3 Results

As discussed in the previous section, we used the catalogue with peculiar velocities as a base catalogue for the comparison.

In order to extract cosmological information, we would like to know which voids are the most affected by peculiar velocities. In such voids, the effect of Cosmology would be dominated by the effect of peculiar velocities. If we found a way to characterize peculiar-velocity dominated voids, we could wisely exclude them from the analysis, as the signal-to-noise ratio for cosmological information with these voids would be low. In the next Subsections, I use the matched fraction of voids and the ellipticities to characterise the effect of

[7]The algorithm is part of the public void finder `VIDE`, at http://bitbucket.org/cosmicvoids/vide_public.

[8]I point out that in this image, the line of sight z is perpendicular to the sheet, i. e. we represent the void on the $x-y$ plane. Thus one might rightfully be worried on why there is any difference due to peculiar velocities, since the velocities should only affect the line-of-sight position of galaxies. The line-of-sight component is, truly, the only affected, but (for clarity) we are representing all galaxies in a slice of z, and not all the projected galaxies of the void. Because of peculiar velocities, the void is changed along the line of sight, as expected. Thus particles flow in and out the z-slice. The $x-y$ shape is changing in the slice, but not for 2-D projection along the line of sight.

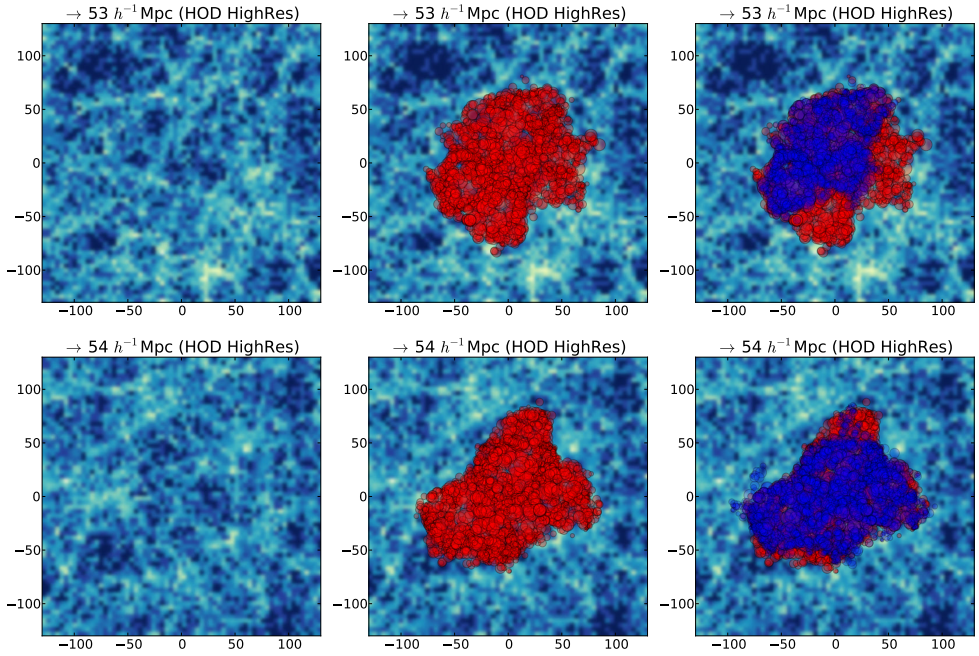

Figure 6.2: Visual impression of the effect of peculiar velocities on voids. Left frame shows a slice of the density field without peculiar velocities. Central frame shows the same slice but with peculiar velocities and the void found in the slice (red). A visual comparison of the density field between the two panels illustrates the effect of peculiar velocities: as expected, structures are enhanced. Right panel shows the void found in the density field without peculiar velocities (blue).

peculiar velocities on cosmic voids.

6.3.1 Matched fraction

A void that is weakly affected by peculiar velocities will have similar properties in both simulations — a direct way to exclude the most affected voids is to consider the matched and unmatched voids. The voids that are unmatched will be the most affected by peculiar velocities.

Taking the peculiar velocity catalogue as a basis for the comparison, unmatched voids from the non-peculiar sample are the most affected by velocities. For this analysis I consider ellipticity and radius of voids, in order to assess which properties of the unmatched voids are a feature of a velocity-dominated void. Figure 6.3 shows the matched and unmatched voids from the catalogues with and without peculiar velocities in the radius-ellipticity plane for both the High density and the Low density sample. The matching is worse for voids with radii lower than ~ 20 h^{-1}Mpc for the High density sample and lower than ~ 35 h^{-1}Mpc for the Low density sample, indicating that, when finding small voids, results are widely affected by peculiar velocities. This seems particularly logical: we might have expected, a priori, that small voids are the most affected by changes in shape due to the velocities, which affected the way `VIDE` defines the Voronoi cells and selects them as belonging to a void.

The finding of these voids is highly affected by peculiar velocities, thus their shape is peculiar-velocity dominated.

For this reason, when extracting cosmological information from these voids, signal-to-noise is low due to the strong impact of velocities. With the aim of extracting cosmological information from voids — for instance using Alcock-Paczyński test — this consideration should be taken into account, as it would greatly improve the result: low radii voids should be wisely excluded from the analysis to maximize the signal-to-noise.

While there is no physical reason for which these voids should not be used (unlike the radius limitation of once the mean particle separation, which is necessary to avoid voids detected as effect of Poisson fluctuations in the tracer

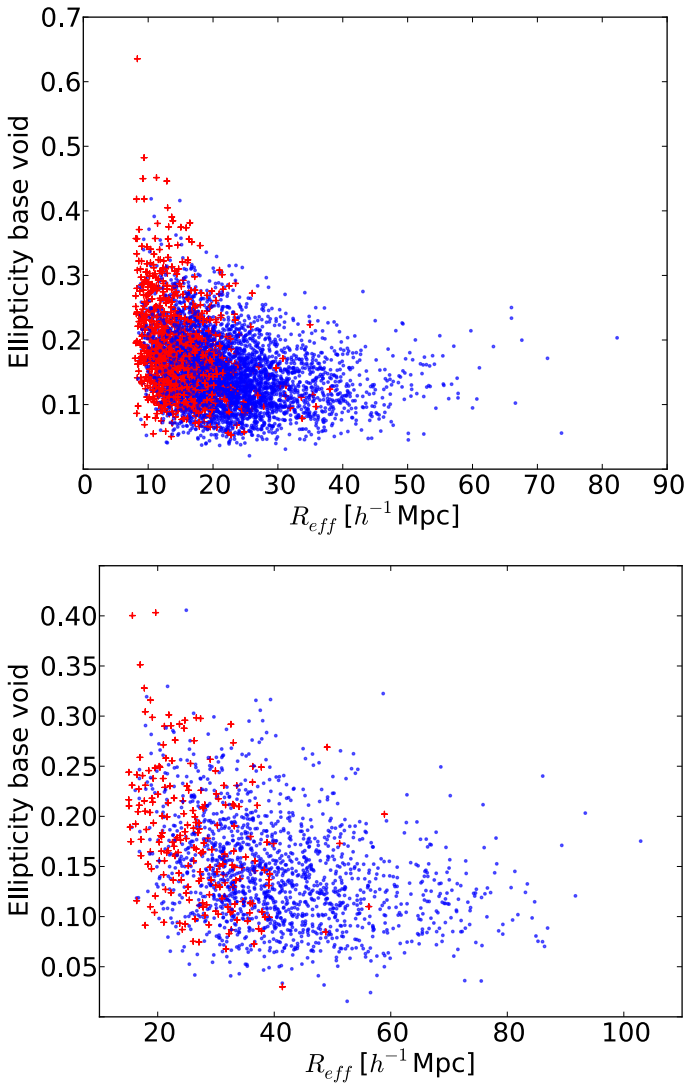

Figure 6.3: We represent the matched and unmatched voids from the catalogues with and without peculiar velocities in the radius-ellipticity plane for both the High and Low density sample. Red crosses represent unmatched voids; blue dots represent matched voids. The small voids are highly affected by peculiar velocities, they are peculiar velocity-dominated; while there is no clear distinction in ellipticity. We show that voids smaller than ~ 20 h^{-1}Mpc for the High density sample and smaller than ~ 35 h^{-1}Mpc in the Low density sample are more affected by peculiar velocities. These limits in radius roughly correspond to twice the mean particle separation. However, we also note that there are a population of well-matched, minimally-affected voids at all scales.

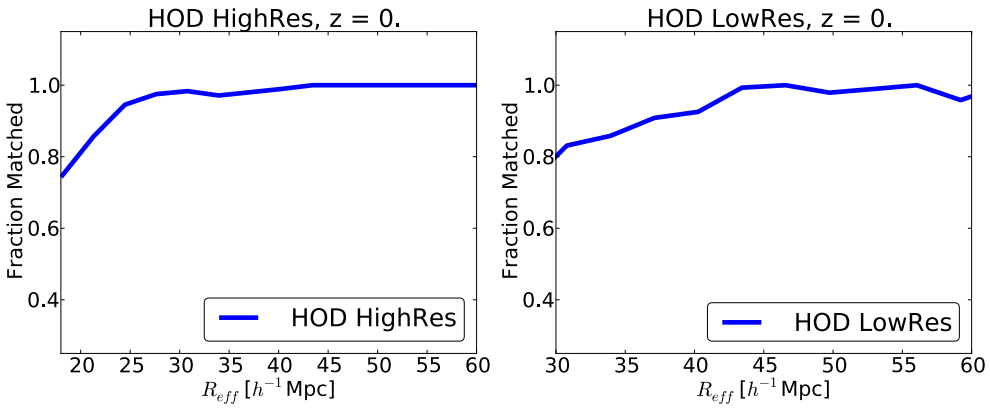

Figure 6.4: The Figure shows the fraction of matched voids. The fraction of matched voids is higher than 80% for voids bigger than 20 h^{-1}Mpc for the High Resolution sample and 30 h^{-1}Mpc for the Low Resolution sample, that corresponds roughly to twice the mean particle separation in both cases.

population and is thus a limit needed because of physical reasons); the use of voids below *twice* the mean particle separation would in principle bring more noise than information, thus highly diminishing the quality of the signal.

Can we infer some property about the unmatched voids that allows us to exclude them from the analysis, as being highly affected by velocities? With the aim of confirming the previous of analysis of matches in the radius-ellipticity plane, we consider, in Figure 6.4, the fraction of unmatched voids: for small voids the matching between voids without and with peculiar is less reliable (see Figure 6.4). Thus when we find voids in redshift space, the smallest voids are the ones most affected by peculiar velocities and for which the matching is often worse, in that case the fraction of matched voids is lower.

The fraction of matched voids is higher than 80% for voids bigger than 20 h^{-1}Mpc for the High Res sample and 30 h^{-1}Mpc for the Low Res sample. It is confirmed that small voids are peculiar-velocity dominated objects, which strongly affects their shape and the finding process by `VIDE`. As expected, we see that the radius limits are more severe in the case of the Low density sample, since the density of tracers is lower.

Before concluding this Section, I consider a further cut that would allow to exclude the non-matched voids. It must be noted that the considered cut

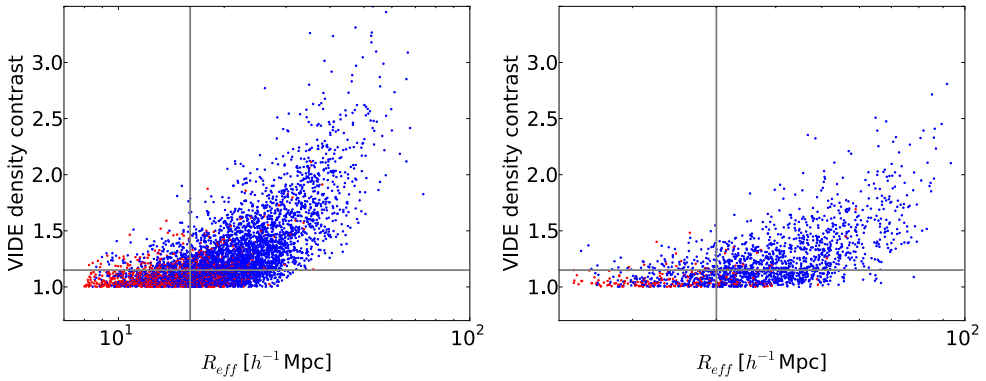

Figure 6.5: The Figure shows in blue the matched voids, which means the voids correctly identified despite the effect of velocities, and in red the unmatched voids. In both the High (left) and Low (right) density cases it is possible to consider a radius cut (twice the mean particle separation) and, additionally, a cut based on the density contrast of the voids (voids with low density contrast are excluded). It must be noted that the considered cuts only use information of the catalogue with peculiar velocities and are therefore applicable to data from real surveys. The cuts aim to exclude from the analysis peculiar-velocities dominated voids, for which the cosmological signal is weaker.

only uses information of the catalogue with peculiar velocities and is therefore applicable to data from real surveys.

As Figure 6.5 shows, it is possible to further isolate unmatched voids by applying, *additionally to the cut in radius*, a cut based on the density contrast of voids (using the density contrast as defined by `VIDE`, which is given by the ratio of the mean density along the ridge of the void versus the minimum density in the void). A good trade-off between cutting too many voids and excluding as many non-matched voids as possible it to exclude voids below 1.15 value for the density contrast. Intuitively, it makes sense to exclude voids with low density contrast, as they are likely to be more affected by peculiar velocities.

I have studied the effect of velocities considering the fraction of unmatched voids. Radial and density contrast cuts might be considered to identify the unmatched voids, that is the voids more affected by peculiar velocities and

thus with low signal-to-noise for cosmological signal. The subsequent stacking of voids can alleviate the effect, but still, stacks of smaller voids and with low density contrast are noise-dominated from a cosmological measurement point of view. The next Section analyses the effect of velocities on the shape of voids. In Section 6.4 I study the effect of velocities on stacks and discuss the use on real data.

6.3.2 Average ellipticity variation due to peculiar velocities

I have analysed the number of matched voids in the cases with and without velocities. I now move to analyse the difference in shape, radius and position of the barycenters for voids.

First I use the comparison of the two voids catalogues — with and without peculiar velocities — to compute the average variation in ellipticity due to peculiar velocities as a function of radius.

For this analysis I consider only voids bigger than the mean particle separation, namely larger than 8 h^{-1}Mpc for the High density sample and 15 h^{-1}Mpc for the low density sample. Furthermore I exclude extremely large voids, that are less reliable due to low number of galaxies and sparsity. This analysis is targeted to provide guidelines on the effect of peculiar velocities to all applications using voids from real data. As discussed above, for such applications, to avoid Poisson noise effects, voids with radii below the mean particle separation are already excluded, as well as too large voids because of the lower number of galaxies. To assess the impact of velocities I consider the matched voids, that is voids we measure in resdhift space corresponding to voids in real space.

The result of the comparison is shown in Figure 6.6. We find an average flattening lower than 10% to the ellipticity of voids for both the High and Low resolution samples. For the High Resolution Sample the ellipticity slightly increases for radii larger than ~ 40 h^{-1}Mpc, these large voids are not flattened.

An interesting conclusion is reached through this work: while voids are expanding and one might expect peculiar velocities to elongate individual

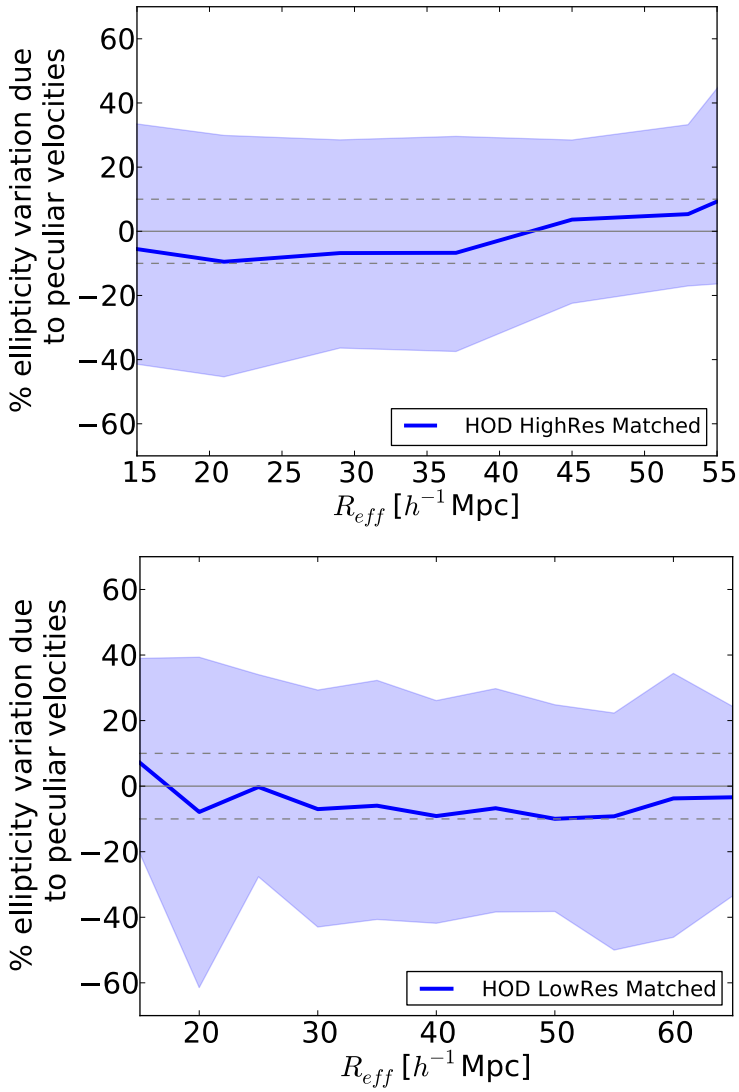

Figure 6.6: The figure shows the percentage ellipticity variation due to peculiar velocities for the High Resolution HOD sample (top) and for the Low Resolution HOD sample (bottom) for matched voids. These are voids that are found in both catalogues. Peculiar velocities contribute on average to a flattening of voids. We find an average flattening lower than 10% to the ellipticity of voids at all scales.

voids, the situation is less clear in a statistical sample of the full cosmic web: the elongation in the dynamically out-flowing portion of voids competes with a thickening of the walls separating them. In addition, peculiar velocities will have an effect on the assignment of a given portion of survey volume to individual voids by `VIDE`.

From this result and the previous considerations about unmatched voids, a first prescription for the use of voids in Cosmology is obtained: one should avoid using small voids, to be more precise voids smaller than *twice the mean particle separation*, and eventually correct the ellipticity for voids of bigger size by the observed constant systematic flattening due to peculiar velocities.

For the High density and Low density samples, this would mean exclude voids smaller than 16 h^{-1}Mpc and 30 h^{-1}Mpc respectively. While this cut might seem drastic for nowadays surveys (such as SDSS DR7) and might excessively reduce the number of voids, since the smaller voids are the ones with higher statistical weight, is can be a good prescription to be adopted for future applications of the Alcock-Paczyński test.

This information gives us the amount of void ellipticity due to peculiar velocities, for the stacked void in redshift space. It means that, if we take voids in redshift space and measure their ellipticity, less than 10 % on average of this ellipticity is due to peculiar velocities — a correction of the ellipticity taking into account this value enhances the robustness of the Alcock-Paczyński test.

Having based the analysis on HOD catalogues, the obtained value is a realistic estimate that can be used to correct applications of the test on real data catalogues (such as Sutter et al. (2012b); Sutter et al. (2014d)[9]). We have also shown that small voids are more affected by peculiar velocities in relative ellipticity. Excluding those voids from the application of the Alcock-Paczyński test is a further way to enhance the signal-to-noise ratio in the measure of the expansion of the Universe.

Aiming to study changes due to peculiar velocities, we compute the relative radius between the peculiar velocity and no peculiar velocity sample

[9]This result has been used in Sutter et al. (2014d) to validate the systematic change in ellipticity due to peculiar velocities.

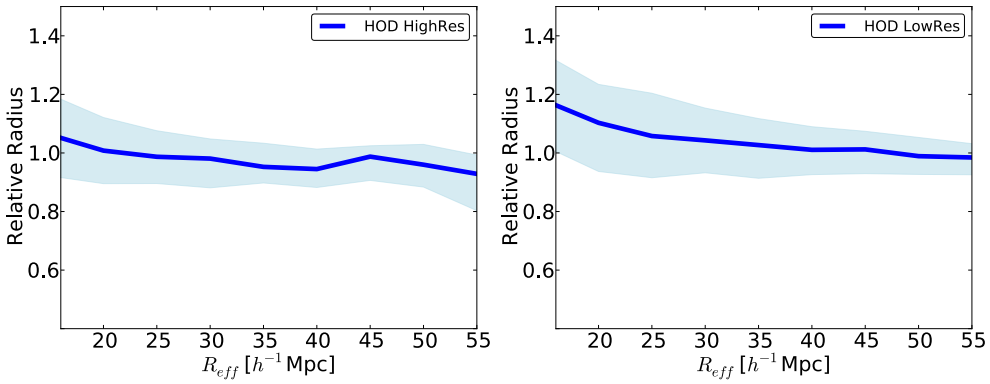

Figure 6.7: The Figure shows the relative radius between the peculiar velocity and no peculiar velocity sample. Interestingly, for voids bigger than twice the mean particle separation the radius remains stable both in the High Res sample and in the Low Res sample.

(see Figure 6.7). Interestingly, for voids bigger than twice the mean particle separation, the radius remains stable both in the High Resolution sample and the Low Resolution sample. The radius of the void is a more stable quantity, because of the way we calculate it. We assume a sphere of equivalent common volume, thus some variation in the shape is averaged out when considering the radius. For applications using the void radius, we conclude that its variation due to peculiar velocities is practically negligible.

Finally we compare the relative distance of barycenters, in Figure 6.8, we see that voids are slightly displaced due to the effect of peculiar velocities. Once again the displacement is larger for small voids. Nevertheless, a change in the position of the voids does not affect much cosmological measurements, that are based on the shape or number of voids and not on their positions. I also point out that this result is important for applications using void abundances: since voids do not change much in radius, the effect of peculiar velocities is negligible for abundances. The only effect is for voids smaller than twice the mean particle separation, for which the abundance can change, as they might be washed out or created by peculiar velocities.

I have studied how peculiar velocities affect the matched fraction of voids, their shape, their radius and their positions. The next Subsection presents

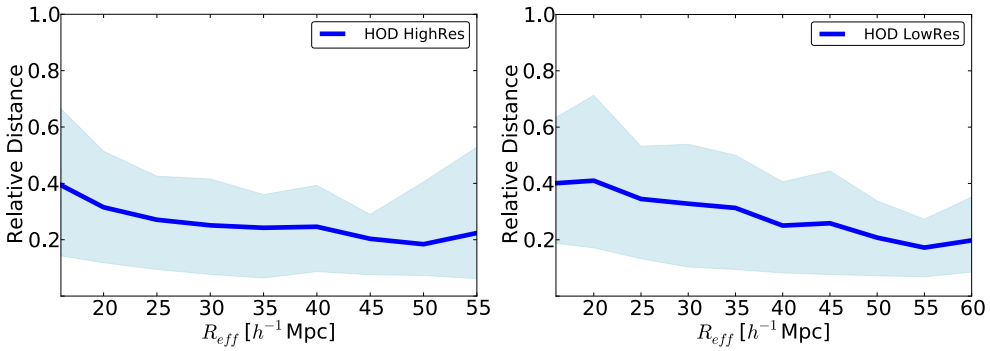

Figure 6.8: We show the relative distance of the position of the barycenter of voids when adding peculiar velocities.

the guidelines emerging from this analysis.

6.3.3 Guidelines

The application of the one-to-one basis comparison allows us to establish guidelines to deal with the effects of peculiar velocities. We can summarise them as following:

- exclude voids with radii below *twice* the mean particle separation, and possibly voids with low density contrast. This prevents the use of voids whose ellipticities are strongly affected by peculiar velocities;
- for the remaining voids, correct for an overall flattening due to peculiar velocities;
- consider that voids radii do not change significantly because of peculiar velocities and that the barycenter of voids is slightly displaced.

I will discuss at the end of the Chapter the implications of these guidelines for real data. In the next Section I analyse the effect of peculiar velocities on the stacked density profiles of voids found in both the Low and High resolution sample.

6.4 Effect of velocities on HOD stacks

I showed in the previous Section that small voids are more affected by peculiar velocities. The stacking of voids can alleviate the effect: even if the shape of the void is not perfectly stable, the averaged density profile that is used for the Alcock-Paczyński test might be more stable. This has been suggested in the case of dark matter particle simulations by Lavaux and Wandelt (2012). We test this claim in a more realistic case using the HOD galaxy samples by comparing the density profiles of stacks in both cases (with and without velocity) for stacks of various radii. Using the technique described in Sutter et al. (2014c), I consider the co-centered density profiles.

The co-centered profiles presented in Figure 6.9 show that the density profiles of stacks are not strongly affected by peculiar velocities, except for the smallest voids. I point out that the use of the co-centering technique is adapted here, since we saw that there is a slight displacement of voids, but the shape and the radii of voids do not change significantly. Thus, when using real data, we can just consider the density profiles, without any need to re-center them, because the density profile is not changed but just displaced.

As a conclusion, current cosmological constraints relying on density profiles of stacks are only very mildly affected by peculiar velocities; as it is shown in Sutter et al. (2014d), where a constant offset can be used as a first approximate way to take into account their effect. This consideration is quite a relief for the applications using the density profiles and for a first use of voids to constrain Cosmology.

Nevertheless, with the aim of attaining the level of precision Cosmology with cosmic voids, a more careful modelling of the velocities is necessary, e.g. to mitigate the peculiar velocity systematics for the Alcock-Paczyński test. Such a model for velocities would allow to extract high-precision cosmological information from stacked voids. As discussed in Section 5.3.2, the goal of a model for peculiar velocities can be reached through the use of the model-independent real-space density reconstruction presented in this thesis.

In the next Section I conclude the Chapter with a discussion on peculiar velocities and on the application of the considered cuts to real data.

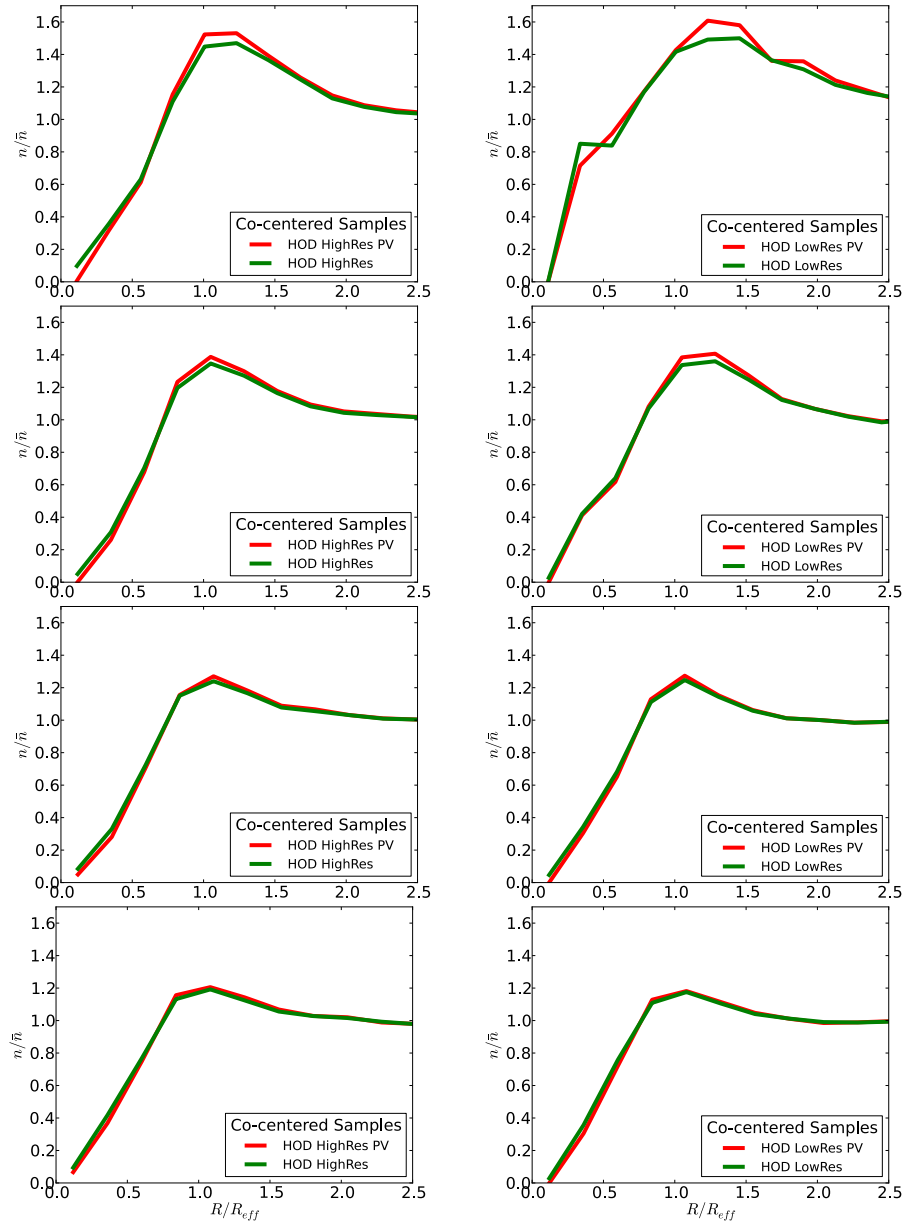

Figure 6.9: The figure shows the density profiles of stacks of different sizes for voids with and without peculiar velocities. For both samples, from top to bottom the stacks are for 15-20, 25-30, 35-40, 45-50 h^{-1}Mpc radii. Left column is the High density sample: the density profile is less affected by peculiar velocities while increasing in radius. Right column shows the Low density sample: we observe the same trend as for the High Resolution sample, but the effect of peculiar velocities is washed out at larger radii. The profiles are co-centered.

6.5 Discussion on peculiar velocities

Voids are mildly affected by peculiar velocities on a one-to-one basis. For most applications that use voids density profiles, voids abundances and voids effective radii, the effect is negligible.

The only feature that is affected by peculiar velocities on a one-to-one basis is the shape of voids. While it is not trivial to find a preferential direction for such an effect, a cut in radius can be applied to ensure minimal effects from peculiar velocities, namely the use of *twice* the mean particle separation. This cut remains drastic for current observations, which are dominated by small voids, but it ensures a limit for the radius of voids above which the effect of peculiar velocities is negligible.

For current observations a lower cut can be applied, still improving the noise in the results. The prescriptions we found allow to understand that small voids remain the most dominated by the effect of peculiar velocities; and, while this might be moderated with averaging techniques such as stacking, the cosmological signal is still strongly washed out for low-radii voids.

Thus it might be convenient, even for applications of the Alcock-Paczyński test to stacked voids from current data, to exclude some of the smallest voids: at the expense of the statistical weight from small voids, there is a gain in signal-to-noise ratio when only limiting the analysis to larger voids. The non-matched voids are the most affected by peculiar velocities, and they reside in the low radius part of the catalogue.

The consideration allowing such analysis is that peculiar velocities mildly affect voids, which is the reason why these structures are less affected by non-linear clustering effects and present themselves as optimal tools to extract cosmological information in a situation with low systematics.

The cut on radius can directly be applied to real data, as well as the further cut on the density contrast in the peculiar velocity case, thus allowing to select the voids which are in absolute the less affected by peculiar velocities. With such methodology, it is possible to preserve the cosmological information through the use of high signal-to-noise data.

As discussed previously, the analysis I have presented in this Chapter is

a first way to tackle the problem of peculiar velocities, which constitutes the main systematic when trying to extract Cosmology from voids. A further step would be the use of the model-independent real-space density profile of voids presented in Chapter 5.1 to obtain a detailed model of the non-linear component of peculiar velocities.

The use of cosmic voids for Cosmology requires careful modelling of systematics. The work presented in this thesis is a crucial step towards the understanding of such effects.

Chapter 7

Constraints from cosmic voids: Alcock-Paczyński test and abundances

Cosmic voids are used to constrain cosmological models, e. g. through Alcock-Paczyński test, or using voids abundances. In this Chapter I discuss the most recent result of the application of the Alcock-Paczyński test to voids. This application is partially based on the results presented in Chapter 6, indicating a constant flattening of voids due to peculiar velocities. Furthermore, the analysis of the effect of peculiar velocities established that the minimum radius to be used when considering number functions is twice the mean particle separation, since voids smaller than that size could be strongly affected by peculiar velocities.

This consideration is used in the second Section of this Chapter to establish a prediction for the abundance of voids that can be obtained by the future ESA Euclid mission, jointly with theoretical considerations based on the two barrier excursion set model for voids proposed by Sheth and Van De Weygaert (2004). The void abundances are then used to calculate a Fisher matrix forecast for voids with Euclid.

7.1 Recent Alcock-Paczyński test application

Recent results on Alcock-Paczyński test show the constraining power of void shapes. For the recent work presented in Sutter et al. (2014d), we have used the conclusions about the effect of velocities discussed in the previous Chapter: the effect of velocities mildly affects the stacked voids shape and the effect is constant at all redshift and radii, once the smallest voids are excluded.

The application to real data does not allow yet to follow the guidelines emerged from the previous analysis, namely to consider only voids of sizes larger than twice the mean particle separation. Indeed for the real data available nowadays a less conservative cut needs to be applied (thus keeping as cut once the mean particle separation), to avoid losing too many small voids, which carry a high statistical weight. The cut still reduces the impact of velocities, and the use of a correction factor widely tested on simulations allows to obtain robust results from the test.

The detected signal from the Alcock-Paczyński test finds a best-fit value of $\Omega_m = 0.15$ (see Figure 7.1). The value is not at the level of precision Cosmology which can be obtained from other probes such as the Planck measured power spectrum, nevertheless it excludes the values of $\Omega_m = 1$, and $\Omega_m = 0$ and constitutes the first cosmological constraint from Alcock-Paczyński test with cosmic voids.

Because of the limited number of voids, the method used to obtain the results in Sutter et al. (2014d) is different from the one used in Lavaux and Wandelt (2012); Sutter et al. (2012b).

The first method, introduced in Lavaux and Wandelt (2012), is a Monte Carlo Markov Chain shape-fitting algorithm that uses as a starting point a non-distorted density profile and fits it to the profile in the observations or simulations. This profile-based shape measurement of voids is more precise in measuring the ellipticity of voids, and thus potentially better to constrain Cosmology with the Alcock-Paczyński test. Nevertheless it needs a sufficient number of voids, otherwise the fit cannot be performed. Sutter et al. (2014d) established a density dependent threshold in the number of voids for this method to work (100 for High density samples and 300 for Low), as well as

the necessity of narrow radii bins.

The second method works better when the number of voids is lower than these thresholds, basically for each stack it takes all particles in an ellipse with a given axis ratio and calculates the ellipticity and inertia tensor. Then, comparing with the expected ellipticity in a ΛCDM model, it is possible to obtain constraints on the model. The second method gives better results with low populated stacks, which is the reason why it has been used in Sutter et al. (2014d).

Nevertheless, applying the real-space density profile reconstruction presented in this thesis on real data and using the model in Hamaus et al. (2014), it could be possible to improve the systematics with the profile fitting method of Lavaux and Wandelt (2012), which uses as a starting point the real-space density profile of voids. The use of this method, improved through the modelling of the real-space shape of voids, appears to greatly reduce the error bars when applying the Alcock-Paczyński test on simulations.

The use of the real-space density profiles described in Section 5.1 is thus a promising avenue to improve such estimates since the more precise method to perform the Alcock-Paczyński test is based on fitting a real-space shape model for the density profile.

Furthermore, as discussed in Section 6, a model independent measure of the non-linear component of peculiar velocities of stacked voids (such as the one that could be obtained using the reconstructed real-space density profiles of voids) can help to reach a careful modelling of the systematics affecting the measurement.

Finally, it is worth studying the optimized application of radius (and possibly density contrast) cuts or re-weightings, guided by the analysis of the effect of peculiar velocities performed in the previous Chapter. Current datasets do not contain a sufficient number of galaxies to fully take into account the guidelines for the Alcock-Paczyński test application to real data and to be able to minimize the effects of peculiar velocities.

This situation will soon change: upcoming datasets such as the results of the full BOSS survey or the future Euclid catalogues will dramatically increase

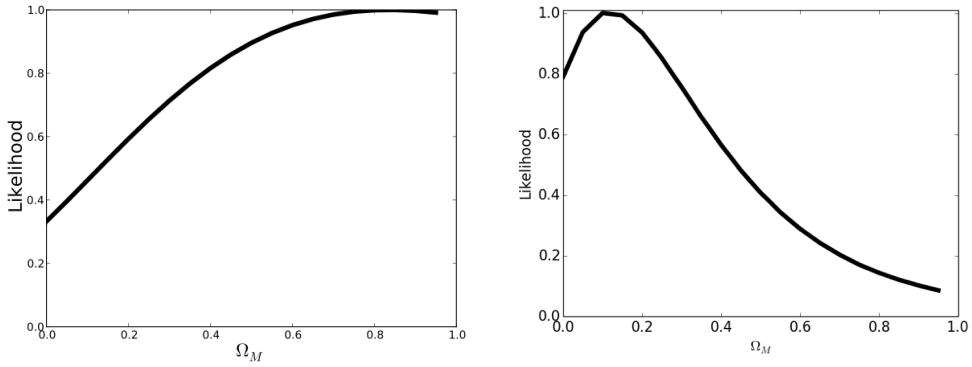

Figure 7.1: Comparison of Alcock-Paczyński test constraints on Ω_m. The left panel shows results from the application of the test to SDSS DR7 voids (Sutter et al., 2012b), while the right panel shows contraints from a most recent analysis using SDSS DR7, DR 10 LOWZ and CMASS (Sutter et al., 2014d). Future data from surveys such as BOSS, Euclid or WFIRST will allow to obtain more stringent constraints with the Alcock-Paczyński test.

the number of galaxies and thus the number of voids, allowing the application of the obtained guidelines. The Alcock-Paczyński test constraints will thus be sharpened and will reach a level competitive with constraints from other cosmological probes.

7.2 Constraints from void abundances

> The results presented in this Section will soon be submitted in Pisani, Sutter, Alizadeh, Biswas and Wandelt (2014) *"Constraining dark energy with cosmic void abundances"* (in prep., Pisani et al. (2014b)), thus are part of a work done in collaboration with Paul M. Sutter, Esfandiar Alizadeh, Rahul Biswas and Benjamin Wandelt.

The abundance of observed cosmic voids in galaxy redshift surveys can be used to forecast the power of voids to constrain the dark energy equation of state through the Fisher matrix formalism (as well as the void ellipticity, see Biswas et al. (2010) and Lavaux and Wandelt (2012)). I consider

the Chevallier-Polarski-Linder (Chevallier and Polarski, 2001; Linder, 2003) parametrisation:

$$w(z) = w_0 + w_a \frac{z}{z+1} \tag{7.1}$$

Once the number of observed voids is known, the Fisher matrices[1] allow to obtain the error ellipses on the $w_0 - w_a$ plane. Thus I can estimate the constraining power that will come from surveys such as the Euclid survey. While this has been done in previous works for the constraints from the shape of voids (Lavaux and Wandelt (2012) calculated constrains using dark matter particle simulations, Biswas et al. (2010) showed void shape Euclid constraints on dark energy), it is interesting to consider constraints from voids abundances.

The model used to obtain constraints can reach now a significant level of precision, thus giving more reliable forecasts of the constraining power of voids. The improvement comes from the fact that recent works on real data (e. g. the SDSS DR7 and DR9 data, see Sutter et al. (2012a, 2013)) shed light on the behaviour of galaxy voids, thus allowing to obtain a much more robust estimation of void abundances based on the use of simulations constructed to reproduce the properties of data in the most realistic possible way.

Furthermore, Euclid has been selected in 2011 (Laureijs et al., 2011) by the European Space Agency — updated details on the mission are available and can be used to model cosmological constraints from voids. For all these reasons, it is interesting to look for an updated and realistic estimate of voids abundances Fisher matrix in the $w_0 - w_a$ plane with the Euclid satellite.

To reach such estimate I first need to determine the number of voids to be found by Euclid. In order to do so, I consider that the formation of a void takes place when there is shell-crossing, analogously to the case of the formation of

[1]The Fisher formalism can give an estimate of the constraints to be obtained from cosmological probes. Nevertheless, while it is a quick and often reliable method, in some cases its performance might not be optimal. As Wolz et al. (2012) point out, it is wise to avoid marginalisation over w_a, since in such cases the Fisher matrix will not be able to correctly reproduce the non-elliptical shape of the likelihood, particularly when referring to geometrical probes. In this case the situation is not critical, since we are using abundances of voids. A possible way to obtain better estimates would be the use of a different parametrization, more optimal for the use of Fisher matrices, based on the parameter $w_s = \ln[-(w_0 + w_a)]$. More details can be found in Wolz et al. (2012).

a halo by collapse as described by the spherical collapse model (Blumenthal et al., 1992). This consideration allowed (Sheth and Van De Weygaert, 2004) constructing a model for the distribution of void sizes that we take as a basis for determining void abundances.

In the galaxy distribution, one identifies voids as the primordial underdensities having reached the linearly extrapolated density contrast $\delta_{\rm v}$, where a spherical void with tophat profile is assumed. To be more clear, $\delta_{\rm v}$ is the density contrast of an underdense sphere at a very early time, linearly extrapolated to the time when a shell forms around that sphere. The Sheth and van de Weygaert formalism (Sheth and Van De Weygaert, 2004) is thus an extension of the Press and Schechter formalism (Press and Schechter, 1974) for voids, were a critical underdensity is defined such that, when it is reached, a void forms (in analogy to the $\delta_{\rm c}$ density threshold above which a halo collapses).

The Sheth and van de Weygaert *two-barrier excursion set model* is an extremely powerful tool to obtain void abundances. I use this model, widely tested with the use of dark matter simulations, to constrain abundances of voids from Euclid.

From the Press-Schechter formalism, it is possible to calculate the number of voids in a given mass interval and at a given redshift, I have:

$$\frac{M^2\, n(M,z)}{\rho_{\rm back}(0)}\frac{{\rm dM}}{M} = \nu f(\nu)\frac{{\rm d}\nu}{\nu}, \tag{7.2}$$

where M is the mass of the void, $\nu f(\nu) = \sqrt{\frac{\nu}{2\pi}}\exp(-\nu/2)$ and I have defined the number density of minima of depth $\delta_{\rm v}$ as:

$$\nu = \frac{\delta_{\rm v}^2}{\sigma^2(M,a)}$$

Recent work with voids allows measuring the abundances of voids in real surveys (e. g. Sutter et al. (2013)). The measurement of void abundances can in principle be used to tune the value of $\delta_{\rm v}$ by matching abundances in real data and in simulations using the Sheth and van de Weygaert two-barrier excursion set model. While this is a first approximation, it uses the

great power of the theoretical description enhanced with the a choice of the parameter based on observations.

Indeed, as indicated by Jennings et al. (2013), the distribution of voids needs to be validated with galaxy mocks in order to be reliable. Thus, in the redshift range of interest to observe voids, we have used HOD dense mocks matched to galaxy density of Euclid and sub-samples of simulations to reach the same density as Euclid and tune the parameter. The value of $\delta_{\rm v}$ obtained with this methodology is -0.35, which has also been tested using different cosmologies[2]. The use of simulations tuned to already observed data enhances the robustness of the abundance estimation for Euclid.

In the definition of ν, we use σ, the linearly extrapolated variance of density fluctuations δ smoothed at the filtering scale $R_{\rm Lag}$ by the Fourier transform of the window function for a top-hat filter $\tilde{W}(x) = 3/x^3\,[\sin(x) - x\cos(x)]$. Using the matter power spectrum $P_\delta(k, a)$, I define:

$$\sigma^2(M, a) = \int_0^\infty \frac{k^3 P_\delta(k, a)}{2\pi^2} \left|\tilde{W}(kR_{\rm Lag}(M))\right|^2 \frac{{\rm d}k}{k}. \tag{7.3}$$

The calculation of σ depends on Cosmology, thus it can be used to constrain Cosmology through the observed abundance of voids in a survey. As Sheth and Van De Weygaert (2004) point out, the *void-in-cloud* problem is affecting the way we estimate the number of small voids, thus the two-barrier excursion set model must be used — the need for two parameters for the void size distribution is unique to the void case.

Furthermore, when considering real surveys, as we wish to do, the power of the survey crucially depends on the minimum size of voids that can be observed. Particular care must be taken to determine the minimum radius for the voids in the survey: the abundance of voids increases rapidly with decreasing radius. Following the methodology described in Biswas et al. (2010), I consider two different criteria and take into account the most stringent, i. e. the higher radius from the two.

[2]Furthermore, we parametrise the uncertainty on the parameter $\delta_{\rm v}$ by marginalisation over it to obtain the constraints. We note that without the marginalisation the constraints shrink slightly.

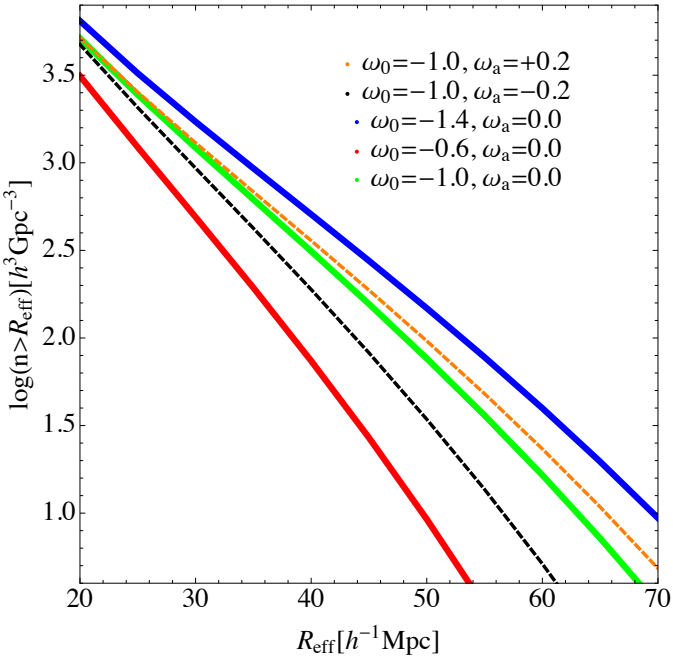

Figure 7.2: Abundances of voids for different cosmologies.

The first and simplest criteria is based on the mean particle separation of galaxies in the survey. Taking into account the features of the survey, we consider as a minimum radius of the void twice the mean particle separation. While we know that voids can be found reliably until one time the mean particle separation, we consider that using twice the mean particle separation $2R_{\rm mps}$ would also guarantee small impact of peculiar velocities, as discussed in the previous Chapter. Indeed, voids below that limit can be washed out or created by the effect of peculiar velocities.

Furthermore, we will consider the "void-in-cloud case", when a void is located inside an overdensity in an earlier redshift and will disappear with the gravitational collapse of the overdense region. In such cases the Press and Schechter formalism is not suitable anymore for small voids. As described above, the excursion set formalism (following Sheth and Van De Weygaert (2004)) involves solving a diffusion equation with two absorbing barriers instead of one, one for halos and one for voids.

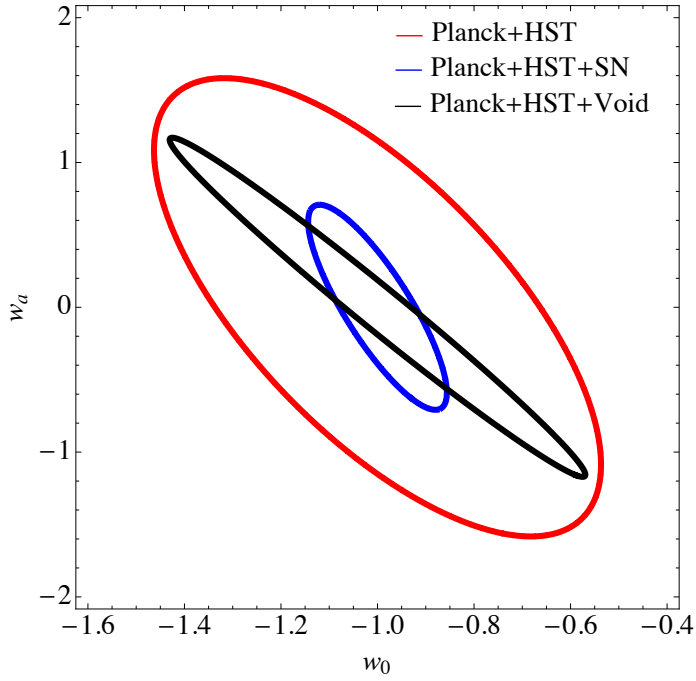

Figure 7.3: Fisher matrix for void abundances.

This leads to a turn-over radius below which the number density of voids decreases as going to small radius due to the void-in-cloud effect. I consider that a void with radius larger than the Lagrangian void-in-cloud radius for which we have $\sigma(R_{\rm Lag}, z) \simeq 1$ is unlikely to be embedded in a halo, thus giving a framework where the Press and Schechter formalism can be applied. Thus I calculate this radius and use it as the second criterion.

At each redshift, the higher radius between $2R_{\rm mps}$ and $R_{{\rm Lag},\sigma\simeq 1}$ is used as the minimum radius to obtain the abundance of voids. Thus, at each redshift I consider the most stringent of the two constraints, one taking into account the surveys features ($2R_{\rm mps}$), the other depending on Cosmology ($R_{{\rm Lag},\sigma\simeq 1}$).

The minimum radius of observable voids is thus an important quantity, as it consider both the survey and the Cosmology. The abundance of voids obtained with this methodology shows the constraints the survey can put on cosmological parameters, and is, as pointed out in the previous discussion, particularly robust, as based on recent observations.

I show in Figure 7.2 the abundances of voids for different cosmologies, and in Figure 7.3 the resulting Fisher matrices obtained from the abundance of voids predicted for Euclid.

I point out that this forecast is based on simulations matched to recent observations to determine the parameters of the model and on simulations matching the features of the future Euclid mission, which enhances the reliability of the constraints (compared to constraints based on dark matter simulations alone); and is using the most recent features of the Euclid space mission. For comparison, I also show constraints from Planck, from the Hubble Space Telescope and from current constraints from supernovae.

Void abundances tighten constraints on the dark energy model: since different probes explore the parameter space in different ways, the addition of a new cosmological probe can shrink the available space for the values by simply having a different orientation (see Figure 7.2).

In this Chapter I discussed the most recent results of the Alcock-Paczyński test and considered possible improvements based on the methods and results presented in this thesis.

Additionally I presented a calculation of constraints from voids abundances we will obtain from the Euclid satellite, showing that voids promise to become a competitive tool to probe dark energy phenomenology in the era of precision Cosmology.

Conclusion

In this thesis I have addressed the particular problem of the use of cosmic voids for Cosmology. While voids have been discovered in 1978 (see Chapter 1), until very recently the potential of these structures to constrain Cosmology has been under-explored. This is mainly due to the difficulty of extracting data from low density zones, which led cosmologists to focus on large-scale structure cosmological probes based on high density probes (such as using luminous red galaxies to trace the baryon acoustic oscillations).

The situation is now changing: modern surveys allow us to access to high quality large-scale-structure measurements, by sampling the galaxy distribution in great detail also in sparse regions. The appeal of cosmic voids becomes thus considerable. Cosmic voids hold cosmological information that remained unused until now and, since they fill most of the Universe and have simpler dynamics than high density regions of the Universe, stand as a new, promising tool to constrain models.

The use of voids to constrain Cosmology is based on studying their shape, their number density and their evolution. These properties are Cosmology dependent, so we can use them to constrain the models to understand and describe the evolution of the universe — e. g. through the Alcock-Paczyński test (see discussion in Chapter 2).

When we observe cosmic voids, however, we observe them in redshift-space: their real shape remains inaccessible to us, thus greatly limiting our knowledge about such structures. To employ voids as a precision tool for Cosmology, it is fundamental to obtain their real-space shape (as explained in Chapter 2).

This thesis presented a model-independent non-parametric algorithm to

reconstruct the spherical density profiles of stacked voids in real space, without any assumption about redshift distortions, but simply based on geometrical considerations — namely the sphericity of a stacked void in a homogeneous and isotropic universe (see Chapter 3).

The method has proven to be robust: it has been tested on a toy model, on a stacked void from a dark matter simulation and on galaxy mocks mimicking the features of the Sloan Digital Sky Survey Data Release 7 (as shown in Chapter 4). The use of different methods to implement the reconstruction further enhances the reliability of the result. Furthermore, the use of the reprojection as a sanity check for the solution of this ill-conditioned problem is a powerful tool to test the reconstruction on real data.

I have thus applied the reconstruction method to stacked cosmic voids from SDSS, obtaining the first ever real-space density profiles of stacked voids (presented in Chapter 5). The obtained real-space density profiles can be used to test cosmological models such as modified gravity models or dark energy models and need no assumptions about redshift-space distortions. Furthermore the application of the Alcock-Paczyński test can be improved, as its most performant method is based on the real-space profile of void stacks.

I have also presented two direct applications of the real-space density profile of stacked voids: the mass compensation and a theoretical prediction for the velocity profiles of voids based on linear theory and assuming cosmological parameters. In parallel, I have discussed the use of the real-space density reconstruction to obtain model-independent information about the peculiar velocity profiles of voids. The use of the real-space density profiles of stacks to constrain higher order terms of peculiar velocities around voids is a novel probe of dynamical structure formation with potential importance for upcoming spectroscopic surveys. This probe acts in a regime where modified gravity effects, if present, would remain unscreened. In addition, information about peculiar velocity effects on cosmic voids would also enhance the understanding of systematics effects in the use of voids for Cosmology and in the study of void evolution.

Using mock catalogues, I analysed the effect of peculiar velocities on the

physical properties of voids, which impacts the way the void finder selects them (discussed in Chapter 6). I have studied the effect of velocities on a one-to-one basis, considering the fraction of unmatched voids depending on the radii of voids and on the density contrasts. Furthermore, studying the effect of velocities on the ellipticities of voids, on their radii and barycenters, I obtained a set of guidelines to master the effect of peculiar velocities when using voids from real data. I also discussed the use of such guidelines for current and future datasets.

Finally I considered the use of void abundances to constrain cosmological parameters: taking into account the suggested guidelines to minimize the effects of velocities jointly with theoretical considerations based on the two barrier excursion set model for voids, I obtained a prediction for the abundance of voids that can be measured by the future Euclid ESA mission and calculated a forecast for the constraint of cosmological parameters through the use of the Fisher matrix formalism (see Chapter 7).

The work presented in this thesis allows to obtain the first real-space density profiles of voids and to reach a deeper understanding of these structures through an analysis of the effect of velocities on voids. By means of their density profiles, of their shapes and of their abundances, voids stand as a powerful probe of Cosmology to be used in the framework of the next generation of surveys, such as the European Space Agency satellite Euclid, but also eBOSS, DESI, and WFIRST. Narrowing constraints on cosmological models, cosmic voids promise to bring independent and complementary information and to shed light on the mystery of dark energy.

Acknowledgements

First of all I would like to thank my supervisor, Ben Wandelt. Ben has the rare capacity of considering his students at his same level, both as friends and colleagues and to always take into account what they think — but at same time he pedagogically transmits his knowledge, passion and creativity. I thank him for the incredible amount of patience he had with me when I was completely lost in impossible problems, for everything he taught me during these three years, and, most of all, for sharing with me his passion for Cosmology.

My deep gratitude goes to all my friends at IAP for their support and friendship, pour les pauses et les bavardages, ainsi que pour les intéressantes discussions scientifiques: Rebekka Bieri, Nicolas Martinet, Guillaume Plum, Jill Chevalier (qui m'a fait découvrir les cannelés), Vivien Scottez, Mélanie Habouzit (sans laquelle aucun doctorant n'aurait mangé cette année, d'après *Martinet and Habouzit (2014)*, in prep.), Clément Ranc, Charlotte Welker, Maxime Kubryk, Julia Gutkin (et ses *superbes* gâteaux au chocolat), Vincent Vennin, Ophélia Fabre, Alba Vidal Garcia (gracias por permitirme practicar mi español), Pierre Fleury, Laura Bernard, Hélène Dupuy (on a vraiment bien rigolé ces dernières années), Clotilde Laigle, Sylvain Marsat, Vincent Bourrier, Guillaume Drouart, Hayley Finley et Sandrine Codis (que je connais maintenant depuis bien longtemps et je remercie pour avoir partagé avec moi ses connaissances sur les grandes structures et... pour les potins déchainés). Enfin, parmi les membres de l'IAP qui ont dû supporter le plus mes bavardages il faut sans doute compter mes co-bureau de ma deuxième moitié de thèse: Thomas Lacroix et Florent Leclercq, merci à tous les deux pour avoir discuté des sujets les plus variés, touchant non seulement à la physique et à

l'informatique, mais aussi à des sujets tels que les banques, la cuisine, la météo (eh oui, c'est décidément un sujet récurrent!)... Et en dernier: le record mondial de tolérance des bavardages revient à Flavien Vansyngel (depuis 2011!), que je soupçonne désormais d'avoir développé une surdité darwinienne pour survivre. D'ailleurs je suis sûre qu'il veut se joindre à mes remerciements pour l'énorme travail qu'a fait Pinot pendant ces trois ans!

Inoltre un enorme grazie a Silvia Galli ed Anna Mangilli per i loro consigli e per aver condiviso con me le lamentele sulla mancanza di sole à Paris (bien que, il faut le dire, nombreux sont ceux qui ont entendu mes plaintes à ce sujet). I express my deep gratitude to Paul Sutter, who (besides of being a very good friend) answered no less than 1942 emails in the last couple of years, starting from May 2012 (according to my Mac mail inbox), he had great patience with all the questions I had, spanning from science and informatics to tourism. I also thank Nico Hamaus and Jens Jasche for their friendship and for enlightening discussions about voids. Enfin je voudrais remercier Guilhem Lavaux, qui a eu la patience de m'expliquer, entre autres, d'obscurs sujets tels que le fonctionnement des Netcdf. Grazie anche a Camilla Pacifici, probabilmente una delle persone piu solari che io conosca, in grado di farti sentire di buon umore anche soltanto entrando nel tuo ufficio!

Joseph Silk deserves a particular thank, because of his inspiring questions, his kindness and profound knowledge of every subject of Astrophysics; it has been a real pleasure to interact with him during these years, I also thank him for the opportunity to participate to the ICAP journal club. Marta Volonteri merita inoltre la mia gratitudine per aver ascoltato i miei dubbi, per i suoi consigli e la sua amicizia. Ensuite, I would like to thank all the members of the Institut d'Astrophysique de Paris, because this place is certainly unique in the world and the opportunity to do research in such an inspiring environment is a real privilege. Among them, I am grateful to Jean-Philippe Uzan, Francis Bernardeau, Christophe Pichon, Valérie de Lapparent, Gary Mamon and Matt Lehnert for useful discussions. Merci aussi aux responsables du cluster Horizon, que j'ai largement utilisé pendant la deuxième partie de ma thèse, à Isabelle Guillerme pour m'avoir conseillé les nombreuses fois où j'ai eu besoin

d'aide pour remplir les formulaires, à Georges Debève, Lionel Provost, Xavier Nathan et Carlos Carvalho pour le soutien informatique (en particulier quand mon Mac "m'a lâché" — tragiquement — pendant ma 3ème année).

It is as well a pleasure to thank John Peacock for his sympathy in our email exchanges and for his interest in my work. I recently had the pleasure to share a dinner with Virginia Trimble and to listen to her comments about my work, she certainly is one of the most inspiring persons I ever met, and an incredibly strong personality (both from a scientific and non-scientific point of view). Inoltre ringrazio Alessandro Melchiorri per il suo supporto, e per il sincero interesse che ha per il mio futuro. Before concluding I would like to thank L'école des Houches, the month I spent there has been a life-enlightening experience. My deep gratitude also goes to the organisers of the IAU Symposium 308 held this June in Tallinn. I participated to the conference while I was finishing to write my thesis, and only those who read the first Chapter of this manuscript can understand how incredible it was for me to participate to that Symposium.

Finally, outside the science world, my gratitude goes to my wonderful family: Mami per il supporto telefonico e per avermi richiamata tutte le migliaia di volte che la linea cadeva; Papi: per l'incoraggiamento costante e per avermi insegnato che fare sport è bellissimo (mi ha davvero salvata, più di una volta); Normi e Robbi, come avrei fatto se non mi aveste suggerito e mandato himym, ouat, bbt, got (ci sono tutte?), e per ogni secondo passato insieme quando riuscivamo a vederci. Robbi, la tua playlist mi ha accompagnato per ogni passo di corsa nel bois, grazie! Alla mia migliore amica Gera, grazie per esserci sempre. Inoltre, thanks to Amélie for that time in Montmartre. I also have to say that Lalli was there for me when I really needed it. Infine grazie anche a Barbara e Riccardo, ad Angelo, a Carlo (che è maturo!), à Vincent et à Marinette.

I realise, writing these lines, that really many people contributed in one way or another to this work with their friendship and support, but sans doute non posso dimenticare l'ultimo: grazie Manu per ogni giorno in cui mi sei stato vicino — il mio lavoro, e la mia vita, non sarebbero gli stessi senza di te.

The work of this thesis has been supported by NSF Grant NSF AST 09-08693 ARRA, by Benjamin Wandelt's Chaire Internationale in Theoretical Cosmology at the Université Pierre et Marie Curie and senior Excellence Chair of the Agence Nationale de la Recherche (ANR-10-CEXC-004-01).

Appendix A: Digression on authorship

This appendix describes details and anecdotes related to the discovery of the expansion of the Universe. While the astronomer Edwin Hubble is the most known for the discovery of the expansion of the Universe, Vesto Melvin Slipher's earlier work had already measured the expansion of the Universe before him and advanced the perceptive hypothesis that galaxies recede in all directions (a detailed analysis can be found in Peacock (2013)). Slipher wrote, in 1917:

> *"The mean of the velocities with regard to sign is positive, implying that the nebulae are receding with a velocity of nearly 500 km. This might suggest that the spiral nebulae are scattering but their distribution on the sky is not in accord with this since they are inclined to cluster."*(Slipher, 1917).

Hubble's result uses most of the redshift measures from Slipher to reach the conclusion that the Universe is expanding. One could be surprised by the insight of Hubble in making this conclusion, if not aware of those times common belief that a relation between the distances of objects and their velocity should exists. In 1924, de Sitter had proposed the first non-static cosmological model. Although some scientists did not agree with it (among them Albert Einstein was known to be hostile to this idea), other started looking for a redshift-distance relation.

The role of Edwin Hubble in establishing the linear relation must thus be correctly analysed and weighted. It is not the purpose of this thesis to repeat

this work, but we refer (and have widely used the material for this discussion) to the particularly detailed study in Peacock (2013) (that points out numerous inconsistencies in Hubble's work) and comments that Slipher should receive credit for the discovery of the expansion of the Universe.

A simple citation from the above paper is quite striking: *"[...] the plot has been manipulated in order to make a linear relation look as good as possible.[...] Hubble's sample is therefore poised to deliver evidence for an expanding Universe, even before adding distance data."*.

Furthermore, the idea of expanding Universe has also been introduced *before* Hubble by another scientist, the Belgian abbey Georges Lemaître. In 1927, Lemaître had published the dynamic solutions to the General Relativity equations, as well as calculations based on the velocity measurements from Vesto Slipher and on the distances determined by Hubble in 1926 (using Leavitt's relation). Lemaître had in fact obtained the expansion rate of the Universe.

This estimate (as discussed by Livio (2011)) gave a very high value for the so-called Hubble constant (625 km s^{-1}Mpc), but not so far from the one inferred by Hubble (500 km s^{-1}Mpc). To correctly trace the origin of data used in this measure, one has to follow the citation path in Lemaître's paper, entitled "Un univers homogène de masse constance et de rayon croissant, rendant compte de la vitesse radiale des nébuleuses extra-galactiques" (Lemaître, 1927)[3].

The Belgian astrophysicist used data from Gustav Strömberg (Stromberg, 1925) and measured magnitudes from Hubble (Hubble, 1926), but Strömberg himself credited Vesto Slipher. Strömberg also cites a paper reaching similar conclusions than him, written by Lundmark (Lundmark, 1924), in which the following sentence also acknowledges the work from Slipher:

> *"The velocities for these objects are mainly due to the wonderful spectrographic work performed at the Lowel Observatory by Dr. V.M. Slipher."*(Lundmark, 1924).

[3]The english version of the paper is "Expansion of the Universe, A homogeneous Universe of constant mass and increasing radius accounting for the radial velocity of extra-galactic nebulae" (Lemaître, 1931).

The theoretical work preceding the measurements had been done by de Sitter (1917) (see also Weyl and Silberstein), such that a relation was expected between velocity and distance. Lundmark[4] and Strömberg investigated the distance-velocity relation — before Hubble — and Lemaître discovered the expansion of the Universe, all of them based on Slipher's radial velocity measurements and apparent magnitudes mostly from Holetschek and Hopmann (Lemaître, 1927; Hubble, 1926, 1929)[5].

We have already seen that Slipher was not acknowledged for his anticipating intuitions, but why is it that also Lemaître did not have the deserved recognition? The truth is that his paper was in french, and when he was asked to translate it — in 1930, after Hubble's paper — he did not translate it entirely, but omitted some parts. Mario Livio found a letter from Lemaître himself, stating:

> *"I send you a translation of the paper. I did not find advisable to reprint the provisional discussion of radial velocities which is clearly of no actual interest, and also the geometrical note, which could be replaced by a small bibliography of ancient and new papers on the subject. I join a french text with indication of the passages omitted in the translation."*.

The Belgian scientist found useless to point out his earlier discovery of the expansion of the Universe in the 1931 translation of his 1927 paper, since this had been shown meanwhile by Hubble 1929 (using Slipher's data).

It appears that most credit for the discovery should have been given to Slipher or Lemaître; furthermore, following the discussion in Peacock (2013), credit has been given before time, since a real proof of the Universe's expansion was actually only reached in 1990 with the Hubble space telescope.

[4]Lundmark's measurements of distance were more accurate than Hubble's measurements. Nevertheless these measurements (unlike Lemaître's) relied on unproven methods, thus Lundmark's research was not adopted (Steer, 2012).

[5]Ian Steer published a paper in which he summarizes the discovery of the expansion of the Universe: *"Lundmark established observational evidence that the Universe is expanding. Lemaître established theoretical evidence. Hubble established observational proof."* (Steer, 2012)

This analysis of attribution for the discovery of the expansion of the Universe is particularly important since countless references seem to have been unfair to the some actors of the discovery (Slipher, for what concerns measurement and a first hypothesis; Lemaître, for what concerns the theoretical discovery of the expansion).

Appendix B

In this appendix I calculate the relation between $\rho(z, r_{\rm p})$ from data and the reconstructed $g(r_{\rm v})$ in two different ways. First I directly calculate $dz/dr_{\rm z}$ by considering:

$$z = H_0 r_{\rm z} + v\left(\sqrt{r_{\rm p}^2 + r_{\rm z}^2}\right)\cos\left[\text{arctg}\left(\frac{r_{\rm p}}{r_{\rm z}}\right)\right] \tag{7.4}$$

From which I get:

$$\begin{aligned}\frac{dz}{dr_{\rm z}} = H_0 + \frac{r_{\rm z}}{\sqrt{r_{\rm p}^2 + r_{\rm z}^2}} v'\left(\sqrt{r_{\rm p}^2 + r_{\rm z}^2}\right)\cos\left[\text{arctg}\left(\frac{r_{\rm p}}{r_{\rm z}}\right)\right] + \\ v\left(\sqrt{r_{\rm p}^2 + r_{\rm z}^2}\right)\left(-\frac{r_{\rm p}}{r_{\rm z}^2}\right)\frac{1}{1+\frac{r_{\rm p}^2}{r_{\rm z}^2}}(-1)\sin\left[\text{arctg}\left(\frac{r_{\rm p}}{r_{\rm z}}\right)\right]\end{aligned} \tag{7.5}$$

Thus

$$\frac{dz}{dr_{\rm z}} = H_0 + \frac{r_{\rm z}}{r_{\rm v}} v'(r_{\rm v})\cos\,\theta + v(r_{\rm v})\sin\,\theta\frac{r_{\rm p}}{r_{\rm z}^2 + r_{\rm p}^2} \tag{7.6}$$

Finally

$$\frac{dz}{dr_{\rm z}} = H_0 + v'(r_{\rm v})\cos^2\theta + \frac{v(r_{\rm v})}{r_{\rm v}}\sin^2\theta \tag{7.7}$$

The same result can be obtained considering:

$$\begin{aligned}\rho(r_{\rm p},z) &= \int dr_{\rm z}\ \delta(z-(H_0 r_{\rm z}+v(r_{\rm v})\cos\,\theta))g(r_{\rm p},r_{\rm z})\\ &= \int dr_{\rm z}\ \delta\left(z-r_{\rm z}\left(H_0+\frac{v(r_{\rm v})}{r_{\rm v}}\right)\right)g(r_{\rm p},r_{\rm z})\\ &= \int dr_{\rm z}\ \frac{\delta(r_{\rm z}-r_{\rm z}^*)}{\frac{\partial f(r_{\rm z})}{\partial r_{\rm z}}\Big|_{r_{\rm z}^*}}g(r_{\rm p},r_{\rm z^*})\\ &= \frac{1}{\frac{\partial f(r_{\rm z})}{\partial r_{\rm z}}\Big|_{r_{\rm z}^*}}g(r_{\rm p},r_{\rm z})\end{aligned} \tag{7.8}$$

where I have defined

$$f(r_{\rm v}) = r_{\rm z}\left(H_0+\frac{v(r_{\rm v})}{r_{\rm v}}\right) \tag{7.9}$$

and $r_{\rm v}=\sqrt{r_{\rm p}^2+r_{\rm z}^2}$.

I calculate:

$$\begin{aligned}\frac{\partial f(r_{\rm z})}{\partial r_{\rm z}}\Big|_{r_{\rm z}^*} &= \left(H_0+\frac{v(r_{\rm v})}{r_{\rm v}}\right)+r_{\rm z}\frac{\partial\left(H_0+\frac{v(r_{\rm v})}{r_{\rm v}}\right)}{\partial r_{\rm z}}\\ = H_0+\frac{v(r_{\rm v})}{r_{\rm v}}+r_{\rm z}&\left[\frac{1}{r}\frac{\partial v(r)}{\partial r_{\rm z}}+v(r_{\rm v})\left(-\frac{1}{r^2}\right)\frac{dr_{\rm v}}{dr_{\rm z}}\right]\\ = H_0+\frac{v(r_{\rm v})}{r_{\rm v}}+r_{\rm z}&\left[\frac{1}{r_{\rm v}}\frac{\partial v(r_{\rm v})}{\partial r_{\rm v}}\frac{\partial r_{\rm v}}{\partial r_{\rm z}}-\frac{v(r_{\rm v})}{r_{\rm v}^2}\frac{r_{\rm z}}{r_{\rm v}}\right]\end{aligned} \tag{7.10}$$

Since

$$\frac{\partial v(r_{\rm v})}{\partial r_{\rm z}} = \frac{\partial v(r_{\rm v})}{\partial r_{\rm v}}\frac{\partial r_{\rm v}}{\partial r_{\rm z}} = \frac{r_{\rm z}}{r_{\rm v}}v'(r_{\rm v}) \tag{7.11}$$

we obtain

$$\begin{aligned}\left.\frac{\partial f(r_{\rm z})}{\partial r_{\rm z}}\right|_{r_{\rm z}*} &= H_0 + \frac{v(r_{\rm v})}{r_{\rm v}} + r_{\rm z}\left[\frac{1}{r_{\rm v}}\frac{r_{\rm z}}{r}v'(r_{\rm v}) - \frac{r_{\rm z}}{r_{\rm v}^3}v(r_{\rm v})\right] \\ &= H_0 + v(r_{\rm v})\frac{r_{\rm v}^2 - r_{\rm z}^2}{r_{\rm v}^3} + \frac{r_{\rm z}^2}{r_{\rm v}^2}v'(r_{\rm v}) \\ &= H_0 + \frac{v(r_{\rm v})}{r_{\rm v}}\sin^2\theta + v'(r_{\rm v})\cos^2\theta\end{aligned} \tag{7.12}$$

where θ is the angle between the direction of line of sight an the radial direction. Thus I find the same result as with the previous method:

$$\rho(r_{\rm p}, z) = \left[H_0 + v'(r_{\rm v})\cos^2\theta + \frac{v(r_{\rm v})}{r_{\rm v}}\sin^2\theta\right]^{-1} g(r_{\rm p}, r_{\rm z}) \tag{7.13}$$

Bibliography

Abel, N. H. *Oeuvres Completes*. SEd. L. Sylow and S. Lie, New York: Johnson Reprint Corp., 1842, reprint 1988.

Abell, G. O. The Distribution of Rich Clusters of Galaxies. *ApJS*, 3:211, May 1958. doi: 10.1086/190036.

Abell, G. O. Evidence regarding second-order clustering of galaxies and interactions between clusters of galaxies. *AJ*, 66:607, December 1961. doi: 10.1086/108472.

Akaike, H. A new look at the statistical model identification. *IEEE Transactions on Automatic Control*, 19:716–723, 1974. doi: 10.1109/TAC.1974.1100705. URL http://dx.doi.org/10.1109/TAC.1974.1100705.

Alcock, C. and Paczynski, B. An evolution free test for non-zero cosmological constant. *Nature*, 281:358, October 1979. doi: 10.1038/281358a0.

Andrae, R., Schulze-Hartung, T., and Melchior, P. Dos and don'ts of reduced chi-squared. *ArXiv e-prints*, December 2010.

Bassett, B. and Hlozek, R. Baryon acoustic oscillations. *Dark energy: observational and theoretical approaches*, 1:246, 2010. URL http://books.google.com/books?hl=en&lr=&id=V3PBqy0aPpcC&oi=fnd&pg=PA246&dq=bao+hlozek&ots=tPFT-WYnxh&sig=MaqqE3JyNu8WiqxUaX2qQbqhdKs.

Belikov, A. V. and Hu, W. Equivalence principle violation in weakly

vainshtein-screened systems. *Physical Review D*, 87(8):084042, 2013. URL http://prd.aps.org/abstract/PRD/v87/i8/e084042.

Biswas, R., Alizadeh, E., and Wandelt, B. D. Voids as a precision probe of dark energy. *Physical Review D*, 82(2):023002, 2010. URL http://prd.aps.org/abstract/PRD/v82/i2/e023002.

Biviano, A. From Messier to Abell: 200 Years of Science with Galaxy Clusters. In *Constructing the Universe with Clusters of Galaxies*, 2000.

Blake, C. and Glazebrook, K. Probing dark energy using baryonic oscillations in the galaxy power spectrum as a cosmological ruler. *The Astrophysical Journal*, 594(2):665, 2003. URL http://iopscience.iop.org/0004-637X/594/2/665.

Blas, D., Lesgourgues, J., and Tram, T. The cosmic linear anisotropy solving system (class). part ii: approximation schemes. *Journal of Cosmology and Astroparticle Physics*, 2011(07):034, 2011. URL http://iopscience.iop.org/1475-7516/2011/07/034.

Blumenthal, G., Da Costa, L. N., Goldwirth, D., Lecar, M., and Piran, T. The largest possible voids. *The Astrophysical Journal*, 388:234–241, 1992.

Bos, E., van de Weygaert, R., Dolag, K., and Pettorino, V. The darkness that shaped the void: dark energy and cosmic voids. *Monthly Notices of the Royal Astronomical Society*, 426(1):440–461, 2012a. URL http://onlinelibrary.wiley.com/doi/10.1111/j.1365-2966.2012.21478.x/full.

Bos, E., van de Weygaert, R., Ruwen, J., Dolag, K., and Pettorino, V. Less is more: How cosmic voids can shed light on dark energy. *arXiv preprint arXiv:1211.3249*, 2012b. URL http://arxiv.org/abs/1211.3249.

Bracewell, R. *The Fourier Transform and Its Applications, 3rd ed.* McGraw-Hill, 1999.

Burnham and Anderson. *Model Selection and Multimodel Inference: A Practical Information-Theoretic Approach (2nd ed.)*. Springer-Verlag, 2002.

Ceccarelli, L., Padilla, N., Valotto, C., and Lambas, D. G. Voids in the 2dfgrs and λcdm simulations: spatial and dynamical properties. *Monthly Notices of the Royal Astronomical Society*, 373(4):1440–1450, 2006.

Chevallier, M. and Polarski, D. Accelerating universes with scaling dark matter. *International Journal of Modern Physics D*, 10(02):213–223, 2001. URL http://www.worldscientific.com/doi/abs/10.1142/S0218271801000822.

Chincarini, G. and Rood, H. J. The Coma supercluster - Analysis of Zwicky-Herzog cluster 16 in field 158. *ApJ*, 206:30–37, May 1976. doi: 10.1086/154353.

Clampitt, J., Cai, Y.-C., and Li, B. Voids in modified gravity: excursion set predictions. *MNRAS*, 431:749–766, May 2013. doi: 10.1093/mnras/stt219.

Colberg, J. M., Sheth, R. K., Diaferio, A., Gao, L., and Yoshida, N. Voids in a λcdm universe. *Monthly Notices of the Royal Astronomical Society*, 360(1):216–226, 2005. URL http://mnras.oxfordjournals.org/content/360/1/216.short.

Colberg, J. M., Pearce, F., Foster, C., et al. The aspen–amsterdam void finder comparison project. *Monthly Notices of the Royal Astronomical Society*, 387(2):933–944, 2008.

Cole, S., Percival, W. J., Peacock, J. A., et al. The 2df galaxy redshift survey: power-spectrum analysis of the final data set and cosmological implications. *Monthly Notices of the Royal Astronomical Society*, 362(2):505–534, 2005.

Cooray, A., Hu, W., Huterer, D., and Joffre, M. Measuring Angular Diameter Distances through Halo Clustering. *ApJL*, 557:L7–L10, August 2001. doi: 10.1086/323323.

Crocce, M., Pueblas, S., and Scoccimarro, R. Transients from initial conditions in cosmological simulations. *Monthly Notices of the Royal Astronomical Society*, 373(1):369–381, 2006. URL http://onlinelibrary.wiley.com/doi/10.1111/j.1365-2966.2006.11040.x/full.

da Costa, L. N., Geller, M. J., Pellegrini, P. S., et al. A complete southern sky redshift survey. *ApJL*, 424:L1–L4, March 1994. doi: 10.1086/187260.

Davis, T. M. and Lineweaver, C. H. Expanding Confusion: Common Misconceptions of Cosmological Horizons and the Superluminal Expansion of the Universe. *Pub. Astr. Soc. Australia*, 21:97–109, 2004. doi: 10.1071/AS03040.

de Bernardis, P., Ade, P., Bock, J., et al. A flat universe from high-resolution maps of the cosmic microwave background radiation. *Nature*, 404(6781): 955–959, 2000. URL http://www.nature.com/nature/journal/v404/n6781/abs/404955a0.html.

de Lapparent, V., Geller, M. J., and Huchra, J. P. A slice of the universe. *The Astrophysical Journal*, 302:L1–L5, 1986.

de Sitter, W. Einstein's theory of gravitation and its astronomical consequences. Third paper. *MNRAS*, 78:3–28, November 1917.

de Vaucouleurs, G. The Case for a Hierarchical Cosmology. *Science*, 167: 1203–1213, February 1970. doi: 10.1126/science.167.3922.1203.

de Vaucouleurs, G., de Vaucouleurs, A., and Corwin, J. Second reference catalogue of bright galaxies. In *Second reference catalogue of bright galaxies, 1976, Austin: University of Texas Press.*, volume 1, page 0, 1976.

Dekel, A. and Rees, M. Omega from velocities in voids. *arXiv preprint astro-ph/9308029*, 1993. URL http://arxiv.org/abs/astro-ph/9308029.

Dodelson, S. *Modern cosmology*. Academic press, 2003.

Eisenstein, D. J., Zehavi, I., Hogg, D. W., et al. Detection of the Baryon Acoustic Peak in the Large-Scale Correlation Function of SDSS Luminous Red Galaxies. *ApJ*, 633:560–574, November 2005. doi: 10.1086/466512.

El-Ad, H., Piran, T., and Dacosta, L. N. A catalogue of the voids in the IRAS 1.2-Jy survey. *MNRAS*, 287:790–798, June 1997.

Fairall, A. P. Large-scale structures in the universe. In *Large-scale structures in the universe/Anthony P. Fairall. New York: Wiley, 1998.(Wiley-Praxis series in astronomy and astrophysics) QB980. F35 1998*, volume 1, 1998.

Fernie, J. D. The Period-Luminosity Relation: A Historical Review. *PASP*, 81:707, December 1969. doi: 10.1086/128847.

Fleury, P., Dupuy, H., and Uzan, J.-P. Can All Cosmological Observations Be Accurately Interpreted with a Unique Geometry? *Physical Review Letters*, 111(9):091302, August 2013. doi: 10.1103/PhysRevLett.111.091302.

Friedmann, A. 125. on the curvature of space. *Zeitschrift für Physik*, 10: 377–386, 1922.

Fujimoto, M. Dynamics of ellipsoidal voids of matter in an expanding universe. *Publications of the Astronomical Society of Japan*, 35:159–171, 1983.

Geller, M. J. and Huchra, J. P. Mapping the universe. *Science*, 246:897–903, November 1989. doi: 10.1126/science.246.4932.897.

Goldwirth, D. S., da Costa, L. N., and Van de Weygaert, R. The two–point correlation function and the size of voids. *Arxiv preprint astro-ph/9503002*, 1995. URL http://arxiv.org/abs/astro-ph/9503002.

Gottlöber, S., Łokas, E. L., Klypin, A., and Hoffman, Y. The structure of voids. *Monthly Notices of the Royal Astronomical Society*, 344(3):715–724, 2003. URL http://mnras.oxfordjournals.org/content/344/3/715.short.

Gregory, S. A. and Thompson, L. A. The Coma/A1367 supercluster and its environs. *ApJ*, 222:784–799, June 1978. doi: 10.1086/156198.

Hamaus, N., Sutter, P., and Wandelt, B. D. A universal density profile for cosmic voids. *arXiv preprint arXiv:1403.5499*, 2014. URL http://arxiv.org/abs/1403.5499.

Hamilton, A. J. S. Linear Redshift Distortions: a Review. In Hamilton, D., editor, *The Evolving Universe*, volume 231 of *Astrophysics and Space Science Library*, page 185, 1998.

Hogg, D. W. Distance measures in cosmology. *arXiv preprint astro-ph/9905116*, 1999. URL http://arxiv.org/abs/astroph/9905116.

Hoyle, F. and Vogeley, M. S. Voids in the Point Source Catalogue Survey and the Updated Zwicky Catalog. *ApJ*, 566:641–651, February 2002. doi: 10.1086/338340.

Hubble, E. A Relation between Distance and Radial Velocity among Extra-Galactic Nebulae. *Proceedings of the National Academy of Science*, 15: 168–173, March 1929. doi: 10.1073/pnas.15.3.168.

Hubble, E. P. Extragalactic nebulae. *ApJ*, 64:321–369, December 1926. doi: 10.1086/143018.

Icke, V. Voids and filaments. *MNRAS*, 206:1P–3P, January 1984.

Icke, V. and van de Weygaert, R. Fragmenting the universe. *Astronomy and Astrophysics*, 184:16–32, 1987.

Jõeveer, M., Einasto, J., and Tago, E. Spatial distribution of galaxies and of clusters of galaxies in the southern galactic hemisphere. *MNRAS*, 185: 357–370, November 1978.

Jennings, E., Li, Y., and Hu, W. The abundance of voids and the excursion set formalism. *Monthly Notices of the Royal Astronomical Society*, 434 (3):2167–2181, 2013. URL http://mnras.oxfordjournals.org/content/434/3/2167.short.

Joeveer, M. and Einasto, J. Has the universe the cell structure. In Longair, M. S. and Einasto, J., editors, *Large Scale Structures in the Universe*, volume 79 of *IAU Symposium*, pages 241–250, 1978.

Kant, I. *Allgemeine Naturgeschichte und Theorie des Himmels*. Johann Friederich Petersen, 1755.

Karachentsev, I. Catalogue of isolated pairs of galaxies in the northern hemisphere. *Soobshcheniya Spetsial'noj Astrofizicheskoj Observatorii*, 7:1, 1972.

Kauffmann, G. and Fairall, A. Voids in the distribution of galaxies: an assessment of their significance and derivation of a void spectrum. *Monthly Notices of the Royal Astronomical Society*, 248(2):313–324, 1991.

Kirshner, R. P., Oemler, A., Jr., Schechter, P. L., and Shectman, S. A. A million cubic megaparsec void in Bootes. *ApJL*, 248:L57–L60, September 1981. doi: 10.1086/183623.

Laureijs, R., Amiaux, J., Arduini, S., et al. Euclid definition study report. *arXiv preprint arXiv:1110.3193*, 2011. URL http://arxiv.org/abs/1110.3193.

Lavaux, G. and Wandelt, B. D. Precision Cosmography with Stacked Voids. *ApJ*, 754:109, August 2012. doi: 10.1088/0004-637X/754/2/109.

Lavaux, G. and Wandelt, B. Cosmic voids as standard rulers for cosmology. In *American Astronomical Society Meeting Abstracts# 219*, volume 219, 2012. URL http://adsabs.harvard.edu/abs/2012AAS...21933602L.

Lavaux, G. and Wandelt, B. D. Precision cosmology with voids: definition, methods, dynamics. *Monthly Notices of the Royal Astronomical Society*, 403 (3):1392–1408, 2010. URL http://onlinelibrary.wiley.com/doi/10.1111/j.1365-2966.2010.16197.x/full.

Leavitt, H. S. 1777 variables in the Magellanic Clouds. *Annals of Harvard College Observatory*, 60:87–108, 1908.

Leavitt, H. S. and Pickering, E. C. Periods of 25 Variable Stars in the Small Magellanic Cloud. *Harvard College Observatory Circular*, 173:1–3, March 1912.

Lemaître, G. Un Univers homogène de masse constante et de rayon croissant rendant compte de la vitesse radiale des nébuleuses extra-galactiques. *Annales de la Societe Scietifique de Bruxelles*, 47:49–59, 1927.

Lemaître, G. Expansion of the universe, A homogeneous universe of constant mass and increasing radius accounting for the radial velocity of extra-galactic nebulae. *MNRAS*, 91:483–490, March 1931.

Li, B. Voids in coupled scalar field cosmology. *Monthly Notices of the Royal Astronomical Society*, 411(4):2615–2627, 2011. URL http://onlinelibrary.wiley.com/doi/10.1111/j.1365-2966.2010.17867.x/full.

Li, X.-F., Huang, L., and Huang, Y. A new Abel inversion by means of the integrals of an input function with noise. *Journal of Physics A Mathematical General*, 40:347–360, January 2007. doi: 10.1088/1751-8113/40/2/012.

Linder, E. V. Exploring the expansion history of the universe. *Physical Review Letters*, 90(9):091301, 2003. URL http://journals.aps.org/prl/abstract/10.1103/PhysRevLett.90.091301.

Livio, M. Lost in translation: Mystery of the missing text solved. *Nature*, 479:171–173, November 2011. doi: 10.1038/479171a.

Longair, M. S. Personal View-The Large Scale Structure of the Universe. In Longair, M. S. and Einasto, J., editors, *Large Scale Structures in the Universe*, volume 79 of *IAU Symposium*, page 451, 1978.

Lundmark, K. The determination of the curvature of space-time in de Sitter's world. *MNRAS*, 84:747–770, June 1924.

Lyth, D. H. and Liddle, A. R. *The Primordial Density Perturbation: Cosmology, Inflation and the Origin of Structure*. Cambridge University Press, 2009.

Majumdar, S. and Mohr, J. J. Self-Calibration in Cluster Studies of Dark Energy: Combining the Cluster Redshift Distribution, the Power Spectrum, and Mass Measurements. *ApJ*, 613:41–50, September 2004. doi: 10.1086/422829.

Marra, V., Amendola, L., Sawicki, I., and Valkenburg, W. Cosmic Variance and the Measurement of the Local Hubble Parameter. *Physical Review Letters*, 110(24):241305, June 2013. doi: 10.1103/PhysRevLett.110.241305.

Martel, H. and Wasserman, I. Simulation of cosmological voids in lambda greater than 0 friedmann models. *The Astrophysical Journal*, 348:1–25, 1990.

Melott, A. L. Voids and velocities in initially gaussian models for large-scale structure. *Monthly Notices of the Royal Astronomical Society*, 228:1001–1023, 1987.

Neyrinck, M. C. ZOBOV: a parameter-free void-finding algorithm. *MNRAS*, 386:2101–2109, June 2008. doi: 10.1111/j.1365-2966.2008.13180.x.

Ostriker, J. P. and Steinhardt, P. J. The observational case for a low-density Universe with a non-zero cosmological constant. *Nature*, 377:600–602, October 1995. doi: 10.1038/377600a0.

Padilla, N., Ceccarelli, L., and Lambas, D. Spatial and dynamical properties of voids in a λ cold dark matter universe. *Monthly Notices of the Royal Astronomical Society*, 363(3):977–990, 2005.

Pan, D. C., Vogeley, M. S., Hoyle, F., Choi, Y.-Y., and Park, C. Cosmic voids in sloan digital sky survey data release 7. *Monthly Notices of the Royal Astronomical Society*, 421(2):926–934, 2012. URL http://mnras.oxfordjournals.org/content/421/2/926.short.

Peacock, J. A. Slipher, Galaxies, and Cosmological Velocity Fields. In Way, M. J. and Hunter, D., editors, *Origins of the Expanding Universe: 1912-1932*, volume 471 of *Astronomical Society of the Pacific Conference Series*, page 3, April 2013.

Peacock, J. A. *Cosmological physics*. Cambridge university press, 1999.

Peebles, P. J. E. *Principles of physical cosmology*. Princeton University Press, 1993.

Perlmutter, S., Aldering, G., and Goldhaber, G. e. a. Measurements of Omega and Lambda from 42 High-Redshift Supernovae. *ApJ*, 517:565–586, June 1999. doi: 10.1086/307221.

Pisani, A. and Wandelt, B. The challenge of cosmic voids. *Proceedings of the International School of Physics "Enrico Fermi" of the Italian Physical Society – SIF-Course CLXXXVI: "New Horizons for Observational Cosmology"*, eds A. Cooray, A. Melchiorri, E. Komatsu, 2013.

Pisani, A., Lavaux, G., Sutter, P. M., and Wandelt, B. D. Real-space density profile reconstruction of stacked voids. *MNRAS*, 443:3238–3250, October 2014a.

Pisani, A., Sutter, P. M., Alizadeh, E., Biswas, R., and Wandelt, B. D. Constraining dark energy with cosmic void abundances (in prep.). *To be submitted to MNRAS*, 2014b.

Pisani, A., Sutter, P. M., and Wandelt, B. D. Mastering the effects of peculiar velocities on voids (in prep.). *To be submitted to MNRAS*, 2014c.

Planck Collaboration. Planck 2013 results. xvi. cosmological parameters. *arXiv preprint arXiv:1303.5076*, 2013. URL http://arxiv.org/abs/1303.5076.

Planck Collaboration, Ade, P. A. R., Aghanim, N., et al. Planck 2013 results. XXVI. Background geometry and topology of the Universe. *ArXiv e-prints*, March 2013.

Platen, E., Van De Weygaert, R., and Jones, B. J. A cosmic watershed: the wvf void detection technique. *Monthly notices of the royal astronomical society*, 380(2):551–570, 2007.

Platen, E., van de Weygaert, R., Jones, B. J., Vegter, G., and Calvo, M. A. A. Structural analysis of the sdss cosmic web–i. non-linear density field reconstructions. *Monthly Notices of the Royal Astronomical Society*, 416 (4):2494–2526, 2011. URL http://mnras.oxfordjournals.org/content/416/4/2494.short.

Press, W. H. and Schechter, P. Formation of galaxies and clusters of galaxies by self-similar gravitational condensation. *The Astrophysical Journal*, 187: 425–438, 1974.

Riess, A. G., Filippenko, A. V., and Challis, P. e. a. Observational Evidence from Supernovae for an Accelerating Universe and a Cosmological Constant. *AJ*, 116:1009–1038, September 1998. doi: 10.1086/300499.

Ryden, B. S. Measuring Q 0 from the Distortion of Voids in Redshift Space. *ApJ*, 452:25, October 1995. doi: 10.1086/176277.

Ryden, B. and Melott, A. Voids in real space and in redshift space. *arXiv preprint astro-ph/9510108*, 1995. URL http://arxiv.org/abs/astro-ph/9510108.

Ryden, B. S. Self-similar expansion of axisymmetric voids. *The Astrophysical Journal*, 423:534, 1994.

Ryden, B. S. *Introduction to cosmology*, volume 523. Addison-Wesley Reading, 2003.

Ryden, B. and Turner, E. A statistical comparison of voids in the galaxy distribution and n-body simulations. *The Astrophysical Journal*, 287:L59–L63, 1984.

Schaap, W. and Van De Weygaert, R. Continuous fields and discrete samples: reconstruction through delaunay tessellations. *Arxiv preprint astro-ph/0011007*, 2000. URL http://arxiv.org/abs/astro-ph/0011007.

Seo, H.-J. and Eisenstein, D. J. Probing dark energy with baryonic acoustic oscillations from future large galaxy redshift surveys. *The Astrophysical Jour-*

nal, 598(2):720, 2003. URL http://iopscience.iop.org/0004-637X/598/2/720.

Shectman, S. A., Landy, S. D., Oemler, A., et al. The Las Campanas Redshift Survey. *ApJ*, 470:172, October 1996. doi: 10.1086/177858.

Sheth, R. K. and Van De Weygaert, R. A hierarchy of voids: much ado about nothing. *Monthly Notices of the Royal Astronomical Society*, 350(2): 517–538, 2004. URL http://onlinelibrary.wiley.com/doi/10.1111/j.1365-2966.2004.07661.x/full.

Slipher, V. M. Nebulae. *Proceedings of the American Philosophical Society*, 56:403–409, 1917.

Smith, R. W. and Berendzen, R. Book-Review - the Expanding Universe - Astronomy's Great Debate 1900-1931. *Journal for the History of Astronomy*, 13:209, 1982.

Spolyar, D., Sahlén, M., and Silk, J. Topology and Dark Energy: Testing Gravity in Voids. *Physical Review Letters*, 111(24):241103, December 2013. doi: 10.1103/PhysRevLett.111.241103.

Springel, V., White, S. D., Jenkins, A., et al. Simulations of the formation, evolution and clustering of galaxies and quasars. *nature*, 435(7042):629–636, 2005. URL http://www.nature.com/nature/journal/v435/n7042/abs/nature03597.html.

Steer, I. History: Who discovered Universe expansion? *Nature*, 490:176, October 2012. doi: 10.1038/490176c.

Strauss, M. A., Weinberg, D. H., Lupton, R. H., et al. Spectroscopic target selection in the sloan digital sky survey: the main galaxy sample. *The Astronomical Journal*, 124(3):1810, 2002. URL http://iopscience.iop.org/1538-3881/124/3/1810.

Stromberg, G. Analysis of radial velocities of globular clusters and non-galactic nebulae. *ApJ*, 61:353–362, June 1925. doi: 10.1086/142897.

Sullivan, R. Celestial motions in the line of sight. *Popular Astronomy*, 24: 109, 1916.

Sutter, P. M., Lavaux, G., Wandelt, B. D., and Weinberg, D. H. A Public Void Catalog from the SDSS DR7 Galaxy Redshift Surveys Based on the Watershed Transform. *ApJ*, 761:44, December 2012a. doi: 10.1088/0004-637X/761/1/44.

Sutter, P. M., Lavaux, G., Wandelt, B. D., and Weinberg, D. H. A First Application of the Alcock-Paczynski Test to Stacked Cosmic Voids. *ApJ*, 761:187, December 2012b. doi: 10.1088/0004-637X/761/2/187.

Sutter, P. M., Lavaux, G., Wandelt, B. D., et al. Voids in the SDSS DR9: observations, simulations, and the impact of the survey mask. *ArXiv e-prints*, October 2013.

Sutter, P. M., Carlesi, E., Wandelt, B. D., and Knebe, A. On the observability of coupled dark energy with cosmic voids. *arXiv preprint arXiv:1406.0511*, 2014a.

Sutter, P., Lavaux, G., Wandelt, B. D., et al. Sparse sampling, galaxy bias, and voids. *arXiv preprint arXiv:1309.5087*, 2013. URL http://arxiv.org/abs/1309.5087.

Sutter, P., Lavaux, G., Hamaus, N., et al. Vide: The void identification and examination toolkit. *arXiv preprint arXiv:1406.1191*, 2014b.

Sutter, P., Lavaux, G., Wandelt, B. D., Weinberg, D. H., and Warren, M. S. The dark matter of galaxy voids. *Monthly Notices of the Royal Astronomical Society*, page stt2425, 2014c. URL http://mnras.oxfordjournals.org/content/early/2014/01/13/mnras.stt2425.short.

Sutter, P., Pisani, A., and Wandelt, B. D. A measurement of the alcock-paczynski test using cosmic voids in the sdss. *arXiv preprint arXiv:1404.5618*, 2014d. URL http://arxiv.org/abs/1404.5618.

Thompson, L. A. Discovery of voids and their relationship to superclusters. *Online*, 2005. URL http://www.astro.bas.bg/~petrov/galaxies_files/voids.html.

Thompson, L. A. and Gregory, S. A. An historical view: The discovery of voids in the galaxy distribution. *arXiv preprint arXiv:1109.1268*, 2011. URL http://arxiv.org/abs/1109.1268.

Tifft, W. G. and Gregory, S. A. Direct observations of the large-scale distribution of galaxies. *ApJ*, 205:696–708, May 1976. doi: 10.1086/154325.

Tifft, W. G. and Gregory, S. A. Observations of the Large Scale Distribution of Galaxies. In Longair, M. S. and Einasto, J., editors, *Large Scale Structures in the Universe*, volume 79 of *IAU Symposium*, page 267, 1978.

Tinker, J. L., Weinberg, D. H., and Zheng, Z. Redshift-space distortions with the halo occupation distribution - I. Numerical simulations. *MNRAS*, 368: 85–108, May 2006. doi: 10.1111/j.1365-2966.2006.10114.x.

van de Weygaert, R. and Schaap, W. The Cosmic Web: Geometric Analysis. *ArXiv e-prints*, August 2007.

van de Weygaert, R. Fragmenting the universe. 3: The constructions and statistics of 3-d voronoi tessellations. *Astronomy and Astrophysics*, 283: 361–406, 1994.

van de Weygaert, R. and Icke, V. Fragmenting the universe. ii-voronoi vertices as abell clusters. *Astronomy and Astrophysics*, 213:1–9, 1989.

van de Weygaert, R. and Schaap, W. The cosmic web: geometric analysis. In *Data Analysis in Cosmology*, pages 291–413. Springer, 2009. URL http://link.springer.com/chapter/10.1007/978-3-540-44767-2_11.

van de Weygaert, R. and van Kampen, E. Voids in gravitational instability scenarios–i. global density and velocity fields in an einstein–de sitter universe. *Monthly Notices of the Royal Astronomical Society*, 263(2):481–526, 1993.

van de Weygaert, R., Pranav, P., Jones, B. J., et al. Probing dark energy with alpha shapes and betti numbers. *arXiv preprint arXiv:1110.5528*, 2011. URL http://arxiv.org/abs/1110.5528.

Verde, L., Jimenez, R., and Feeney, S. The importance of local measurements for cosmology. *Physics of the Dark Universe*, 2:65–71, June 2013. doi: 10.1016/j.dark.2013.04.003.

Weinberg, D. H., Mortonson, M. J., Eisenstein, D. J., et al. Observational probes of cosmic acceleration. *arXiv preprint arXiv:1201.2434*, 2012. URL http://arxiv.org/abs/1201.2434.

Weinberg, S. Gravitation and cosmology: principles and applications of the general theory of relativity. *John Wiley & Sons, Inc.*, 1972.

Wolz, L., Kilbinger, M., Weller, J., and Giannantonio, T. On the validity of cosmological fisher matrix forecasts. *Journal of Cosmology and Astroparticle Physics*, 2012(09):009, 2012. URL http://iopscience.iop.org/1475-7516/2012/09/009.

Wright, T. O. D. and Hoskin, M. A. Review of Publications- An Original Theory or New Hypothesis of the Universe (1750). *J. Royal Astr. Soc. Canada*, 66:280, October 1972.

Zehavi, I., Zheng, Z., Weinberg, D. H., et al. Galaxy clustering in the completed sdss redshift survey: the dependence on color and luminosity. *The Astrophysical Journal*, 736(1):59, 2011. URL http://iopscience.iop.org/0004-637X/736/1/59.

Zeldovich, I. B. The theory of the large scale structure of the universe. In Longair, M. S. and Einasto, J., editors, *Large Scale Structures in the Universe*, volume 79 of *IAU Symposium*, pages 409–420, 1978.

Zheng, Z., Coil, A. L., and Zehavi, I. Galaxy evolution from halo occupation distribution modeling of deep2 and sdss galaxy clustering. *The Astrophysical Journal*, 667(2):760, 2007. URL http://iopscience.iop.org/0004-637X/667/2/760.

Zwicky, F. Die Rotverschiebung von extragalaktischen Nebeln. *Helvetica Physica Acta*, 6:110–127, 1933.

Zwicky, F. Non-Uniformities in the Apparent Distribution of Clusters of Galaxies. *PASP*, 69:518, December 1957. doi: 10.1086/127139.

La Cosmologie avec les Vides Cosmiques

Résumé de la thèse en français

Introduction

La Cosmologie est la science qui étudie l'Univers dans son ensemble, avec l'objectif de comprendre sa structure et son évolution. Afin d'obtenir des informations sur l'Univers, il est possible de l'observer à grande échelle; dés lors considérant les galaxies — groupes d'étoiles unies pas la force de gravité — comme des points et étudiant leurs positions et mouvements. Le mouvement des galaxies trace pour nous l'évolution de l'Univers. À très grandes échelles, des amas de galaxies, des feuilles et des vides constituent l'Univers — c'est la "toile cosmique".

Alors que le travail de recherche pour comprendre la structure de l'Univers à très grande échelle s'est jusqu'à présent plutôt concentré sur l'étude des régions les plus denses, l'intérêt des Cosmologues se porte aujourd'hui aussi sur les régions à faible densité: les vides cosmiques. Ces régions, découvertes en 1978, ont des dimensions entre les dizaines et les centaines de Mpcs.

À cause de la difficulté pour obtenir des données dans les zones à faible densité, le potentiel des vides a été sous-estimé. Les télescopes et satellites modernes nous permettent à présent d'accéder à des mesures de haute précision de la structure à grande échelle de l'Univers: l'appel des vides cosmiques devient

considérable.

Étant dévidés de matière, les vides cosmiques pourraient être principalement composés d'énergie obscure — ce qui justifie largement leur importance pour la Cosmologie, vu que l'énergie obscure constitue environ le 70% de l'Univers et nous ne la comprenons pas encore. Les efforts des cosmologues semblent converger vers un modèle cosmologique (appelé ΛCDM) qui laisse de nombreux énigmes. La nature — et pour en dire plus, l'existence même — de l'énergie obscure reste un mystère; ainsi que la nature de la matière noire. Dans ce contexte, les vides cosmiques constituent un nouvel atout dans notre quête d'un modèle correct pour la Cosmologie.

Les vides remplissent la plus grande partie de l'Univers, et ont une dynamique plus simple que les zones à haute densité de l'Univers. En tant que tels, ils se présentent comme un laboratoire idéal pour tester l'énergie obscure, contraindre l'expansion cosmique et discriminer parmi les différents modèles cosmologiques, tels que les modèles de gravité modifiée.

Bien que promettant d'être plus simple, la Cosmologie avec les vides cosmiques n'en est qu'à ses débuts. Dans l'ère de la Cosmologie de haute précision, toute méthode ou tout nouvel outil cosmologique nécessite d'une compréhension profonde des effets systématiques qui affectent les mesures et d'une étude détaillée, afin de devenir aussi compétitif que les autres outils cosmologiques. Dans le but de contraindre les paramètres caractérisant notre Univers avec les vides cosmiques, nous devons les comprendre et les modéliser correctement.

L'utilisation des vides pour contraindre la Cosmologie est basée sur l'étude de leur formes, de leur nombre et de leur évolution. Ces propriétés dépendent en effet du modèle cosmologique et peuvent donc être utilisées pour contraindre ce modèle. Dans ce contexte la source majeure d'effets systématiques est la présence des vitesses particulières des galaxies.

Quand nous observons les vides cosmiques, nous les observons dans *l'espace des redshifts*: leur forme réelle reste inaccessible pour nous, limitant donc grandement notre connaissance de ces structures. Pour utiliser les vides en tant que outils de précision pour la Cosmologie, il est crucial d'obtenir

leur forme dans l'espace réel et, éventuellement, de comprendre comment les vitesses particulières les affectent.

Le but de cette thèse est de trouver une méthode pour accéder à la forme réelle des vides cosmiques, méthode qui soit autant que possible indépendante du modèle cosmologique — c'est à dire accéder à l'information de l'espace réel avec le mineur nombre possible d'assomptions sur les paramètres cosmologiques.

Ce travail vise à répondre aux questions suivantes: comment peut-on extraire des information sur les vides dans l'espace réel de manière indépendante du modèle? Pouvons-nous comprendre quels sont les effets systématiques dans l'utilisation des vides? Est-il possible d'obtenir des informations sur l'espace réel à partir de vraies données?

L'application de la méthode à développer aux données est un autre point fondamental de ce travail: nous ne pouvons nous affranchir des données, qui ont toujours le dernier mot pour évaluer la qualité d'un modèle. De plus l'utilisation de modèles HOD (Halo Occupation Distribution; distribution de l'occupation de halos) permet de simuler les donnés; il est donc possible d'étudier les effets systématiques qui affectent l'utilisation des vides pour contraindre les modèles cosmologiques: les vitesses particulières.

Obtenir la forme des vides dans l'espace réel et comprendre comment les vitesses influent sur nos mesures sont des étapes cruciales pour atteindre le but de la Cosmologie de précision avec les vides cosmiques.

Nous allons décrire dans une première partie l'utilisation des vides pour contraindre les modèles cosmologiques, ainsi que les effets systématiques qui affectent leur utilisation.

Ensuite nous allons présenter, dans une deuxième partie, la méthode pour obtenir des informations sur les vides dans l'espace réel. Dans cette partie nous présentons également un test de l'algorithme sur une simulation et l'application de la méthode aux données, qui nous permet d'obtenir les premiers profils de vides dans l'espace réel.

Dans la troisième partie nous résumons le résultat d'une analyse visant à établir l'effet des vitesses particulières sur les vides. Enfin nous présentons

une discussion sur l'emploi des vides pour contraindre la cosmologie avec les missions futures.

Contraindre les paramètres cosmologiques avec les vides

En 1995, Barbara Ryden propose d'utiliser les vides pour contraindre les modèles cosmologiques. En particulier, dans Ryden and Melott (1995) elle suggère d'utiliser les vides pour l'application du test de Alcock-Paczyński.

Le test de Alcock-Paczyński permet, en principe, de mesurer l'expansion de l'Univers. Les bases théoriques de cette méthode ont été établies par Charles Alcock and Bohdan Paczyński in 1979: en supposant de pouvoir peupler l'Univers de sphères, on pourrait observer ces objets et mesurer le diamètre angulaire $\Delta\theta$ et leur dimension le long de la ligne de visée, dans l'espace des redshift Δz. Comme pour les règles standard, la manière avec laquelle ces mesures se rapportent aux dimensions physiques dépend de la Cosmologie.

Nous savons que l'objet est une sphère, donc le rapport de ses longueurs radiales et transversales (qui sont des diamètres) doit être égal à un. Quand nous convertissons cela dans des observables cosmologiques, cela signifie que notre sphère standard est un object pour lequel le rapport entre sa dimension dans l'espace des redshift et sa dimension angulaire est connu.

Si ce n'est pas le cas, cela signifie que le modèle cosmologique utilisé pour relier les quantités mesurées (dimension angulaire et dimension le long de la ligne de visée) aux quantités physiques (dimensions radiales et transversales) est faux[6]. Donc si nous avions des sphères placées à différents redshifts dans l'Univers, nous pourrions tester la validité des modèles cosmologiques.

En se basant sur la supposition que les vides soient des objets sphériques (Icke, 1984), Barbara Ryden propose de mesurer l'extension des vides le long de la ligne de visée, ainsi que leur dimension angulaire, pour contraindre les paramètres cosmologiques (Ryden, 1995; Ryden and Melott, 1995). Malheureusement cette idée brillante est destinée à échouer: la forme d'un vide cosmique est en réalité très compliquée, et loin d'être sphérique. Cela porte à des erreurs systématiques considérables qui empêchent l'extraction du signal

[6]En particulier le test de Alcock-Paczyński contraint le produit $H(z)d_A(z)$; pour plus de détails voir le texte de la thèse en anglais.

cosmologique en utilisant le test de Alcock-Paczyński sur les vides.

Récemment, Lavaux and Wandelt (2012) ont introduit un détour astucieux pour permettre l'application du test de Alcock-Paczyński sur les vides cosmiques: l'article propose d'utiliser pour le test des vides empilés. La procédure prévoit donc des trouver les vides dans un intervalle de redshift donné et de faire des moyennes par dimensions. Dans un univers homogène et isotrope il n'y a pas de raison possible pour laquelle la forme *moyenne* des vides cosmiques pourrait avoir des directions préférentielles. Donc les vides sont, en moyenne, sphériques; ce qui signifie que nous pouvons les utiliser comme les sphères standards nécessaires pour le test de Alcock-Paczyński.

Mais l'application du test de Alcock-Paczyński pour mesurer l'expansion de l'Univers n'est pas la seule raison pour laquelle les vides sont intéressants. Le vides sont dévidés de matière, leur principale composante est l'énergie obscure. Donc leur évolution sera dominée par cette composante mystérieuse (Bos et al., 2012a). De nombreux groupes ont étudié l'évolution des vides (entre autres Icke (1984); Fujimoto (1983); Gottlöber et al. (2003); Colberg et al. (2005) et, surtout, Sheth and Van De Weygaert (2004); van de Weygaert et al. (2011)); de manière simplifiée, les vides sont en expansion — toutefois des simulations numériques à haute résolution montrent que certains vides peuvent disparaître dans des régions à haute densité.

De plus, il a été montré que le profil de densité des vides est particulièrement adapté pour tester les modèles de gravité massive, où l'équation d'état dépend de la densité, ce qui rend les zones à densité extrême (amas, c'est à dire maxima de densité; vides, c'est à dire minima de densité) particulièrement sensibles au modèle. Spolyar et al. (2013) et Belikov and Hu (2013) ont montré que cet effet est plus marqué pour les vides: pour la gravité massive, le changement dans les potentiels est négligeable dans les zones à densité élevée, mais considérable dans les vides.

En utilisant les vides cosmiques, il est aussi possible de contraindre les modèles de champ scalaire couplé: dans ces modèles les vides auraient commencé à se développer plus tôt et auraient donc des dimensions majeures (Li, 2011). En outre les vides sont particulièrement sensibles aux composantes

diffuses telles que les neutrinos; qui pourraient modifier la forme des vides dans l'espace réel et leur évolution.

Enfin, les vides sont des structures non-virialisées. En tant que telles, ils gardent une meilleure mémoire des conditions initiales — ils ont évolué moins et d'une manière plus simple que les régions à densité élevée. L'étude de leur profil de densité et de son évolution est donc une fenêtre sur l'Univers primordial.

Les vides sont donc en train de devenir des outils cosmologiques à plein titre. Cependant, nous restons incapables — jusqu'à présent — d'accéder à la forme réelle de ces objets, vu que nous les observons dans l'espace des redshift. En effet quand nous observons les galaxies dans l'Univers avec des télescopes comme le Sloan Digital Sky Survey (SDSS), nous mesurons leur position dans l'espace des redshift. Ceci modifie la forme des vides (comme décrit par Lavaux and Wandelt (2012) et Sutter et al. (2012b)).

Les *distorsions dans l'espace des redshift* modifient le profile de densité que nous obtenons pour les vides. Pour comprendre les vides et les utiliser en tant qu'outils cosmologiques il est d'importance cruciale d'avoir accès au profil de densité dans *l'espace réel*. Malheureusement s'affranchir des distorsions dans l'espace des redshift est l'un des points les plus difficiles dans l'extraction d'information cosmologique à partir des grandes structures de l'Univers. La présence des distorsions en redshift est l'un des effets systématiques les plus importants pour les vides qui sont, sans cela, des objets à évolution simple qui peuvent être décrits dans le cadre de la théorie linéaire.

Le but de cette thèse est de reconstruire le profil de densité des vides dans l'espace réel, en permettant ainsi d'améliorer l'application du test de Alcock-Paczyński, de comprendre l'évolution des vides, mais aussi d'étudier les modèles de gravité modifiée. Dans la prochaine partie nous allons présenter la méthode utilisée pour la reconstruction des vides, ainsi que son application aux données de SDSS.

Reconstruction des vides cosmiques dans l'espace réel

Pour obtenir un profile de densité des vides dans l'espace réel qui soit utilisable pour contraindre les paramètres cosmologiques, il est nécessaire de se baser sur le mineur nombre possible d'assomptions. En particulier il faut que la reconstruction n'utilise aucun modèle pour les distorsions en redshift.

L'idée fondamentale pour résoudre le problème d'une reconstruction des vides (qui soit autant que possible indépendante des modèles cosmologiques[7] et des modèles de distorsions en redshift) est la suivante: les distorsions en redshift vont affecter la position des galaxies *seulement* le long de la ligne de visée.

Si nous étions capables de reconstruire la forme des vides empilés sans utiliser la composante le long de la ligne de visée — c'est à dire si nous pouvions reconstruire le profil des vides à partir de sa projection sur le plan x-y, perpendiculaire à la ligne de visée — nous pourrions obtenir le vide dans l'espace réel. La Figure 1 illustre l'idée que nous venons d'introduire.

Nous considérons la densité dans l'espace des redshift, où par densité nous considérons le nombre de galaxies par élément de volume; ensuite nous la projetons sur le plan x-y en contant toutes les galaxies dans des intervalles en rayon, nous obtenons ainsi la densité projetée. Pour reconstruire le profil de densité du vide à partir de la projection, on utilise la transformée inverse de Abel (Abel, 1842, reprint 1988; Bracewell, 1999):

$$g(r_{\rm v}) = -\frac{1}{\pi}\int_{r_{\rm v}}^{1}\frac{I'(r_{\rm p})}{\sqrt{r_{\rm p}^2 - r_{\rm v}^2}}dr_{\rm p} \tag{1}$$

où $g(r_{\rm v})$ est le profil de densité sphérique des galaxies dans l'espace réel que nous voulons reconstruire, $r_{\rm v} = \sqrt{x^2+y^2+z^2}$ est le rayon du vide, $r_{\rm p} = \sqrt{x^2+y^2}$ est le rayon de la projection sur un plan perpendiculaire à la ligne de visée et $I(r_{\rm p})$ est la densité projetée.

Le problème principal est que la transformée inverse de Abel, bien que

[7]Nous rappelons que nous assumons un univers homogène et isotrope.

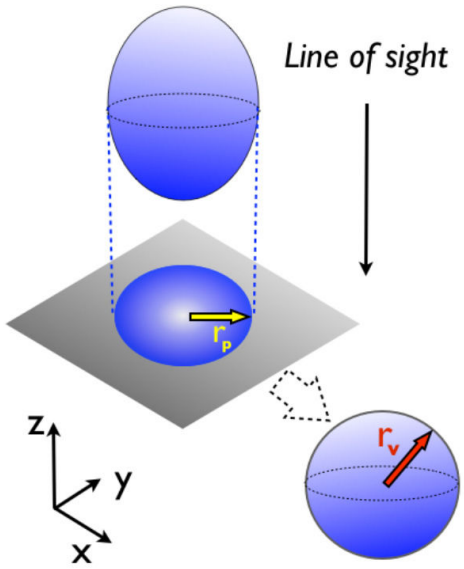

Figure 1: Representation de la méthode pour obtenir la sphère dans l'espace réel à partir de la sphère déformée dans l'espace des redshift: le vide déformé est projeté le long de la ligne de visée (les vitesses n'affectent pas la projection). À partir de la projection nous reconstruisons la sphère dans l'espace réel. La flèche rouge représente le rayon du vide dans l'espace réel $r_{\rm v}$, la flèche jaune représente le rayon de la projection $r_{\rm p}$.

mathématiquement définie par l'équation 1, est *mal-conditionnée*: s'il y a du bruit dans la fonction d'entrée $I(r_{\rm p})$ (dont $I'(r_{\rm p})$ est la dérivée par rapport à $r_{\rm p}$), la reconstruction sera dominée par le bruit.

En physique nous traitons souvent avec des problèmes inverses, qui relient les mesures à partir d'observations aux propriétés physiques que nous voulons établir. À cause du bruit dans les données, les problèmes inverses sont souvent mal-conditionnés, donc des petites erreurs dans les données en entrée vont donner des résultats complètement dominés par le bruit.

Lorsque nous utilisons les données des vides nous sommes dans cette condition: si nous considérons un vide empilé obtenu en lançant un algorithme capable de détecter les vides dans un catalogue de galaxies, le profil de densité dans l'espace des redshift sera bruité, ainsi que sa projection sur le plan x-y. Le bruit dans la projection $I(r_{\rm p})$ va fortement affecter la reconstruction obtenue moyennant la transformée inverse de Abel.

Le profil obtenu dans l'espace réel $g(r_{\rm v})$ sera donc dominé par le bruit: toutes les caractéristiques physiques du profil de densité seront dominées et effacées par le bruit, rendant impossible l'utilisation du profil pour contraindre la Cosmologie. Pour résoudre le problème du mauvais conditionnement nous avons implémenté dans le cas des vides une régularisation polynomiale de l'inversion (comme proposé par Li et al. (2007)). L'algorithme pour la reconstruction permet d'obtenir les profils de densité dans l'espace réel. Pour tester la reconstruction nous avons construit un modèle simple de vide empilé, nous l'avons déformé selon les distorsions et nous avons appliqué notre algorithme de reconstruction pour retrouver le profile dans l'espace réel. Pour simuler les effets dus au faible nombre de galaxies et au bruit dans le profil de densité, le modèle construit inclus aussi du bruit.

La reconstruction permet de contrôler le mal-conditionnement de l'inverse et de reconstruire le profil du vide empilé dans l'espace réel. La Figure 2 montre une illustration pédagogique de la reconstruction sans et avec la méthode de régularisation. Il est à noter que la fonction choisie pour ce modèle simple est une fonction pour laquelle l'inversion peut se calculer analytiquement (appelée paire de Abel); dans le cas d'un profil de vide plus vraisemblable,

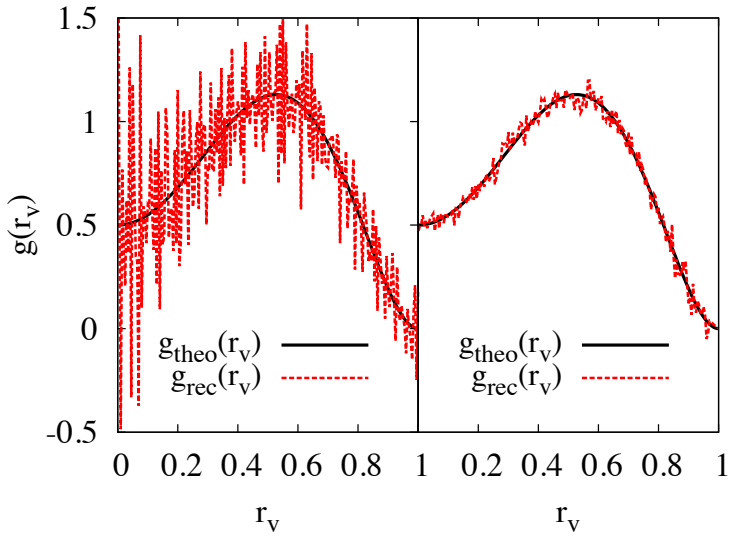

Figure 2: *Droite*: Profil théorique de la densité $g(r_v)$ (ligne noire) et profil reconstruit (pointillés rouges) dans le cas avec un bruit Gaussien de %1 dans la fonction d'entrée. À gauche nous représentons le profil obtenu en implémentant l'inversion de Abel sans aucune régularisation. À droite nous montrons la reconstruction avec la méthode pour régulariser l'inversion. Il est à noter que la fonction choisie pour ce modèle simple est une fonction pour laquelle l'inversion peut se calculer analytiquement (appelée paire de Abel); dans le cas d'un profil de vide plus vraisemblable, la reconstruction serait encore plus dominée par le bruit.

le signal cosmologique serait ultérieurement perdu dans le bruit. Avec le but de tester ultérieurement la méthode nous avons aussi développé une autre méthode de régularisation de l'inversion basée sur la décomposition en valeurs singulières. Pour une présentation de cette méthode et une comparaison avec la reconstruction polynomiale, voir la version anglaise de la thèse.

Pour valider la méthode, nous avons aussi utilisé un vide empilé obtenu à partir d'une simulation de particules de matière noire. Un test avec une simulation est en effet nécessaire, car il permet d'évaluer la méthode dans une situation aussi proche que possible de la réalité, qui tient donc en compte les erreurs dus au bruit de manière vraisemblable. Le résultat de la reconstruction est montré en Figure 3.

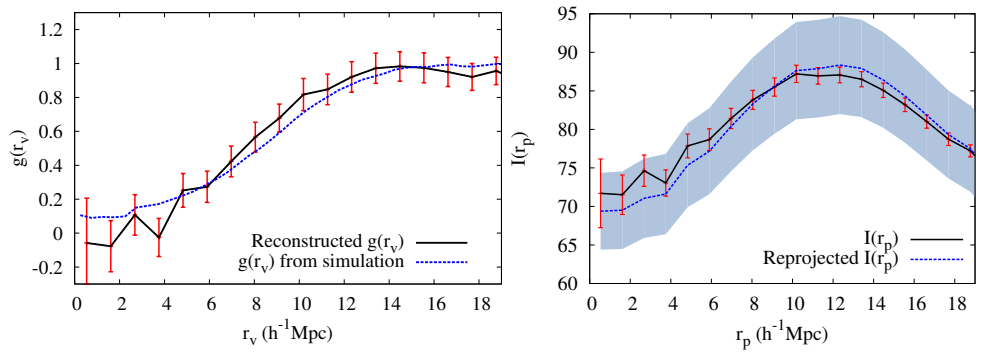

Figure 3: *Gauche:* La reconstruction avec la méthode polynomiale correspond bien au profil sphérique connu de la simulation. La reconstruction est obtenue à partir d'un échantillon de 200,000 particules de matière noire (sur un total de 10^9 particules). *Droite:* Pour le profil de la simulation, nous montrons la correspondance entre la projection $I(r_\mathrm{p})$ de la simulation et la reprojection après reconstruction. Plus de détails se trouvent dans la version complète de la thèse.

Enfin après avoir testé la reconstruction avec une simulation[8] nous avons utilisé des vides empilés du catalogue publié dans Sutter et al. (2012a) pour obtenir les premiers profils de densité de vides dans l'espace réel sans autre assomption que la sphéricité du vide. Les vides utilisés sont décrits dans le Tableau 1.

Rayon du vide	Redshift	Dataset	Galaxies	Vides
5-15	0.05-0.10	dim2	173929	173
10-15	0.05-0.10	dim2	43527	41
20-25	0.10-0.15	bright1	21241	17
25-45	0.15-0.20	bright2	51913	37

Tableau 1: Vides cosmiques empilés extraits du catalogue de vides de SDSS.

À titre d'exemple nous représentons en Figure 4 la reconstruction dans l'espace réel d'un vide empilé avec rayon entre 10 et 15 h^{-1}Mpc.

Nous avons construit et testé un algorithme pour obtenir les profils de vides

[8]Un test avec une simulation enrichie avec un modèle HOD est aussi présent dans la version complète de la thèse.

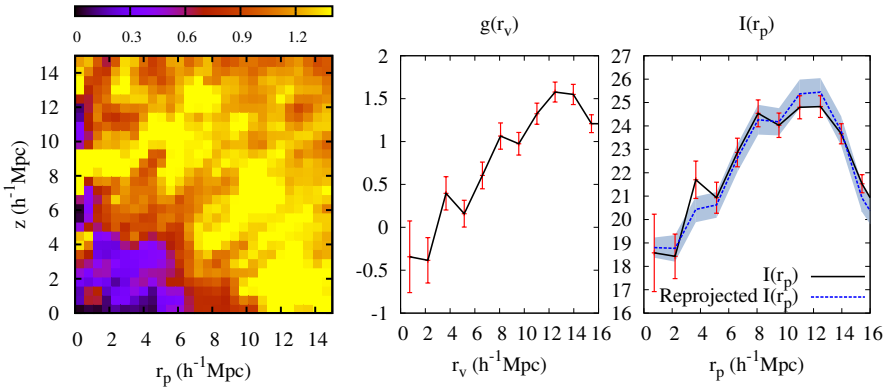

Figure 4: Résultats pour un vide empilé de rayon 10-15 h^{-1}Mpc: de gauche à droite nous représentons la densité dans l'espace des redshift $\rho(r_p, z)$, la densité reconstruite $g(r_v)$ et enfin la comparaison entre la densité projetée à partir des données $I(r_p)$ et la densitee re-projetée $I(r_p)$ à partir de notre reconstruction. Nous avons normalisé à la densité moyenne pour g et ρ, alors que les unités pour $I(r_p)$ sont en nombre de galaxies par $(h^{-1}\text{Mpc})^2$.

dans l'espace réel. L'application de cet algorithme aux données de SDSS nous a permis de reconstruire les premiers profils de densité pour les vides dans l'espace réel.

Une première application pour ces résultats est le calcul de la masse non-compensée présente dans le vide. On dit qu'un vide est compensé quand la masse présente à l'intérieur du vide balance la masse présente dans le mur du vide, dans ce cas la masse non-compensée est nulle. Les profils de densité dans l'espace réel obtenus des vides empilés de SDSS restent assez bruités. En utilisant une moyenne de ces profils de densité(pour plus de détails voir le texte original), nous pouvons toutefois obtenir la masse non-compensée:

$$\delta M(r) = 4\pi \int_0^r \Delta g r'^2 dr' \tag{2}$$

où $\Delta g = g(r) - \bar{g}(r)$.

Nous représentons la masse et le profil de densité en Figure 5.

De plus, le profil de densité peut être utilisé pour obtenir une prédiction théorique de la vitesse d'expansion des vides, représentée en Figure 6. Nous

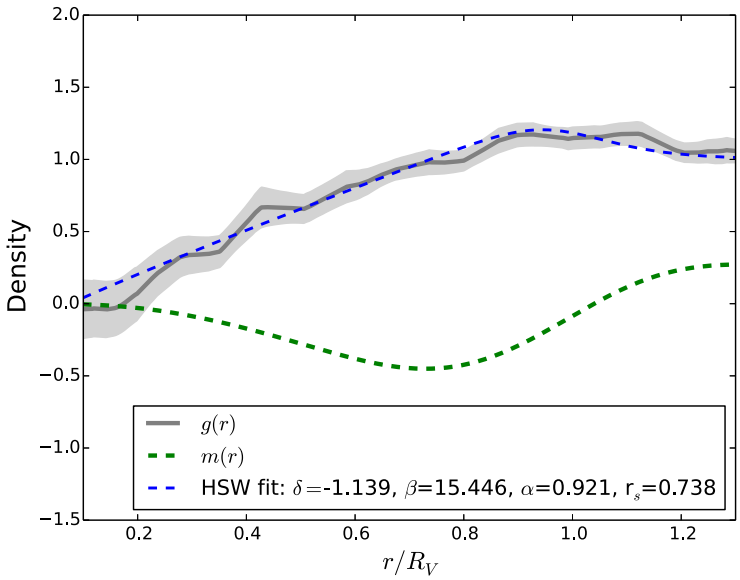

Figure 5: Masse non-compensée en fonction du rayon.

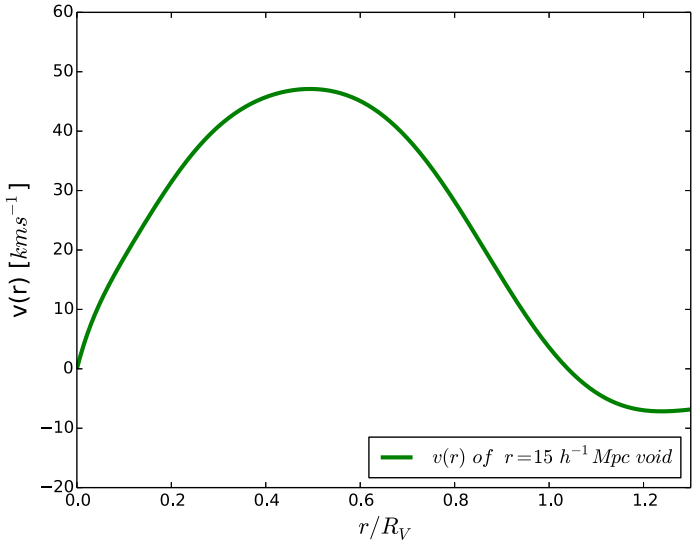

Figure 6: Prédiction théorique pour le profil de vitesse du vide en fonction du rayon, obtenue en considérant la théorie linéaire et en assumant un modèle cosmologique ΛCDM.

avons donc présenté deux applications immédiates de la reconstruction de vides dans l'espace réel. Dans la prochaine partie nous présenterons une analyse de l'effet des vitesses particulières des vides basée sur des simulations HOD.

L'effet des vitesses particulières sur les vides

Pour comprendre l'effet des vitesses particulières il est nécessaire d'analyser quelle différence celles-ci comportent en ce qui concerne les propriétés physiques des vides *et* en ce qui concerne la sélection des vides avec l'algorithme capable d'extraire les vides dans une distribution de traceurs de densité. Pour étudier cet l'impact des vitesses, nous comparons la même simulation HOD avec et sans l'ajout de vitesses particulières.

En particulier, nous comparons le nombre de vides qui sont relevés dans le deux cas, à travers la fonction de couplage de `VIDE`. Cette fonction permet de comparer deux catalogues de vides en se basant sur l'identifiant des cellules de chaque vide, et sur la superposition des cellules pour vérifier si le même vide est bien sélectionné dans les deux cas. En particulier nous étudions les nombre de vides couplés en dépendance du rayon, de l'ellipticité du vide et du contraste de densité (défini par `ZOBOV` comme le rapport de la densité minimale le long du bord de la région sélectionnée pour le vide et de la densité minimale de toute la région). La Figure 8 illustre le résultat de cette analyse.

De plus nous analysons la variation en pourcentage de l'ellipticité due aux vitesses particulières (en Figure 7).

L'analyse résultante est présente dans le texte intégral de la thèse, en anglais, et permet d'aboutir à une série de consignes permettant de réduire l'impact des vitesses pour les applications avec les vides en excluant de l'analyse les vides pour lesquels l'effet des vitesses est dominant. Ces consignes sont:

- exclure de l'analyse les vides avec rayon mineur que *deux fois* la séparation moyenne de traceurs, et éventuellement les vides avec un contraste de densité faible. Ceci éviterait l'utilisation de vides dont les ellipticités sont fortement affectées par les vitesses particulières;

- pour les vides restants corriger l'ellipticité en tenant compte de la valeur de l'aplatissement moyen causé par la présence de vitesses particulières (dû à l'élargissement des murs des vides);

- considérer que les vides ne changent pas de rayon de manière signifiante

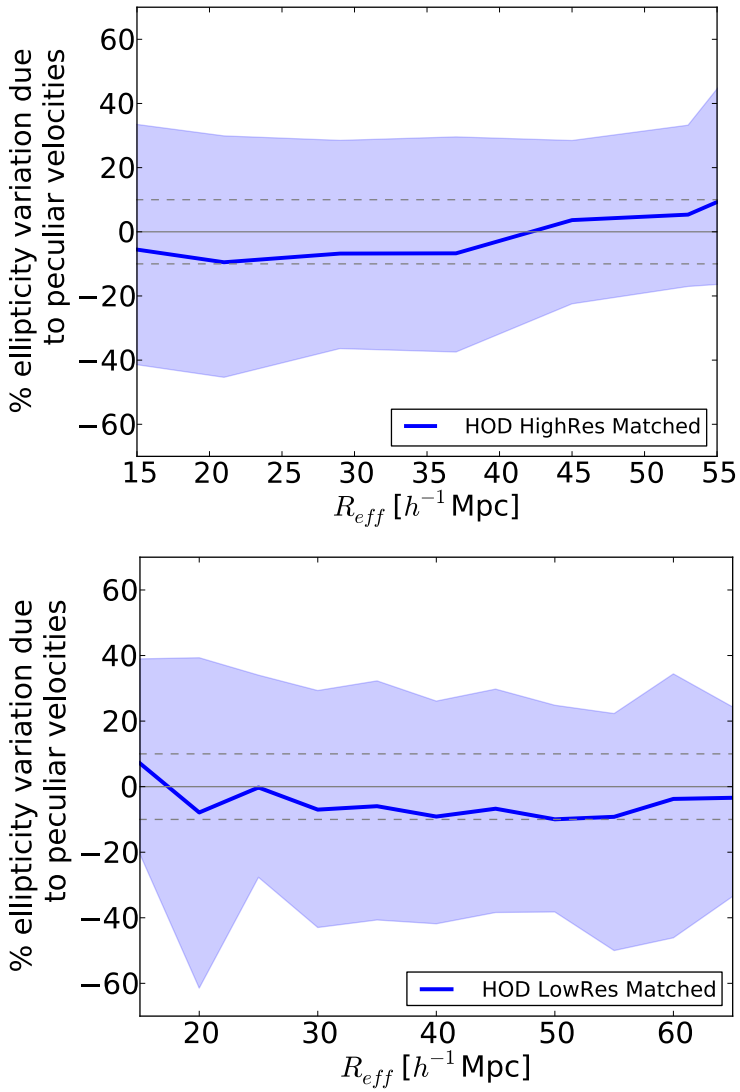

Figure 7: Pourcentage de variation de l'ellipticité due aux vitesses particulières pour la simulation HOD à haute densité (haut) et à faible densité (bas). Les vitesses particulières contribuent en moyenne à un aplatissement des vides.

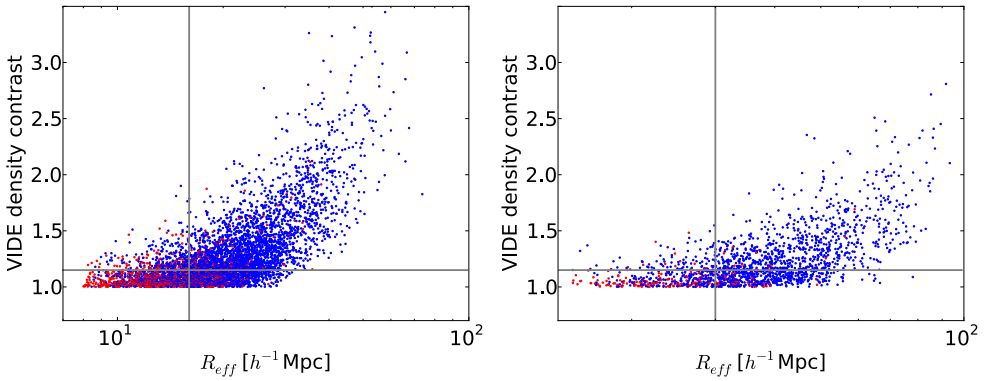

Figure 8: En bleu les vides couplés (c'est à dire les vides correctement identifiés malgré l'effet des vitesses particulières) et en rouge les vides non couplés. Dans les deux cas il est possible de considérer des sélections par rayon et par contraste de densité permettant de sélectionner les vides les plus affectés par les vitesses pariculières.

à cause des vitesse particulières et que les barycentres des vides sont légèrement déplacés.

Ces consignes peuvent être appliquées aux données, permettant de réduire les effets systématiques dus à la présence de vitesses.

Vides cosmiques et futures missions

L'application du test de Alcock-Paczyński présentée récemment dans Sutter et al. (2014a) montre qu'il est possible d'extraire l'information cosmologique des vides. Les études sur les vitesses particulières présentés dans cette thèse ont permit d'établir une correction globale à effectuer pour tenir en compte des vitesses.

L'application aux données ne permet pas encore de suivre les consignes dans les détails, car cela réduirait le nombre de vides de manière trop drastique dans le cas des données. Toutefois des critères de sélection semblables, mais plus relâchés, permettraient tout de même de réduire les effets systématiques dans les applications du test de Alcock-Paczyński.

De plus la reconstruction du profil de densité des vides dans l'espace réel permettrait d'améliorer la méthode la plus performante actuellement utilisée pour le test, qui se base sur la forme du vide dans l'espace réel.

En ce qui concerne une application des consignes plus sévère, qui permette de réduire l'impact des vitesses, la situation va bientôt changer. Des nouvelles données de missions telles que BOSS (avec les résultats complets) et Euclid vont améliorer de manière consistante le nombre de vides et donc l'application du test de Alcock-Paczyński. Les contraintes sur les modèles cosmologiques promettent donc d'atteindre le niveau de précision nécessaire dans le contexte de la Cosmologie moderne.

De plus, dans le contexte de ces nouvelles missions, une manière innovatrice d'utiliser les vides pour contraindre les modèles cosmologiques est l'utilisation du nombre de vides observés. En considérant le formalisme de Chevallier-Polarski-Linder (Chevallier and Polarski, 2001; Linder, 2003), nous avons:

$$w(z) = w_0 + w_a \frac{z}{z+1} \tag{3}$$

Une fois que le nombre de vides observés est connu, l'utilisation de matrices de Fisher permet d'obtenir les erreurs sur le plan $w_0 - w_a$. Ceci permet d'estimer le pouvoir contraignant des futures missions, telles que Euclid.

Le modèle utilisé pour obtenir ces contraintes est assez précis, dans la

mesure où il se base sur les détails les plus récents au sujet de la mission ESA Euclid. De plus il considère le modèle de Sheth and Van De Weygaert (2004) pour obtenir la distribution de vides en fonction du rayon. Les paramètres de ce modèle sont établis en se basant sur les catalogues HOD construits pour reproduire les détails de Euclid. Nous obtenons donc une estimation du nombre de vides trouvé par Euclid, ainsi que de la précision qui peut être atteinte par cette mission pour contraindre w_0 et w_a.

Le nombre de vides (pour plus de détails voir la version anglaise de la thèse) est donc un outil cosmologique à grand potentiel dans le cadre des missions modernes, qui promet de contraindre l'espace des paramètres de manière complémentaire avec les autres méthodes.

Conclusion

Dans cette thèse nous avons considéré le problème particulier de l'utilisation des vides cosmiques en Cosmologie. Alors que les vides sont des structures connues depuis 1978, jusqu'à présent le potentiel de ces structures pour contraindre les paramètres cosmologiques a été négligé. Cela est principalement dû aux difficultés que l'on rencontre pour extraire des données des zones à faible densité; ce qui a porté les cosmologues à se focaliser sur les outils cosmologiques pouvant utiliser les zones à densité élevée (par exemple les galaxies rouges lumineuses pour tracer les oscillations acoustiques des baryons).

La situation est maintenant en train de changer: les missions modernes nous permettent d'accéder à des mesures de haute qualité pour les grandes structures, en échantillonnant la distribution de galaxies en détail jusque dans les régions les moins denses. L'appel des vides cosmiques devient donc considérable. Le vides cosmiques sont donc une source d'information cosmologique, source qui demeure inutilisée jusqu'à présent. Dans la mesure où les vides remplissent l'Univers et ont une dynamique plus simple que les zones à densité élevée, ils s'affirment maintenant comme un outil innovateur et prometteur pour contraindre les modèles.

L'utilisation des vides pour contraindre la Cosmologie est basée sur leur forme, leur nombre et leur évolution. Ces propriétés dépendent de la Cosmologie, il est donc possible de les utiliser pour tester les modèles visant à comprendre et décrire l'évolution de l'Univers — e. g. en utilisant le test de Alcock-Paczyński.

Quand nous observons les vides, toutefois, nous les observons dans l'espace des redshift: leur forme réelle reste inaccessible pour nous, ce qui limite grandement notre connaissance de ces structures. Pour utiliser les vides en tant qu'outils cosmologiques de précision, il est fondamental d'obtenir leur forme dans l'espace réel.

Dans cette thèse nous avons présenté un algorithme non-paramétrique et indépendant du modèle assumé, permettant de reconstruire les profils de densité sphériques des vides empilés dans l'espace réel, sans aucune assomption au

sujet des distorsions en redshift, mais simplement basé sur des considérations géométriques — la sphéricité des vides empilés dans un univers homogène et isotrope.

La méthode de reconstruction est robuste: elle a été testée avec un modèle simplifié de vide, avec des vides empilés obtenus à partir d'une simulation de particules de matière noire et sur des catalogues simulés de galaxies construits pour simuler les caractéristiques de la Sloan Digital Sky Survey Data Release 7. L'utilisation de différentes méthodes pour obtenir la reconstruction améliore ultérieurement la fiabilité des résultats. De plus, l'utilisation de la re-projection pour contrôler la solution de ce problème mal-conditionné est un outil puissant pour valider la reconstruction dans le cas de l'application aux données.

Nous avons donc appliqué la méthode de reconstruction à des vides empilés extrait des données de SDSS et nous avons obtenu pour la première fois les profils de densité des vides empilés dans l'espace réel. Les profils obtenus peuvent être utilisés pour tester des modèles cosmologiques tels que les modèles de gravité modifiée ou les modèles d'énergie obscure et ne nécessitent d'aucune assomption sur les distorsions en redshift. De plus l'application du test de Alcock-Paczyński peut être améliorée, vu que la méthode la plus performante pour conduire le test est basée sur les profils de vides empilés dans l'espace réel.

Nous avons aussi présenté deux applications directes pour les profils de densité dans l'espace réel: la compensation de masse et une prédiction théorique pour les profils de vitesses particulières des vides (utilisant la théorie linéaire et assumant les valeurs des paramètres cosmologiques[9]).

En utilisant des catalogues de galaxies simulés, nous avons analysé l'effet des vitesses particulières sur les propriétés physiques des vides, qui ont un impact sur la manière dont l'algorithme pour trouver les vides sélectionne ces régions. Nous avons étudié l'effet des vitesses en comparant les vides un par un, en considérant la fraction de vides ayant une correspondance entre les deux catalogues et de ceux n'ayant pas de correspondance, en fonction du contraste

[9]La version complète de la thèse présente aussi une discussion sur la manière d'extraire des informations sur les vitesses particulières des vides de manière indépendante.

de densité et du rayon du vide. De plus, en étudiant l'effet des vitesses sur l'ellipticité des vides, sur leur rayons et sur leurs barycentres, nous avons obtenu des consignes à prendre en compte pour contrôler l'effet des vitesses particulières lors de l'utilisation des vides obtenus des données. Nous avons aussi discuté l'application de ces consignes dans le cas des missions courantes et futures.

Enfin nous avons considéré l'utilisation du nombre de vides pour contraindre les paramètres cosmologiques: en prenant en compte les consignes considérées pour minimiser l'effet des vitesses et les considérations théoriques basées sur le modèle "excursion set" à deux barrières pour les vides, nous avons obtenu une prédiction pour le nombre de vides qui peut être mesuré par le futur satellite Euclid de l'ESA (Agence Spatiale Européenne). En utilisant le formalisme des matrices de Fisher, nous avons aussi calculé une prédiction des contraintes de paramètres cosmologiques qui peuvent être obtenues grâce à cette mission.

Le travail présenté dans cette thèse permets d'obtenir les premiers profils de densité de vides dans l'espace réel et d'atteindre une compréhension plus profonde de ces structures à travers une analyse de l'effet des vitesses particulières sur les vides. Par moyen des leurs profils de densité, de leurs formes et de leur nombre, les vides s'imposent comme un outil cosmologique puissant dans le contexte de la nouvelle génération de missions, telles que le satellite de l'ESA Euclid, mais aussi eBOSS, DESI et WFIRST. En améliorant les contraintes sur les modèles cosmologiques, les vides cosmiques promettent d'apporter des informations indépendantes et complémentaires et d'éclairer le mystère de l'énergie obscure.